Quantitative MR in dystrophic muscle : It's more than fat

Hooijmans, M.T.

Lay-out and Printing: Guus Gijben; Proefschrift-aio.nl
Cover design by: Guus Gijben

ISBN: 978-94-92801-15-9

The research described in this thesis was supported by a grant from the Netherlands Organization for Health Research and Development (ZonMW) (grant number 113302001).

Quantitative MR in Dystrophic Muscle
It's more than fat

Proefschrift

ter verkrijging van
de graad van doctor aan de Universiteit van Leiden
op gezag van de Rector Magnificus prof. mr. C.J.J.M. Stolker,
volgens besluit van het College voor Promoties
te verdedigen op woensdag 13 december 2017
klokke 15:00 uur

door

Melissa Tamara Hooijmans

geboren te Zoetermeer
in 1989

Promotor:	Prof. Dr. A.G. Webb
Co-promotores:	Dr. H.E. Kan
	Dr. E.H. Niks
Leden promotie-commissie:	Prof. Dr. G.J. Strijkers
	(Amsterdam Medical Center)
	Dr. J.J. Prompers
	(Technical University Eindhoven)
	Prof. Dr. A.A.M. Aartsma-Rus

The work presented in this thesis was carried out at the C.J. Gorter Center, department of Radiology at the Leiden University Medical Center.

Financial support for printing of this thesis was kindly provided by Philips healthcare, the Netherlands.

Contents

1

Chapter 1

General introduction

1. General Introduction

Magnetic Resonance Imaging (MRI) and Magnetic Resonance Spectroscopy (MRS) are both important non-invasive tools in the field of biomedical research. The most common application is in the brain: however, adaptation of these MR techniques make them applicable to many other tissues and organs. One of these fields is musculoskeletal imaging where many different techniques are available to map various characteristics of healthy and diseased skeletal muscle. An important development in this field is the switch from qualitative visual assessment to quantitative measurements of tissue properties, which can be used to map the course of a disease, to evaluate potential therapeutic effects, and to investigate the effects of potential confounding factors on interpretation. One of the most common applications is in muscular dystrophies.

1.1 Skeletal muscle

Skeletal muscle is a highly ordered structure surrounded by connective tissue called the epimysium. The epimysium encloses the whole muscle and protects it from friction against other muscles and bones. A muscle consists of multiple fascicles, each surrounded by the perimysium and containing multiple fibers, which are in turn enclosed by the endomysium. All these connective tissue layers are interconnected and play an important role in force transmission. Small blood vessels and motor axons cross the perimysial space to make connections with muscle fibers. An individual muscle fiber is filled with sarcoplasm in which the myofibrils, ribosomes and mitochondria are located. In the myofibril, protein filaments (myofilaments) are organized in repeating units called sarcomeres. A sarcomere includes actin and myosin, contractile proteins which are essential for the generation of a muscle contraction. In addition to these contractile proteins, there is a wide variety of structural proteins in the sarcomere such as titin, nebulin and dystrophin, whose function is to maintain the architecture of the sarcomere. These organized repeating units are surrounded by the endoplasmic reticulum (Figure. 1.1). The endoplasmic reticulum stores calcium ions which are released when an action potential arrives at the T-tubulus. The rapid release of calcium ions activates the myofilaments that work together to generate force. The force developed in an individual muscle cell needs to be transferred to the musculoskeletal system in order to facilitate movement. The interconnection of all the connective tissue layers ensures that force is transferred to the tendon which is connected to the skeleton and finally results in movement.

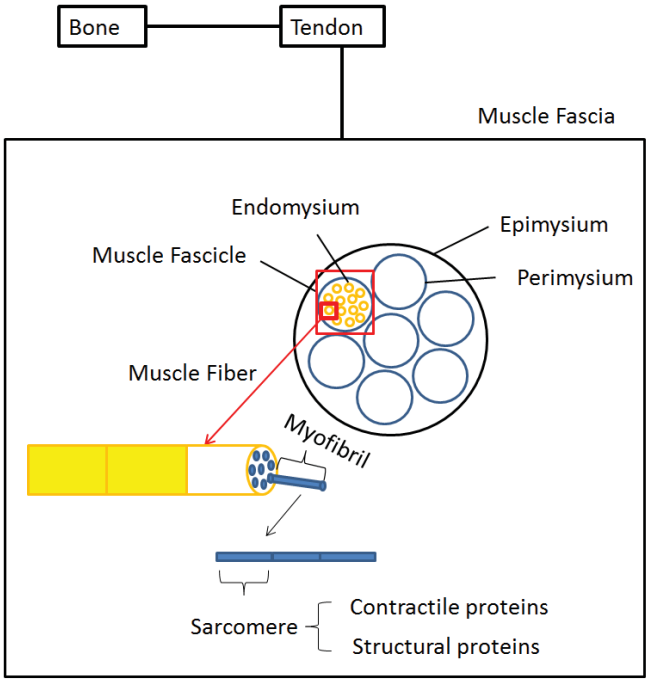

Figure 1. A schematic overview of skeletal muscle showing the arrangement of the various components.

1.2 Duchenne Muscular Dystrophy

Clinical phenotype

Duchenne Muscular Dystrophy (DMD) is the most common neuromuscular disorder, with an incidence of 1 in 3500 newborn boys. [1] It is an X-linked disease caused by a mutation in the *DMD* gene which codes for the protein dystrophin within the muscle cell. [2] The disease is characterized by progressive muscle damage, weakness and functional impairment. In DMD patients, the first symptoms often become apparent between the ages of 2 and 4 years old and consist of walking abnormalities, difficulties in climbing stairs, rising from the floor and running. [3] Many patients show pseudo-hypertrophy of the muscles, most notably in the calf muscles. The progressive loss of muscle strength results in wheelchair dependence in their early teens, after which upper limb function starts to decrease and frequently, scoliosis occurs. [4-6] In the late teens, patients develop respiratory impairments and need assisted ventilation.[7,8] In all DMD patients the heart muscle also becomes affected with age and mainly results in dilated cardiomyopathy.[9] Some patients suffer from learning and behavioral disabilities and the Intelligence Quotient (IQ) has been found to be one standard deviation below the general population.[10-12] Although life expectancy and quality of

life gradually increased due to treatment with corticosteroids, assisted ventilation and spinal fixation for severe scoliosis, most DMD patients die in their mid-thirties due to cardiac and respiratory failure. [13]

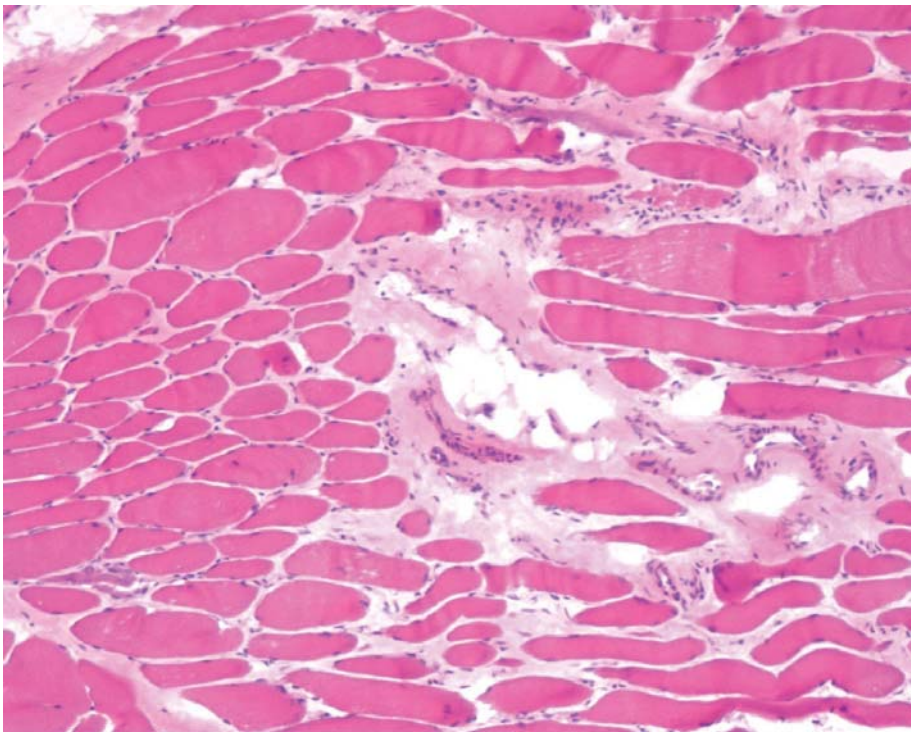

Figure 2. Cross-section of a muscle biopsy of the tibialis anterior muscle of a DMD patient showing the variations in fiber size, fibrosis, regeneration and degeneration of fibers, inflammatory cells and fat infiltration.

Muscle pathology

In muscle, dystrophin anchors the contractile apparatus to the muscle basement membrane via connections with the dystroglycoprotein complex.[14,15] Absence of dystrophin results in ongoing muscle damage, but the exact mechanism of how deficiency of dystrophin causes degeneration of muscle fibers is not fully understood. [16] Within muscle tissue different pathophysiological events take place, such as changes in energy metabolism, inflammation, fibrosis and fat replacement. These pathological hallmarks are clearly visible in muscle biopsies which contain an increased variation in fiber size, fibrotic and fatty tissue as well as groups of necrotic or degenerated fibers (Figure2). [17] The exact time course of these various processes is not fully understood, but it is thought that fiber necrosis induces a chronic inflammatory response that triggers fibrosis. At the same time, regeneration takes place through activation of

satellite cells.[4,18] Nonetheless, exhaustion of this regeneration capacity of the muscle eventually results in the replacement of muscle tissue by fat and connective tissue which is considered to be the end stage of the disease. [19] It is not completely clear whether the initial increase in muscle mass through hypertrophy is to compensate in part for the loss of force-generating capacity or should be considered an intrinsic aspect of this type of muscular dystrophy. [20,21]

1.3 Quantitative MR in skeletal muscle.

MR contrast

In MR the effect of two primary relaxation mechanisms on water protons is used to create image contrast, T_1 and T_2 relaxation. T_1 relaxation is the mechanism by which the longitudinal magnetization returns to its thermal equilibrium and reflects the energy transfer from spins to the environment, consisting of atoms and macromolecules. Each of these structures has its own characteristic tumbling rate (motion of the spin) which depends on the size and structure of the molecule and is driven by the thermal energy. The T_1 is shortest when the tumbling rate is almost equivalent to the Larmor frequency of the spin in the main magnetic field, both faster and slower tumbling rates are less efficient and result in longer T_1's. T_2 relaxation is the dephasing of the transverse magnetization and is determined by the interactions between spins in the tissue, which will lead to slight differences in resonance frequency. This difference in frequencies is measured by the dephasing of spins and generates T_2 contrast. By varying of sequence parameters, such as echo time (TE) and repetition time (TR), different image contrasts can be generated based on the T_1 and T_2 of the tissue.

MR in Skeletal muscle

Skeletal muscle has a short T_2 relaxation time, long T_1 relaxation time and high diffusivity of water protons. Consequently, application of MR techniques in skeletal muscle is challenging, as these tissues intrinsic MR properties all act to reduce the MR signal in a given sequence. These intrinsic tissue characteristics can change due to damage and disease, and as such can be a direct reflection of the disease. However, these pathology-related changes, for example muscle inflammation, metabolic alterations, or the replacement of muscle tissue by fat, can also act as confounders in the MR measurement. The recent switch from qualitative to quantitative assessment of skeletal muscle tissue properties with MR stresses the importance of high quality data, and the need to correct for such confounding effects. Acquisition of high quality data can naturally be achieved by using long measurement times. However, these long measurement times are generally experienced as uncomfortable and increase the risk of, for example, movement during the measurements which can

directly affect data-quality. In addition, a wide variety of MR-related parameters need to be assessed in order to be able to correct for any potential confounding factors, which is a time-consuming process. For newly-introduced techniques, it is generally unclear if there are any confounding factors and what, in the end, the effect might be on the measurements: the existence of confounding factors needs to be investigated to determine their effects on the final quantitative information from the scans.

Magnetic Resonance Imaging and Spectroscopy in DMD

Quantitative MR techniques have been frequently used to assess individual pathophysiological processes in Duchenne Muscular Dystrophy (DMD). [22] To start with, the replacement of muscle tissue by fat and connective tissue has been studied extensively. Both quantitative and semi-quantitative techniques showed variations in the extent and the rate of disease progression between different leg muscles.[20,23-29] In addition, quantitative techniques also showed that muscle fat fraction correlated well with disease progression and functional measures. Another MR measure which is often used in DMD, and is thought to reflect the inflammation component of the disease, is water T_2 relaxation times. Water T_2 values have shown to be elevated compared to healthy controls and to decrease with age and disease progression in DMD. [30-32] Moreover, water T_2 values have been shown to decrease towards more healthy values after three months of corticosteroid treatment. [33] Consequently, both muscle fat fraction and water T_2 values are frequently used as outcome measures in therapeutic evaluations (https://clinicaltrials.gov/search?cond=DMD+Therapy+MRI). Finally, changes in energy metabolism can be detected with phosphorous spectroscopy (^{31}P MRS). Elevated phosphodiesters levels, reduced phosphocreatine levels and a more alkaline intracellular tissue pH have been detected in DMD.[34-37] In addition, changes in energy metabolites have been found in relation to age, disease progression and functional measures. [37-41] So far the main focus of the field has been on quantifying individual pathophysiological processes in relation with function, disease progression, therapy and on detecting differences between individual muscles. However, to date, very little is known about how these individual pathophysiological processes relate to each other as well as to differences within an individual muscle.

Challenges in scanning of (young) children

Imaging studies in young pediatric populations remain relatively scarce due to the practical and technical challenges imposed during scanning of non-sedated subjects. Those challenges include motivation, alertness and cooperation of the child, but also anxiety caused by loud noise and the confined space of an MR scanner.

Various strategies have been proposed to improve a child's compliance during scanning without using sedation. [42] In the studies described in this thesis we used a mock scanner combined with a clear explanation of the procedure in appropriate terminology and a flexible approach based on the needs of the participant to improve the compliance. In addition to this, wearing their own metal-free clothing, bringing their own stuffed animal, and listening to their own music can result in a more familiar situation which improves the state of the patient. The presence of a parent, sibling or friend of the family in the MRI room can also put the child at ease. Alternatively, the presence of parents, sibling or guardians can also negatively influence the child which complicates the scanning procedure. During scanning, it is highly important to be aware of the state of the participant, as children sometimes do not express their feelings. Boredom, anxiety, discomfort and frustrations need to be detected and dealt with properly to ensure data quality: for example by using compliments, positive feedback and reminders about the essential things during scanning.

A number of MRI and MRS techniques applied in skeletal muscle will be discussed in more detail in the following section, as they are an essential part of this thesis. The discussion will focus on the basic characteristics of the method, confounders, data quality and factors which need to be considered during quantification.

1.4 Water fat imaging and ^{1}H MRS to assess muscle fat infiltration

One of the most common pathophysiological changes in damaged and diseased skeletal muscle is the progressive replacement of muscle tissue by fat. [43,44] [45,46] There are two main approaches used to assess muscle fat infiltration in skeletal muscle.

^{1}H MRS

The first approach is single voxel (SV) proton spectroscopy (^{1}H MRS) which is based on the difference in resonance frequency between water and fat protons. This technique measures the net equilibrium precessing magnetization of a desired nucleus, in this case protons, in a specific volume of interest, and depicts it as a function of their resonance frequency. This results in a frequency spectrum in which the resonances can be assigned to known functional groups, such as water and lipid (and also other macromolecules), and can be quantified. The total lipid signal in a typical ^{1}H spectrum consists of a number of spectral peaks at varying resonances and with varying amplitudes, while the water protons resonate at a single frequency (Figure 3). The lipid signal measured at clinical field strengths is represented by six fat peaks. It is dominated by lipid frequencies resonating between 0.5-2.75 ppm, and is often referred to as the aliphatic fat peak.[47] The lipid signal resonating at 5.3 ppm,

very close to the water signal, is called the olefinic fat peak. The apparent fat fraction can be derived from the integrated area of all the lipid signals and the water signal. One of the disadvantages of this method is that it only reflects a specific volume of interest. Therefore, it is less representative in heterogeneous tissue types, or in situations where one needs information from multiple muscles at once.

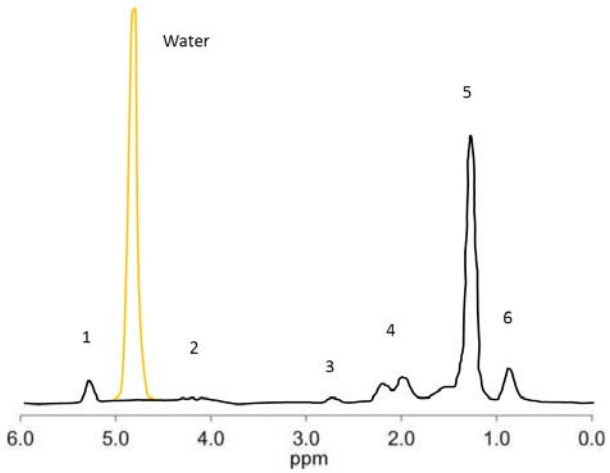

Figure 3. A proton MR spectrum at 3T. Water signal appears as a single peak at 4.7ppm (orange), whereas the fat signal is represented by six peaks (black), including the olefinic fat peak at 5.3 ppm (1), the peak at 4.1 ppm (2), the diacyl peak 2.7 ppm (3), the a-olefinic and a-carboxyl peak at 2.1 ppm (4), the dominant methylene peak at 1.3 ppm (5) and the methyl peak at 0.9 ppm (6).

Water Fat Imaging

The second approach is a quantitative imaging technique called Dixon, first introduced in 1984.[48] This method also allows separation of water and fat tissue based on the difference between the precessional frequencies of protons in water and fat. The conventional 2-point-DIXON method relies on the acquisition of two images with a gradient echo sequence, one in which water and fat are in-phase (IP) and one in which water and fat are out-of-phase (OP). Adding and subtracting these two images generates water and fat images, which combined can be used to quantitatively calculate an apparent fat fraction (Figure 4). One of the drawbacks of this method is that the reliability of the fat and water separation, by adding and subtracting images, is highly dependent on the magnetic field (B_o) inhomogeneities. This conventional method has been extended to the so-called 3-point-Dixon method which contains an additional third echo resulting in the ability to account for phase differences introduced by minor field inhomogeneities.[49] However, the situation described above is oversimplified, since it assumes a single resonance frequency

for water and fat, whereas the fat signal consists of a number of spectral peaks all contributing differently to the total fat signal. [47,50] The underlying algorithm of the 3-point Dixon can be modified to account for the individual fat spectral peaks.[51 52]

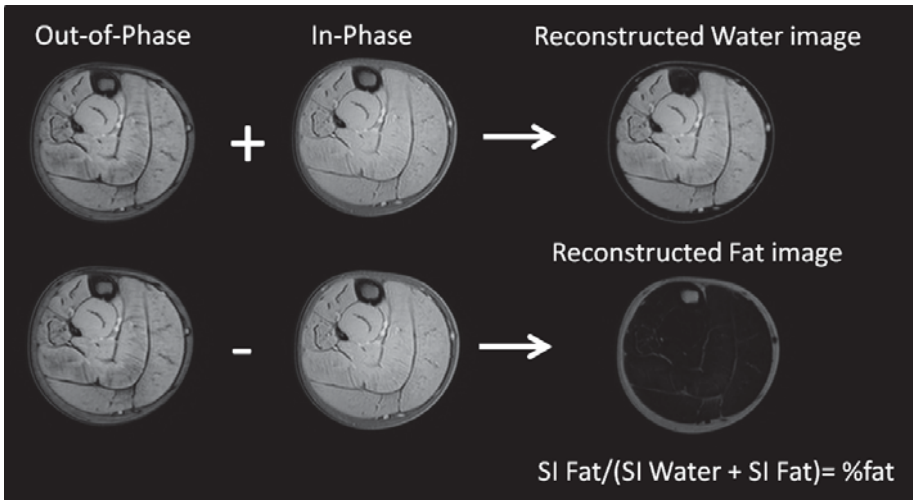

Figure 4. Axial in-phase (IP) and out-of-phase (OP) images and their reconstructed water and fat map of a right lower leg of a DMD patient. Note that the bright signal in the water images originates from muscle while in the fat images the bright signal is located in the subcutaneous fat.

The gradient echo 3-point Dixon method is used for all studies quantitatively assessing fat fraction in this thesis. A few factors will be discussed that need to be considered during the Dixon quantification process. First, the T_1 relaxation effect which could result in an overestimation of the fat fraction, due to a shorter T_1 of fat, as this difference in T_1 relaxation time between water and fat protons results in quicker relaxation of the fat signal within a short sequence TR.[53,54] For the data to be truly quantitative, this effect has to be minimized by using appropriate sequence parameters, for instance by using an optimized combination of a specific flip angle and TR. Secondly, the number of peaks taken into account in the reconstruction algorithm has a pronounced effect on the accuracy of the assessed fat fraction. Single peak models, solely aimed at the dominant methylene fat peak, responsible for 70% of the total fat signal, have shown to underestimate the total fat fraction compared to multi-peak models.[55,56] Another confounder is the T_2* relaxation effect, which originates from signal relaxation between echoes due to minor field inhomogeneities. [57] Despite the fact that this effect is small in tissues with no significant iron concentrations, this could result in an overestimation of fat fractions in low fat ranges. These effects can be accounted for in post-processing, where a minimum of three echoes is essential to generate a proper T_2* correction. [58]

1.5 (Water) T_2 relaxation time to assess inflammation and edema-like processes

The T_2 relaxation time is a tissue specific constant which reflects the interaction of a group of proton spins dephasing with respect to each other. The T_2 relaxation behavior should be mono-exponential in case of a single component, such as protons in water that reside in the same compartment. However, the transverse relaxation behavior of most biological tissues, including muscle, has shown to be multi-exponential. [59] Changes in T_2 are often associated with pathology, for example elevated water T_2 values in skeletal muscle are thought to reflect processes such as inflammation or edema. Elevated water T2 values are also found after exercise. By contrast, reduced water T_2 values in skeletal muscle have been associated with fibrosis. [60,61]

^{1}H MRS to assess water T_2

There are two main techniques used to quantitatively assess water T_2 relaxation time in skeletal muscle. First of all, SV ^{1}H MRS which measures the T_2 relaxation behavior of any tissue component independently of others, in this case water, and is *in-vivo* generally reflected by a mono-exponential fit. This MRS method with mono-exponential fit is assumed to be the gold standard and has been shown to be a robust and quantitative measure to assess water T_2 within a specific region of interest in both healthy and diseased tissue. [62-64] However, as mentioned before, this method can only generate information from one specific region of interest and is therefore not representative in heterogeneous tissue types.

Quantitative T_2 imaging to assess water T_2

The second approach is a Multi Spin Echo (MSE) acquisition, which is a quantitative imaging method that can cover a large region of interest (ROI) and contains information from multiple muscles at once. This approach is based on a simple Carr-Purcell-Meiboom-Gill sequence, where a 90-degree pulse is followed by a series of 180-degree pulses at multiple echo times, which allows assessment of the relaxation behavior of protons bound to various tissue components. The T_2 relaxation times of these tissue components can differ. For example, the T_2 relaxation time of fat protons is relatively long (> 90ms) compared to that of water (25-30ms). These two components together, when originating from the same tissue compartment, create a bi-exponential signal. However, the relaxation behavior of these two tissue components can still be approximated by a mono-exponential fit. [65,66] This combined relaxation behavior of protons in water and fat is then referred to as global T_2 values. In healthy skeletal muscle, global T_2 values and water T_2 values are almost equivalent, due to the only very minor contributions of the protons in fat. However, one of

the most common pathophysiological changes in damaged and diseased muscle is the replacement of muscle tissue by fat. Consequently, an increase in muscle fat fraction will result in more slowly decaying signal that results in measuring a prolonged T_2 relaxation time. This increase in the T_2 relaxation time is proportional to the fat fraction, and may falsely indicate muscle inflammation. Hence, additional approaches are necessary to separate the contribution of the fat and water protons to the total T_2 signal in order to derive the true water T_2. This is particularly important in situations where a significant amount of fat is present.

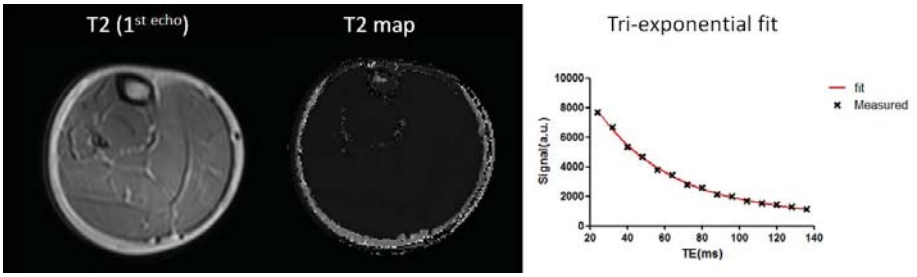

Figure 5. Axial multi-spin echo images of the right lower leg of non-fat infiltrated muscles of a DMD patient showing the 1st echo (TE: 8ms); the reconstructed T_2 map based on a tri-exponential fit; and the corresponding fit of a single point located in the Soleus muscle.

There are multiple approaches to separate the contribution of the water and fat protons. Two of these approaches are often used in skeletal muscle T_2 measurements and will be discussed in more detail. The first one is based on an addition to the acquisition scheme, a Spectrally Adiabatic Inversion Recovery (SPAIR) fat suppression pulse aimed at the main methylene and methyl fat peak.[67] (Figure 2) This resonance-specific method is based on the idea that when fully suppressing the main fat peak one can solely acquire the water signal. This method then assumes mono-exponential behavior of the water protons. It is important to note that this approach is highly sensitive to B_0 inhomogeneities as it has a resonance-specific fat suppression pulse. As a result, one should be extremely careful when using this method for quantification purposes because the fat suppression pulse can be inconsistent between examinations. In addition, previous work also showed that the significant influence of the fat signal on the measurement increased in the higher fat ranges.[68] This suggests that this measurement does not purely reflect the water signal. The second approach separates the multi-exponential behavior of the T_2 signal in post-processing by either a tri-exponential or an Extended Phase Graph (EPG) based fit. [43,69,70] A minimum number of echoes is essential to obtain a proper fit of the signal and advanced post-processing is needed to obtain quantitative values.

The MSE in combination with the advanced tri-exponential fitting method has been used in all studies assessing water T_2 in this thesis (Figure 5).

There are a few factors which need to be considered during quantification. First of all, the MSE method is more sensitive to B_1^+ field inhomogeneities compared to the MRS approach due to the larger field of view (FOV). The effect of these potential B_1^+ inhomogeneities should be taken into account when using the MSE approach. The EPG based fit incorporated these B_1^+ field fluctuations in the model, but that is not the case for the advanced tri-exponential signal fit. Consequently, in that case additional approaches, for example mapping of the B_1^+ field, are necessary to correct for these B_1^+ inhomogeneities (see the next section). Secondly, relatively high water T_2 values have been found with the advanced fit MSE approach compared to the MRS approach.[71] This difference in T_2 values has been attributed to imperfect slice profiles in the MSE approach caused by the absence of adequate RF-spoiling schemes on most clinical systems.[66,71] These RF imperfections result in stimulated echoes (additional signal) which can result in measuring elevated water T_2 values. This needs to be considered when comparing water T_2 values between studies.

1.6 B_1^+ field mapping approaches

There are two approaches often used to map the B_1^+ field: the double angle method (DAM) and the double TR method for actual flip angle imaging (AFI). [72,73] The double angle method acquires two images, one at flip angle α and one at $2*\alpha$, whereby the true flip angle can be derived from those two images by calculation. The double TR method uses two varying repetition times to derive the actual Flip Angle. This B_1^+ field information can be used as prior knowledge or as cut-off values in post-processing to ensure data-quality in any B_1^+ field sensitive acquisition. To date, this is still a relatively time-consuming process without any direct diagnostic value, so acceleration of this process is highly desirable. Recently, a relatively new fast Dual Refocusing Echo Acquisition Mode (DREAM) B_1^+ mapping technique has been proposed which allows acceleration by two orders of a magnitude. This method seems very promising but needs further evaluation in clinical applications.[74,75]

1.7 Diffusion Tensor Imaging to assess muscle structure

Diffusion Tensor Imaging (DTI) is a quantitative imaging technique aimed at probing water diffusion, the random microscopic movement of water, which in skeletal muscle is hindered by structures such as mitochondria, the sarcoplasmic reticulum, macromolecules and the cell membrane. This hindered diffusion can be described by a parameter called the apparent diffusion coefficient (ADC), which is an indirect reflection of the muscle microstructure. Introducing diffusion weighting into the

sequence attenuates the signal more from tissues which allow unrestricted diffusion of water, thus producing higher relative signals from tissues in which the movement is restricted. By using two or more diffusion-weighted sequences and comparing the relative tissue signal intensities it is possible to calculate ADC maps, showing diffusive properties of tissue in different regions of interest.

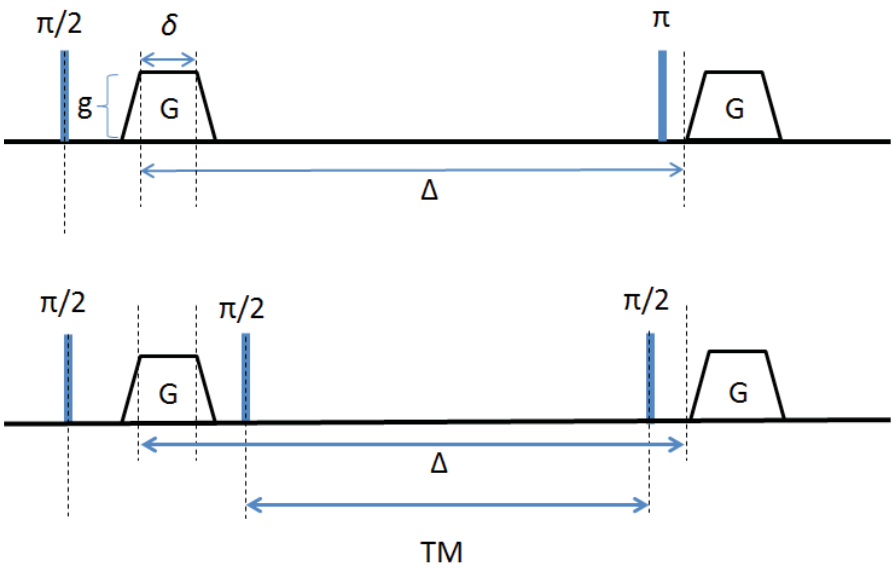

Figure 6. A schematic representation of the different diffusion modules: Spin Echo sequence (top) and a Stimulated Echo Sequence (bottom). g is the gradient amplitude, δ is the gradient duration, Δ is the spacing, and TM is the mixing time.

There are two main MR techniques used to map the diffusion properties of water in skeletal muscle. The first is the spin-echo echo-planar imaging sequence (SE-EPI), a fast, movement-robust and intrinsically T_2-weighted method, most commonly used with Stejskal-Tanner diffusion encoding (Figure 6 (top)).[76] The main challenge for this method is to achieve sufficient diffusion weighting within reasonable echo times since muscle tissue has a relatively short T_2 relaxation time. The amount of diffusion weighting is directly related to the *b*-value, a higher *b*-value generates more diffusion weighting. A given *b*-value is dependent on the gradient amplitude (g), gradient strength, the gyromagnetic ratio of the nucleus and the gradient spacing duration between the dephasing and rephrasing gradients (Δ). There are two ways to increase diffusion weighting: higher gradient strength (g) or longer gradient duration (*δ*). (Figure 6) However, the maximal gradient strength on most clinical scanners is limited due to subject safety limitations. In order to reach

higher *b*-values one has to increase the gradient spacing or duration. Both of these adjustments result in longer TE's which has a high impact on Signal to Noise Ratio (SNR) due to the muscle tissue's short T_2. An alternative approach is the Stimulated Echo (STE) sequence which avoids the T_2 decay by storing the magnetization in the longitudinal plane, which causes the signal to be attenuated by T_1 decay, and $T_1 > T_2$ for all tissues.[77] The 180-degree refocusing pulse is replaced by two 90-degree radio frequency pulses which are separated by the mixing time (TM). (Figure 6 (bottom)) This results in a direct loss of approximately 50% of the signal but allows much longer mixing times within the same echo time. These longer mixing times result in the ability to probe longer distances which can be advantageous in larger structures.

A minimum of six non-collinear diffusion directions are necessary in order to quantify the directionality of the diffusion within one individual voxel by calculating the diffusion tensor. The tensor can be diagonalized to obtain three eigenvectors (v_1, v_2, v_3) and their corresponding eigenvalues (λ_1, λ_2, λ_3). These eigenvalues are commonly used as DTI based outcome parameters. The first eigenvalue (λ_1) represents the direction in which diffusion is dominant. As such, in skeletal muscle this represents diffusion along the fiber length; the first eigenvector defines the fiber orientation with respect to the scanner coordinate system. The second eigenvalue (λ_2) points along a direction that is orthogonal to the first eigenvector (v_1). The third eigenvalue (λ_3) is orthogonal to both the first eigenvector (v_1) and the second eigenvector (v_2). If diffusion is isotropic all eigenvalues ($\lambda_1 = \lambda_2 = \lambda_3$) are equal, whereas when it is anisotropic the first eigenvalue is larger than the other two eigenvalues ($\lambda_1 > \lambda_2 = \lambda_3$ or $\lambda_1 > \lambda_2 > \lambda_3$). Radial diffusivity is the average of the second and third eigenvalue (λ_2 and λ_3) and represents the average diffusion orthogonal to the dominant direction. The radial diffusivity is thought to be most sensitive to changes in muscle due to the elongated shape of the fibers. From these three eigenvalues two other measures can be computed. The mean diffusivity (MD) is the average of the three eigenvalues and reflects the average diffusion in tissue. The fractional anisotropy (FA) is a dimensionless scalar index which varies between zero (isotropic) and one (anisotropic) and reflects the amount of directionality in the tissue. [78,79] These five measures are generally used to describe tissue microstructure and have been shown to change with respect to age, gender, exercise, injury and disease; and to vary between individual muscles.[80-94] [95]

High quality data is essential to obtain reliable estimates of these DTI-based parameters. However, reaching sufficient SNR is challenging in skeletal muscle due to the tissue's short T_2, long T_1 and relatively high diffusivity of water. Simulation studies have evaluated the effect of SNR on the DTI parameter estimation. They predicted

an underestimation of MD and the three eigenvalues, and an overestimation of FA in low SNR data.[80,89] In addition, changes in $T_{2,}$ often associated with muscle damage may indirectly influence the DTI parameter estimation in the SE-EPI sequence due to associated changes in SNR. Finally, simulation studies showed that the presence of fat signal can result in an inaccurate DTI parameter estimation due to the fact that fat has a diffusion coefficient two orders of magnitude lower than water. [96] This is particularly important in applications where there is a significant amount of fat tissue present in the region of interest, such as in muscular dystrophies. Multiple approaches have been investigated in order to suppress the effect of the fat signal.[97] One of the methods which generates good overall suppression of the spectrum is a combination of a SPAIR pulse and a Slice Selective Gradient Reversal (SSGR) technique both aimed at the main methylene and methyl fat peaks, together with a second spectral suppression pulse aimed at the olefinic fat peak. (Figure 3) Essential to keep in mind is that this method needs adjustments on the acquisition side and is highly sensitive to B_0 field inhomogeneities.[96] Recently, a relatively new method has been introduced which uses an arbitrary chemical-shift angle dual echo Dixon method to perform image reconstruction of diffusion-weighted images with suppression of the entire fat spectrum. [98] The SE-EPI sequence in combination with the three-component fat saturation technique was used for all DTI measurements in this thesis.

1.8 Phosphorous Magnetic Resonance Spectroscopy (^{31}P MRS) to assess energy metabolism

^{31}P MRS is a quantitative technique used to assess energy metabolism in skeletal muscle either in rest or in non-steady state conditions. As mentioned previously, this technique is based on the concept that nuclei of the same type, in this case ^{31}P, resonate at slightly different frequencies in different chemical environments, due to minor differences in shielding exerted by the electron cloud. This gives rise to a spectrum of frequencies which can be assigned to known metabolites. A ^{31}P spectrum of skeletal muscle contains a variety of peaks from (muscle) metabolites including Inorganic Phosphate (Pi), Phosphocreatine (PCr), Phosphodiesters (PDE), Phosphomonoesters (PME) and Adenine-Tri-Phosphate (ATP). An example of a spectrum obtained in skeletal muscle at a 7T MR system is shown in figure 7.

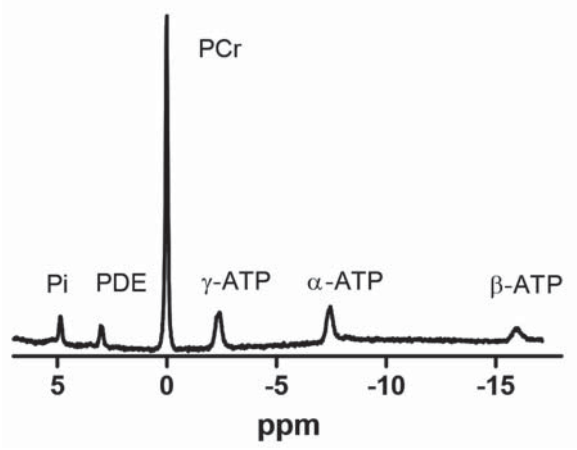

Figure. 1.7: Typical ^{31}P spectra of the Soleus muscle of a healthy (adult) control subject.

Ratios between these phosphorous compounds can reflect for instance muscle metabolic reserve and oxidative phosphorylation capacity. [99,100] In addition, the shift in resonance between the Pi and PCr peak can be used to calculate the intracellular tissue pH. These ratios and intracellular tissue pH slightly vary between the individual muscles at rest.[101,102]

MRS measurements are commonly based on a simple free induction decay (FID) readout without gradients during the spatial encoding which results in signal without any spatial information. There are three ways commonly used to spatially localize MRS data: surface coil localization, single voxel localization and spectroscopic imaging. Surface coil localization is most commonly used for ^{31}P MRS measurements in skeletal muscle and is based on measuring one single FID for all the signal picked up by the coil. This method is very fast and has short TE's which is advantageous since ^{31}P compounds have relatively short T_2 relaxation times. The sensitivity of this method is highly influenced by the shape and size of the coil, and the signal is weighted towards tissue located more closely to the surface. Consequently, the signal obtained with this method is a mixture of multiple tissue types and has a high inter-subject variability which needs to be considered when interpreting the results. Secondly, there are single-voxel localization approaches which generate rapid information from a well-defined small ROI with a relatively homogeneous magnetic field. This method uses a combination of three slice-selective RF pulses in orthogonal planes through which a signal arises at the intersection of these three planes. This localization method is highly sensitive to the chemical shift displacement artefact (CSDA), especially at high magnetic fields, and works less efficiently in heterogeneous tissue types. In addition, the relatively long TE's, pertinent to this

method, in combination with the relatively short T_2 times of the various phosphorous compounds result in a lot of signal loss. [103] Lastly, there are Chemical Shift Imaging (CSI) methods which became increasingly more popular with the availability of higher field magnets. The acquisition of this technique is based on a simple FID readout, spatially localized in 1D, 2D or 3D by a combination of a single excitation pulse and phase encoding steps. This technique is very well suited for heterogeneous tissue types, is relatively efficient in terms of SNR per unit of time but has long acquisition times and less well-defined voxels. Besides spectroscopy, one could also use spectrally sensitive ^{31}P imaging. This imaging technique can be used to map PCr with high temporal and spatial resolution compared to spectroscopy approaches. This is advantageous in exercise settings and heterogeneous tissue types. However, this method is only aimed at one or two resonances, which limits application possibilities.[104] The 2D chemical shift imaging method was used for all ^{31}P MRS studies in this thesis.

There are a few general points which need to be considered when quantitatively assessing energy metabolism with ^{31}P MRS. First, one of the most essential points for MRS in general is adequate shimming of the B_0 field which has a direct relation to SNR and linewidth. Generally, a drop in SNR and an increase in linewidth result in a less accurate estimation of the area under curve and thus of the metabolite ratios. These effects can be minimized by enforcing strict acceptance criteria that limit spectra to minimum SNR and maximum linewidths to ensure proper quantification and comparisons of energy metabolism among individuals. Second, the saturation effect due to variation in T_1 relaxation of the various phosphorus compounds needs to be considered. In practice, the T_1 relaxation times of ^{31}P metabolites are too long to allow complete saturation before the next excitation pulse. These relaxation effects can be accounted for in post-processing using literature values, or by measuring the full relaxation of the various compounds. They can also be reduced during acquisition by using the Ernst angle for excitation. [103] Last, all individual phosphorous compounds are generally presented as a ratio over β-ATP. This quantification method assumes that muscle ATP is constant or at least is preserved as long as possible in skeletal muscle. However, this might not always be the case.

1.9 Objectives of this thesis

The overall aim of this thesis was to combine various quantitative MR measurements and to compare these between DMD patients and healthy age-matched controls, both on a cross-sectional and longitudinal level, to generate a better understanding of the underlying pathophysiology and ideally to explore the value of these MR outcome parameters to monitor muscle tissue changes in a clinical setting. In order to achieve this aim we:

1. measured muscle fat infiltration, inflammation, fiber architecture and energy metabolism in healthy and diseased muscle on a cross-sectional and longitudinal level.
2. combined these MR techniques to assess the effect of spatial localization, data quality and confounding factors on the quantification process of MR outcome measures.
3. combined these MR parameters to have a better understanding of the underlying pathophysiology of DMD.

Thesis Outline

This thesis is divided into two main parts, preceded by an introduction and followed by a general discussion. The first part focuses on the effect of methodological factors such as data-quality, accurate spatial localization and confounding factors on quantification of MR outcome measures in skeletal muscle applications. In chapter 2, the effect of %fat, SNR and T_2 changes on the DTI measurements in skeletal muscle of DMD patients and healthy controls has been evaluated using multi-parametric MRI. In chapter 3, the accuracy of spatial localization is stressed using 3-point-dixon imaging for fat quantification along the proximodistal muscle axis in DMD patients. In chapter 5, the effect of data quality, accuracy and reproducibility of quantifying PDE-levels with ^{31}P MRS was assessed in healthy control subjects. The second part of this thesis is focused on the importance of combining various imaging techniques in order to have a better understanding of the underlying pathophysiology in DMD and to explore the value of MR measures to monitor muscle tissue changes. Chapter 3 assessed variations in muscle degeneration within individual leg muscles of DMD patients. Chapter 4 presents combined qMRI and spatially-resolved (2D-CSI) ^{31}P MRS data of the leg muscles in DMD patients to determine metabolic changes and inflammation in muscles with and without fat infiltration, to assess if metabolic changes and inflammation vary in different stages of the disease process. Chapter 5 presents longitudinal and spatially resolved ^{31}P MRS and qMRI data of lower leg muscles that represent varying levels of muscle deterioration, aimed to assess whether phosphodiester (PDE)-levels detected by ^{31}P MRS could be a marker for muscle tissue changes. In addition, the course of the other metabolic indices over two-year time-period was assessed. Finally, chapter 6 aims to bridge the gap between the research field and clinical practice by accelerating of sequences, as it focuses on the implementation of a fast B_1^+ shimming technique to improve image quality, in whole body imaging at 3T, without loss of essential scan time.

1.10 References

1 Ryder, S. *et al.* The burden, epidemiology, costs and treatment for Duchenne muscular dystrophy: an evidence review. *Orphanet J Rare Dis* **12**, 79, doi:10.1186/s13023-017-0631-3 (2017).

2 Hoffman, E. P., Brown, R. H. & Kunkel, L. M. Dystrophin - the Protein Product of the Duchenne Muscular-Dystrophy Locus. *Cell* **51**, 919-928, doi:Doi 10.1016/0092-8674(87)90579-4 (1987).

3 Jennekens, F. G., ten Kate, L. P., de Visser, M. & Wintzen, A. R. Diagnostic criteria for Duchenne and Becker muscular dystrophy and myotonic dystrophy. *Neuromuscul Disord* **1**, 389-391 (1991).

4 Blake, D. J., Weir, A., Newey, S. E. & Davies, K. E. Function and genetics of dystrophin and dystrophin-related proteins in muscle. *Physiol Rev* **82**, 291-329, doi:10.1152/physrev.00028.2001 (2002).

5 Kinali, M. *et al.* Muscle histology vs MRI in Duchenne muscular dystrophy. *Neurology* **76**, 346-353, doi:Doi 10.1212/Wnl.0b013e318208811f (2011).

6 Eagle, M. *et al.* Managing Duchenne muscular dystrophy--the additive effect of spinal surgery and home nocturnal ventilation in improving survival. *Neuromuscul Disord* **17**, 470-475, doi:10.1016/j.nmd.2007.03.002 (2007).

7 Ishikawa, Y. *et al.* Duchenne muscular dystrophy: survival by cardio-respiratory interventions. *Neuromuscul Disord* **21**, 47-51, doi:10.1016/j.nmd.2010.09.006 (2011).

8 Eagle, M. *et al.* Survival in Duchenne muscular dystrophy: improvements in life expectancy since 1967 and the impact of home nocturnal ventilation. *Neuromuscul Disord* **12**, 926-929 (2002).

9 Nigro, G., Comi, L. I., Politano, L. & Bain, R. J. The incidence and evolution of cardiomyopathy in Duchenne muscular dystrophy. *Int J Cardiol* **26**, 271-277 (1990).

10 Cotton, S. M., Voudouris, N. J. & Greenwood, K. M. Association between intellectual functioning and age in children and young adults with Duchenne muscular dystrophy: further results from a meta-analysis. *Dev Med Child Neurol* **47**, 257-265 (2005).

11 Mehler, M. F. Brain dystrophin, neurogenetics and mental retardation. *Brain Res Brain Res Rev* **32**, 277-307 (2000).

12 Cyrulnik, S. E., Fee, R. J., De Vivo, D. C., Goldstein, E. & Hinton, V. J. Delayed developmental language milestones in children with Duchenne's muscular dystrophy. *J Pediatr* **150**, 474-478, doi:10.1016/j.jpeds.2006.12.045 (2007).

13 Kieny, P. *et al.* Evolution of life expectancy of patients with Duchenne muscular dystrophy at AFM Yolaine de Kepper centre between 1981 and 2011. *Ann Phys Rehabil Med* **56**, 443-454, doi:10.1016/j.rehab.2013.06.002 (2013).

14 Ervasti, J. M., Ohlendieck, K., Kahl, S. D., Gaver, M. G. & Campbell, K. P. Deficiency of a glycoprotein component of the dystrophin complex in dystrophic muscle. *Nature* **345**, 315-319, doi:10.1038/345315a0 (1990).

15 Rybakova, I. N., Patel, J. R. & Ervasti, J. M. The dystrophin complex forms a mechanically strong link between the sarcolemma and costameric actin. *J Cell Biol* **150**, 1209-1214, doi:DOI 10.1083/jcb.150.5.1209 (2000).

16 Allen, D. G., Whitehead, N. P. & Froehner, S. C. Absence of Dystrophin Disrupts Skeletal Muscle Signaling: Roles of Ca2+, Reactive Oxygen Species, and Nitric Oxide in the Development of Muscular Dystrophy. *Physiol Rev* **96**, 253-305, doi:10.1152/physrev.00007.2015 (2016).

17 Peverelli, L. *et al.* Histologic muscular history in steroid-treated and untreated patients with Duchenne dystrophy. *Neurology* **85**, 1886-1893, doi:10.1212/Wnl.0000000000002147 (2015).

18 Deconinck, N. & Dan, B. Pathophysiology of duchenne muscular dystrophy: current hypotheses. *Pediatr Neurol* **36**, 1-7, doi:10.1016/j.pediatrneurol.2006.09.016 (2007).

19 Bell, C. D. & Conen, P. E. Histopathological changes in Duchenne muscular dystrophy. *J Neurol Sci* **7**, 529-544 (1968).

20 Wokke, B. H. *et al.* Quantitative MRI and strength measurements in the assessment of muscle quality in Duchenne muscular dystrophy. *Neuromuscular Disord* **24,** 409-416, doi:10.1016/j.nmd.2014.01.015 (2014).

21 Karpati, G., Carpenter, S. & Prescott, S. Small-caliber skeletal muscle fibers do not suffer necrosis in mdx mouse dystrophy. *Muscle Nerve* **11,** 795-803, doi:10.1002/mus.880110802 (1988).

22 Straub, V. *et al.* Stakeholder cooperation to overcome challenges in orphan medicine development: the example of Duchenne muscular dystrophy. *Lancet Neurol* **15,** 882-890 (2016).

23 Fischmann, A. *et al.* Muscular involvement assessed by MRI correlates to motor function measurement values in oculopharyngeal muscular dystrophy. *J Neurol* **258,** 1333-1340, doi:10.1007/s00415-011-5937-9 (2011).

24 Fischmann, A. *et al.* Quantitative MRI can detect subclinical disease progression in muscular dystrophy. *J Neurol* **259,** 1648-1654, doi:10.1007/s00415-011-6393-2 (2012).

25 Fischmann, A. *et al.* Quantitative MRI and loss of free ambulation in Duchenne muscular dystrophy. *J Neurol* **260,** 969-974, doi:10.1007/s00415-012-6733-x (2013).

26 Hollingsworth, K. G., Garrood, P., Eagle, M., Bushby, K. & Straub, V. Magnetic Resonance Imaging in Duchenne Muscular Dystrophy: Longitudinal Assessment of Natural History over 18 Months. *Muscle Nerve* **48,** 586-588, doi:10.1002/mus.23879 (2013).

27 Ricotti, V. *et al.* Upper Limb Evaluation in Duchenne Muscular Dystrophy: Fat-Water Quantification by MRI, Muscle Force and Function Define Endpoints for Clinical Trials. *Plos One* **11,** e0162542, doi:10.1371/journal.pone.0162542 (2016).

28 Bonati, U. *et al.* Quantitative muscle MRI: A powerful surrogate outcome measure in Duchenne muscular dystrophy. *Neuromuscul Disord* **25,** 679-685, doi:10.1016/j.nmd.2015.05.006 (2015).

29 Wren, T. A., Bluml, S., Tseng-Ong, L. & Gilsanz, V. Three-point technique of fat quantification of muscle tissue as a marker of disease progression in Duchenne muscular dystrophy: preliminary study. *AJR Am J Roentgenol* **190,** W8-12, doi:10.2214/AJR.07.2732 (2008).

30 Willcocks, R. J. *et al.* Longitudinal measurements of MRI-T-2 in boys with Duchenne muscular dystrophy: Effects of age and disease progression. *Neuromuscular Disord* **24,** 393-401, doi:10.1016/j.nmd.2013.12.012 (2014).

31 Arpan, I. *et al.* T-2 mapping provides multiple approaches for the characterization of muscle involvement in neuromuscular diseases: a cross-sectional study of lower leg muscles in 5-15-year-old boys with Duchenne muscular dystrophy. *Nmr Biomed* **26,** 320-328, doi:10.1002/nbm.2851 (2013).

32 Forbes, S. C. *et al.* Magnetic Resonance Imaging and Spectroscopy Assessment of Lower Extremity Skeletal Muscles in Boys with Duchenne Muscular Dystrophy: A Multicenter Cross Sectional Study. *Plos One* **9,** doi:ARTN e106435
10.1371/journal.pone.0106435 (2014).

33 Arpan, I. *et al.* Examination of effects of corticosteroids on skeletal muscles of boys with DMD using MRI and MRS. *Neurology* **83,** 974-980, doi:10.1212/WNL.0000000000000775 (2014).

34 Kemp, G. J., Taylor, D. J., Dunn, J. F., Frostick, S. P. & Radda, G. K. Cellular Energetics of Dystrophic Muscle. *J Neurol Sci* **116,** 201-206, doi:Doi 10.1016/0022-510x(93)90326-T (1993).

35 Griffiths, R. D., Cady, E. B., Edwards, R. H. & Wilkie, D. R. Muscle energy metabolism in Duchenne dystrophy studied by 31P-NMR: controlled trials show no effect of allopurinol or ribose. *Muscle Nerve* **8,** 760-767, doi:10.1002/mus.880080904 (1985).

36 Newman, R. J. *et al.* Nuclear Magnetic-Resonance Studies of Forearm Muscle in Duchenne Dystrophy. *Brit Med J* **284,** 1072-1074 (1982).

37 Younkin, D. P. *et al.* 31P NMR studies in Duchenne muscular dystrophy: age-related metabolic changes. *Neurology* **37,** 165-169 (1987).

38 Hogrel, J. Y. *et al.* Longitudinal functional and NMR assessment of upper limbs in Duchenne muscular dystrophy. *Neurology* **86,** 1022-1030, doi:10.1212/Wnl.0000000000002464 (2016).

39 Wary, C. *et al.* Quantitative NMRI and NMRS identify augmented disease progression after loss of ambulation in forearms of boys with Duchenne muscular dystrophy. *Nmr Biomed* **28**, 1150-1162, doi:10.1002/nbm.3352 (2015).

40 Wary, C. *et al.* Nuclear Magnetic Resonance imaging and spectroscopy provide quantitative indices of disease severity in forearms of boys with Duchenne Muscle Dystrophy. *Neuromuscular Disord* **23**, 810-810, doi:10.1016/j.nmd.2013.06.600 (2013).

41 Wary, C. *et al.* One year follow-up of Duchenne muscle dystrophy with nuclear magnetic resonance imaging and spectroscopy indices. *Neuromuscular Disord* **24**, 853-853, doi:10.1016/j.nmd.2014.06.201 (2014).

42 de Amorim e Silva, C. J., Mackenzie, A., Hallowell, L. M., Stewart, S. E. & Ditchfield, M. R. Practice MRI: reducing the need for sedation and general anaesthesia in children undergoing MRI. *Australas Radiol* **50**, 319-323, doi:10.1111/j.1440-1673.2006.01590.x (2006).

43 Azzabou, N., Loureiro de Sousa, P., Caldas, E. & Carlier, P. G. Validation of a generic approach to muscle water T2 determination at 3T in fat-infiltrated skeletal muscle. *J Magn Reson Imaging* **41**, 645-653, doi:10.1002/jmri.24613 (2015).

44 Janssen, B., Voet, N., Geurts, A., van Engelen, B. & Heerschap, A. Quantitative MRI reveals decelerated fatty infiltration in muscles of active FSHD patients. *Neurology* **86**, 1700-1707, doi:10.1212/WNL.0000000000002640 (2016).

45 Choi, S. J. *et al.* Intramyocellular Lipid and Impaired Myofiber Contraction in Normal Weight and Obese Older Adults. *J Gerontol A Biol Sci Med Sci* **71**, 557-564, doi:10.1093/gerona/glv169 (2016).

46 Son, J. W. *et al.* Low muscle mass and risk of type 2 diabetes in middle-aged and older adults: findings from the KoGES. *Diabetologia*, doi:10.1007/s00125-016-4196-9 (2017).

47 Reeder, S. B. *et al.* Quantification of hepatic steatosis with MRI: the effects of accurate fat spectral modeling. *J Magn Reson Imaging* **29**, 1332-1339, doi:10.1002/jmri.21751 (2009).

48 Dixon, W. T. Simple proton spectroscopic imaging. *Radiology* **153**, 189-194, doi:10.1148/radiology.153.1.6089263 (1984).

49 Glover, G. H. & Schneider, E. Three-point Dixon technique for true water/fat decomposition with Bo inhomogeneity correction. *Magn Reson Med* **18**, 371-383 (1991).

50 Kuroda, K., Oshio, K., Mulkern, R. V. & Jolesz, F. A. Optimization of chemical shift selective suppression of fat. *Magn Reson Med* **40**, 505-510 (1998).

51 Hernando, D., Kellman, P., Haldar, J. P. & Liang, Z. P. Robust water/fat separation in the presence of large field inhomogeneities using a graph cut algorithm. *Magn Reson Med* **63**, 79-90, doi:10.1002/mrm.22177 (2010).

52 Hu, H. H. *et al.* ISMRM workshop on fat-water separation: insights, applications and progress in MRI. *Magn Reson Med* **68**, 378-388, doi:10.1002/mrm.24369 (2012).

53 Liu, C. Y., McKenzie, C. A., Yu, H., Brittain, J. H. & Reeder, S. B. Fat quantification with IDEAL gradient echo imaging: correction of bias from T(1) and noise. *Magn Reson Med* **58**, 354-364, doi:10.1002/mrm.21301 (2007).

54 Bydder, M. *et al.* Relaxation effects in the quantification of fat using gradient echo imaging. *Magn Reson Imaging* **26**, 347-359, doi:10.1016/j.mri.2007.08.012 (2008).

55 Reeder, S. B. *et al.* Water-fat separation with IDEAL gradient-echo imaging. *J Magn Reson Imaging* **25**, 644-652, doi:10.1002/jmri.20831 (2007).

56 Wokke, B. H. *et al.* Comparison of dixon and T1-weighted MR methods to assess the degree of fat infiltration in duchenne muscular dystrophy patients. *J Magn Reson Imaging* **38**, 619-624, doi:10.1002/jmri.23998 (2013).

57 Yu, H. Z. *et al.* Multiecho Water-Fat Separation and Simultaneous R-2* Estimation With Multifrequency Fat Spectrum Modeling. *Magn Reson Med* **60**, 1122-1134, doi:10.1002/mrm.21737 (2008).

58 Loughran, T. *et al.* Improving Highly Accelerated Fat Fraction Measurements for Clinical Trials in Muscular Dystrophy: Origin and Quantitative Effect of R2*Changes. *Radiology* **275**, 570-578, doi:10.1148/radiol.14141191 (2015).

59 Araujo, E. C., Fromes, Y. & Carlier, P. G. New insights on human skeletal muscle tissue compartments revealed by in vivo t2 NMR relaxometry. *Biophys J* **106**, 2267-2274, doi:10.1016/j.bpj.2014.04.010 (2014).

60 McCully, K. & Posner, J. Measuring exercise-induced adaptations and injury with magnetic resonance spectroscopy. *Int J Sports Med* **13 Suppl 1**, S147-149, doi:10.1055/s-2007-1024621 (1992).

61 Damon, B. M. *et al.* Intracellular acidification and volume increases explain R(2) decreases in exercising muscle. *Magn Reson Med* **47**, 14-23 (2002).

62 Arpan, I. *et al.* Examination of effects of corticosteroids on skeletal muscles of boys with DMD using MRI and MRS. *Neurology* **83**, 974-980 (2014).

63 Willcocks, R. J. *et al.* Longitudinal measurements of MRI-T2 in boys with Duchenne muscular dystrophy: effects of age and disease progression. *Neuromuscul Disord* **24**, 393-401, doi:10.1016/j.nmd.2013.12.012 (2014).

64 Willcocks, R. J. *et al.* Magnetic resonance imaging and spectroscopy detect changes with age, corticosteroid treatment, and functional progression in DMD. *Neuromuscular Disord* **23**, 810-810, doi:10.1016/j.nmd.2013.06.599 (2013).

65 Fullerton, G. D., Cameron, I. L., Hunter, K. & Fullerton, H. J. Proton magnetic resonance relaxation behavior of whole muscle with fatty inclusions. *Radiology* **155**, 727-730, doi:10.1148/radiology.155.3.4001376 (1985).

66 Carlier, P. G. Global T2 versus water T2 in NMR imaging of fatty infiltrated muscles: Different methodology, different information and different implications. *Neuromuscular Disord* **24**, 390-392, doi:10.1016/j.nmd.2014.02.009 (2014).

67 Bley, T. A., Wieben, O., Francois, C. J., Brittain, J. H. & Reeder, S. B. Fat and water magnetic resonance imaging. *J Magn Reson Imaging* **31**, 4-18, doi:10.1002/jmri.21895 (2010).

68 Wokke, B. H. *et al.* T2 relaxation times are increased in Skeletal muscle of DMD but not BMD patients. *Muscle Nerve* **53**, 38-43, doi:10.1002/mus.24679 (2016).

69 Lebel, R. M. & Wilman, A. H. Transverse relaxometry with stimulated echo compensation. *Magn Reson Med* **64**, 1005-1014, doi:10.1002/mrm.22487 (2010).

70 Marty, B. *et al.* Simultaneous muscle water T2 and fat fraction mapping using transverse relaxometry with stimulated echo compensation. *Nmr Biomed* **29**, 431-443, doi:10.1002/nbm.3459 (2016).

71 Forbes, S. C. *et al.* Skeletal Muscles of Ambulant Children with Duchenne Muscular Dystrophy: Validation of Multicenter Study of Evaluation with MR Imaging and MR Spectroscopy. *Radiology* **269**, 198-207, doi:10.1148/radiol.13121948 (2013).

72 Stollberger, R. & Wach, P. Imaging of the active B1 field in vivo. *Magn Reson Med* **35**, 246-251 (1996).

73 Yarnykh, V. L. Actual flip-angle imaging in the pulsed steady state: a method for rapid three-dimensional mapping of the transmitted radiofrequency field. *Magn Reson Med* **57**, 192-200, doi:10.1002/mrm.21120 (2007).

74 Nehrke, K. & Bornert, P. DREAM--a novel approach for robust, ultrafast, multislice B(1) mapping. *Magn Reson Med* **68**, 1517-1526, doi:10.1002/mrm.24158 (2012).

75 Sacolick, L. I., Wiesinger, F., Hancu, I. & Vogel, M. W. B1 mapping by Bloch-Siegert shift. *Magn Reson Med* **63**, 1315-1322, doi:10.1002/mrm.22357 (2010).

76 Steidle, G. & Schick, F. Echoplanar diffusion tensor imaging of the lower leg musculature using eddy current nulled stimulated echo preparation. *Magn Reson Med* **55**, 541-548, doi:10.1002/mrm.20780 (2006).

77 Karampinos, D. C., Banerjee, S., King, K. F., Link, T. M. & Majumdar, S. Considerations in high-resolution skeletal muscle diffusion tensor imaging using single-shot echo planar imaging with stimulated-echo preparation and sensitivity encoding. *Nmr Biomed* **25**, 766-778, doi:10.1002/nbm.1791 (2012).

78 Basser, P. J. & Pierpaoli, C. Microstructural and physiological features of tissues elucidated by quantitative-diffusion-tensor MRI. *J Magn Reson B* **111**, 209-219 (1996).

79 Pierpaoli, C. & Basser, P. J. Toward a quantitative assessment of diffusion anisotropy. *Magn Reson Med* **36**, 893-906 (1996).

80 Damon, B. M. Effects of image noise in muscle diffusion tensor (DT)-MRI assessed using numerical simulations. *Magn Reson Med* **60**, 934-944, doi:10.1002/mrm.21707 (2008).

81 Damon, B. M., Ding, Z., Anderson, A. W., Freyer, A. S. & Gore, J. C. Validation of diffusion tensor MRI-based muscle fiber tracking. *Magn Reson Med* **48**, 97-104, doi:10.1002/mrm.10198 (2002).

82 Damon, B. M., Heemskerk, A. M. & Ding, Z. Polynomial fitting of DT-MRI fiber tracts allows accurate estimation of muscle architectural parameters. *Magn Reson Imaging* **30**, 589-600, doi:10.1016/j.mri.2012.02.003 (2012).

83 Zaraiskaya, T., Kumbhare, D. & Noseworthy, M. D. Diffusion tensor imaging in evaluation of human skeletal muscle injury. *J Magn Reson Imaging* **24**, 402-408, doi:10.1002/jmri.20651 (2006).

84 Qi, J., Olsen, N. J., Price, R. R., Winston, J. A. & Park, J. H. Diffusion-weighted imaging of inflammatory myopathies: polymyositis and dermatomyositis. *J Magn Reson Imaging* **27**, 212-217, doi:10.1002/jmri.21209 (2008).

85 Galban, C. J., Maderwald, S., Uffmann, K. & Ladd, M. E. A diffusion tensor imaging analysis of gender differences in water diffusivity within human skeletal muscle. *Nmr Biomed* **18**, 489-498, doi:10.1002/nbm.975 (2005).

86 Budzik, J. F. *et al.* In vivo MR tractography of thigh muscles using diffusion imaging: initial results. *Eur Radiol* **17**, 3079-3085, doi:10.1007/s00330-007-0713-z (2007).

87 Heemskerk, A. M. & Damon, B. M. Diffusion Tensor MRI Assessment of Skeletal Muscle Architecture. *Curr Med Imaging Rev* **3**, 152-160, doi:10.2174/157340507781386988 (2007).

88 Heemskerk, A. M., Strijkers, G. J., Drost, M. R., van Bochove, G. S. & Nicolay, K. Skeletal muscle degeneration and regeneration after femoral artery ligation in mice: monitoring with diffusion MR imaging. *Radiology* **243**, 413-421, doi:10.1148/radiol.2432060491 (2007).

89 Froeling, M., Nederveen, A. J., Nicolay, K. & Strijkers, G. J. DTI of human skeletal muscle: the effects of diffusion encoding parameters, signal-to-noise ratio and T2 on tensor indices and fiber tracts. *Nmr Biomed* **26**, 1339-1352, doi:10.1002/nbm.2959 (2013).

90 Froeling, M. *et al.* Muscle changes detected with diffusion-tensor imaging after long-distance running. *Radiology* **274**, 548-562, doi:10.1148/radiol.14140702 (2015).

91 Froeling, M. *et al.* Reproducibility of diffusion tensor imaging in human forearm muscles at 3.0 T in a clinical setting. *Magn Reson Med* **64**, 1182-1190, doi:10.1002/mrm.22477 (2010).

92 Oudeman, J. *et al.* Techniques and applications of skeletal muscle diffusion tensor imaging: A review. *J Magn Reson Imaging* **43**, 773-788, doi:10.1002/jmri.25016 (2016).

93 Schlaffke, L. *et al.* Diffusion tensor imaging of the human calf: Variation of inter- and intramuscle-specific diffusion parameters. *J Magn Reson Imaging*, doi:10.1002/jmri.25650 (2017).

94 Scheel, M. *et al.* Diffusion tensor imaging of skeletal muscle--correlation of fractional anisotropy to muscle power. *Rofo* **185**, 857-861, doi:10.1055/s-0033-1335911 (2013).

95 Sinha, S., Sinha, U. & Edgerton, V. R. In vivo diffusion tensor imaging of the human calf muscle. *J Magn Reson Imaging* **24**, 182-190, doi:10.1002/jmri.20593 (2006).

96 Williams, S. E. *et al.* Quantitative effects of inclusion of fat on muscle diffusion tensor MRI measurements. *J Magn Reson Imaging* **38**, 1292-1297, doi:10.1002/jmri.24045 (2013).

97 Hernando, D. *et al.* Removal of olefinic fat chemical shift artifact in diffusion MRI. *Magn Reson Med* **65**, 692-701, doi:10.1002/mrm.22670 (2011).

98 Burakiewicz, J. *et al.* Improved olefinic fat suppression in skeletal muscle DTI using a magnitude-based dixon method. *Magn Reson Med*, doi:10.1002/mrm.26655 (2017).

99 Taylor, D. J., Bore, P. J., Styles, P., Gadian, D. G. & Radda, G. K. Bioenergetics of intact human muscle. A 31P nuclear magnetic resonance study. *Mol Biol Med* **1**, 77-94 (1983).

100 Prompers, J. J. *et al.* Dynamic MRS and MRI of skeletal muscle function and biomechanics. *Nmr Biomed* **19,** 927-953, doi:10.1002/nbm.1095 (2006).
101 Meyerspeer, M. *et al.* Direct noninvasive quantification of lactate and high energy phosphates simultaneously in exercising human skeletal muscle by localized magnetic resonance spectroscopy. *Magn Reson Med* **57,** 654-660, doi:10.1002/mrm.21188 (2007).
102 Vandenborne, K. *et al.* Metabolic heterogeneity in human calf muscle during maximal exercise. *Proc Natl Acad Sci U S A* **88,** 5714-5718 (1991).
103 Bogner, W. *et al.* Assessment of (31)P Relaxation Times in the Human Calf Muscle: A Comparison between 3 T and 7 T In Vivo. *Magn Reson Med* **62,** 574-582, doi:10.1002/mrm.22057 (2009).
104 Parasoglou, P., Feng, L., Xia, D., Otazo, R. & Regatte, R. R. Rapid 3D-imaging of phosphocreatine recovery kinetics in the human lower leg muscles with compressed sensing. *Magn Reson Med* **68,** 1738-1746, doi:10.1002/mrm.24484 (2012).

1

2

Chapter 2

Evaluation of skeletal muscle DTI in patients with Duchenne Muscular Dystrophy

M.T. Hooijmans, B.M. Damon, M. Froeling, M.J. Versluis, J. Burakiewicz, J.J.G.M Verschuuren, A.G. Webb, E.H. Niks, H.E. Kan

NMR Biomed. 2015 Nov;28(11):1589-97.

Abstract

Diffusion tensor imaging (DTI) is a popular method to assess differences in fiber organization in diseased and healthy muscle tissue. Previous work has shown that muscle DTI measurements depend on signal-to-noise ratio (SNR), %fat, and tissue T_2. The goal of this study was to evaluate the potential biasing effects of these factors on skeletal muscle DTI data in patients with Duchenne Muscular Dystrophy (DMD). MR images were obtained of the right lower leg of 21 DMD patients and 12 healthy controls on a Philips 3T system. DTI measurements were combined with quantitative *in-vivo* measures of mean water T_2, %fat and SNR to evaluate their effect on DTI parameter estimation. All outcome measures were determined within ROIs drawn for six lower leg muscles. Between group analysis, using all ROIs, revealed a significantly elevated FA in the GCL, SOL and PER muscles ($p<0.05$) and an increased mean diffusivity ($p<0.05$) and λ_3 ($p<0.05$) in the TA muscle of DMD patients. *In-vivo* evaluation of the individual confounders showed behaviour in line with predictions from previous simulation work. To account for these confounders, subsequent analysis used only ROIs with SNR greater than 20. With this criterion we found significantly greater MD in the TA muscle of DMD patient ($p<0.009$) and λ_3 in the TA and GCL muscles ($p<0.001$) of DMD patients, but no differences in FA. As both increased %fat and lower SNR are expected to reduce the apparent MD and λ_3, these between-group differences are likely due to pathophysiology. However, the increased FA, observed when using all ROIs, likely reflects the effect of low SNR and %fat on the DTI parameter estimation. These findings suggest that measuring mean water T_2, %fat and SNR is essential to ascribe changes in DTI measures to intrinsic diffusion changes or to confounding influences.

Introduction

Spin-echo-based diffusion tensor imaging (DTI) is an intrinsically T_2-weighted method to measure the apparent diffusion of water molecules in tissue. Water diffusion can be hindered by structures such as mitochondria, sarcoplasmic reticulum, macromolecules and the cell membrane. [1] DTI is commonly used as a non-invasive and quantitative method to assess fiber organization in healthy, diseased and damaged skeletal muscle. [2-8] Changes in DTI parameters have been observed with respect to age, gender, injury, disease and exercise, as well as between individual muscles, showing the potential of DTI as a measure for overall muscle quality. [9-15] DTI has also been used to assess changes in fiber type distributions, to monitor muscle recovery after marathon running, and to discriminate between different phases of the recovery after artery ligation. [16-19] As DTI is a quantitative technique, high quality data are necessary to obtain reliable estimates of DTI based parameters. Even in healthy muscle tissue it is challenging to achieve high signal-to-noise-ratio (SNR) due to the tissue's short T_2, long T_1, and a relatively high diffusivity of water. Recently, several simulation studies have shown that the reliability of estimating DTI parameters is substantially affected by the SNR, water T_2 value, and percentage fat composition (%fat). [20-22] These simulation studies predicted that low SNR data result in an overestimation of fractional anisotropy (FA) and an underestimation of the three eigenvalues (λ_1, λ_2, λ_3) and mean diffusivity (MD). [20, 22] Increases in T_2, often associated with muscle damage, may indirectly affect the diffusion parameters due to the associated increase in SNR. [20, 22] In addition, the increases in fat % associated with age and pathology may alter the diffusion parameters due to increased partial volume effects. [20, 22] DMD is an X-linked disease caused by a mutation in the dystrophin gene, and is characterized by progressive muscle weakness and muscle damage. [23] In many muscular dystrophies, muscles show structural changes such as fat infiltration and fibrosis that increase with age, as well as oedema and/or inflammatory processes which increase the mean water T_2. As a result, true differences in DTI measurements in this population may be obscured by MR confounders such as increased fat fraction and increased T_2. [24-26] The majority of previous skeletal muscle DTI studies have focused on its properties as a non-invasive and quantitative method to assess differences in microstructural organization and on performing fiber tractography. However, the potential role that confounders such as SNR, %fat and water T_2 values could have on the detected differences in DTI parameters in healthy and diseased muscle has not been addressed experimentally in patients with a muscle disease. The overall purpose of this study was to acquire skeletal muscle DTI measurements in patients with DMD and healthy controls, combined with measurements to assess mean water T_2, %fat and SNR for an in–vivo

evaluation of their effect on the DTI measurements. Furthermore, DTI was used as a non-invasive and quantitative method to assess changes in DTI parameters between these groups. Finally, the feasibility of ascribing these changes to pathology or confounding effects using multi-parametric MRI was assessed. As such we obtained data in a group of DMD patients and age-matched healthy controls and looked at the differences in DTI parameters between groups.

Methods

Study population

Twenty-one DMD patients (9.5± 3.1 yrs; range, 5-16 yrs) and 12 age-matched healthy controls (9.7± 2.9 yrs, range: 5-14 yrs) participated in the study. The DMD patients were recruited from the Dutch Dystrophinopathy Database, while the controls were recruited from local schools. The diagnosis DMD was confirmed by a mutation in the DMD gene and lack of dystrophin expression in the muscle biopsy. Of the 21 DMD patients, 8 were wheelchair bound, 13 were fully ambulant and all boys used corticosteroids. The study was approved by the local medical ethics committee. All participants or their legal representatives signed informed consent.

MR examination

MR datasets of the right lower leg were acquired on a 3T MR scanner (Ingenia, Philips, Best, Netherlands) with a 16-element anterior body receive coil. Patients were positioned in a feet-first supine position in the scanner. The total duration of the scan was 25 minutes and contained:

(i) a SE-EPI DTI sequence to obtain DTI parameters (TR/TE 2990/49 ms; number of signal averages (NSA) 6; number of gradient directions 16; b-value 0,450 s/mm2; voxel size 2x2x6 mm; 12 contiguous slices; half scan 0.7; SENSE factor in RL direction; spectrally adiabatic inversion recovery (SPAIR) and slice-selection gradient reversal (SSGR) fat suppression on the aliphatic fat peak with spectrally selective suppression of the olefinic fat peak; [21]

(ii) SE-EPI without diffusion weighting to determine the SNR (TR/TE 3020/49 ms; NSA 6; b-value 0 s/mm2; voxel size 2x2x6 mm; 12 contiguous slices; 10 dynamics, SPAIR and SSGR fat suppression on the aliphatic fat and selective suppression of the olefinic fat peak) [21];

(iii) TSE T_1-weighted images for anatomical reference (TR/TE 630/30ms; voxel size 1.5x1.5x6 mm; no gap, 12 slices),

(iv) Three point Dixon images to determine the amount of fat infiltration

(TR/TE/ΔTE 210/4.41/0.76 ms; NSA 2; flip angle 8°; voxel size 1x1x10 mm; slice gap 5 mm; 23 slices)

(v) Multi turbo spin echo sequence to measure the water T_2 relaxation time (17 echoes; TR/TE/ΔTE 3000/8/8 ms; refocussing angle 180°;voxel size 1.4x1.8x10 mm; slice gap 20 mm;; 5 slices, no fat suppression).

Data-analysis

DTI-analysis was performed using a custom-built toolbox in Mathematica. [5, 27] Data were de-noised, registered and corrected for eddy currents before the tensor calculation and estimation of the individual eigenvalues (λ_1, λ_2, λ_3), mean diffusivity (MD) and the fractional anisotropy (FA). A Weighted-Linear-Least-Squares (WLLS) method was used for tensor calculation and MD and FA were determined with standard equations using these eigenvalues. A separate SE-EPI sequence with 10 dynamics was used to assess the SNR, which was defined as the mean signal over the 10 dynamics divided by the standard deviation over the same 10 dynamics. The SNR was determined per pixel and presented as a mean of all pixels within a region of interest (ROI), as described below. The determination of the water T_2-relaxation times used a tri-exponential fitting routine written in MATLAB based on a previously described method. [28] Quantitative fat fractions were calculated as signal intensity (SI) fat/ (SI fat+ SI water))*100 from the 3-point Dixon images. Fat and water images were generated using a multi-peak model based on a six fat peak spectrum. Values were not corrected for T_2* relaxation effects. Even though the relaxation between the echoes is small in tissues with no significant iron concentrations, this could have resulted in a small overestimation of fat fractions in the low fat ranges. [29] Subsequently, the sequence was optimized with respect to TR and flip angle to minimize T_1 relaxation effects. ROIs were manually drawn for the 3P-Dixon, MSE and the T_1-weighted sequence, using Medical Image Processing, Analysis and Visualization (MIPAV) software (http://mipav.cit.nih.gov) for six individual lower leg muscles: the lateral head of the gastrocnemius (GL), medial head of the gastrocnemius (GM), soleus (SOL), tibialis anterior (TA), peronei (PER) and the tibialis posterior (TP) muscles (Figure 1f). Boundaries of the ROIs were identified to always fall within a muscle in order to avoid contamination of subcutaneous fat and fatty septa between muscles. The ROIs from the T_1-weighted images were used for anatomical reference in the DTI and SNR assessments. All outcome measures are reported as a mean value of all pixels within a ROI over multiple slices. Because of sequence-specific differences in slice thickness, the number of slices used in the analysis varied between sequences. However, all sequences covered the same volume of tissue as the DTI sequence.

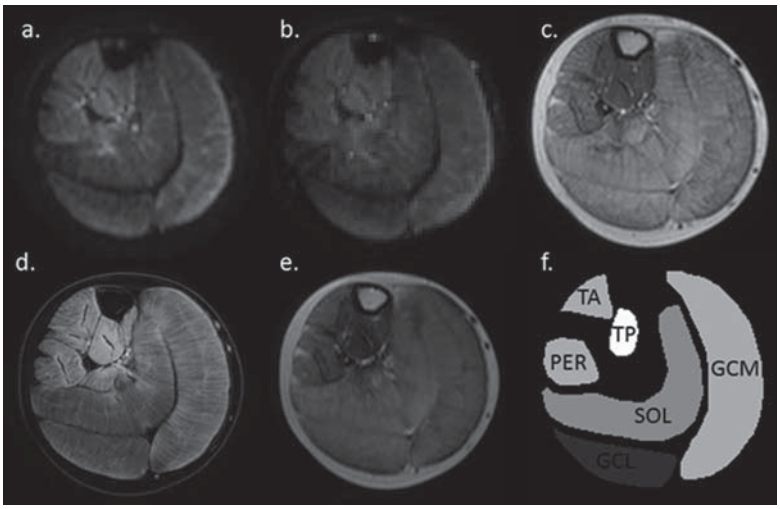

Figure 1. Axial multi-parametric images of the lower leg of a DMD patient: a fat-suppressed diffusion weighted SE-EPI image (b-value of 450 mm/s2) (a); a fat-suppressed SE-EPI image without diffusion weighting (b); T_1-weighted image; (c) a 3-point Dixon water image; (d) the 7th echo of a multi-spin-echo image (TE: 56 ms); (e) and a representation of the masks created for the 6 lower leg muscles - medial and lateral head of gastrocnemius (GM, GL), soleus (SOL), anterior tibialis (TA), peroneus (PER) and posterior tibialis (TP)) (f). Note the complete suppression of the fat signal in (a) and (b), resulting from the use of the combined fat suppression method.

Simulations

Simulations were performed according to Froeling *et al.* and Damon *et al.*. For the simulations the parameters were set identical to the MRI experiments (TE = 49 ms, TR = 2990 ms, 16 gradient directions and b = 450 s/mm2). The fat compartment was simulated using T_2 = 80/550 ms with a ratio of 2:1, T_1 = 300 ms, proton density ρ = 0.1 and MD = 0.6 mm2/2 and FA=0. For the muscle compartment T_2 = 37 ms (the mean of all muscles), T_1 = 1200 ms and ρ = 0.8 were used. Two simulation experiments were performed: simulation 1 - diffusion parameters as a function of SNR, simulation 2 – diffusion parameters as a function of the fat fraction. The muscle diffusion properties were set to values estimated from the normal distribution given by all muscles of healthy subjects with an SNR > 25 and from all muscles of Duchene patients with a fat fraction < 10%, for simulation 1 and 2 respectively. The fat fractions and the SNR was also estimated form the same subsets for each simulation. For each SNR value, ranging from 1 to 55 with steps of 2, and for each fat fraction, ranging from 0 to 60 % with steps of 2 %, 5000 virtual subjects were simulated by generating a noisy diffusion signal using randomly selected values using the previously determined normal distributions of the diffusion properties, SNR and fat fraction using,

$$S(\rho, T_1, T_2, TR, TE) = \rho \cdot (1 - e^{-TR/T_1}) \cdot e^{-TE/T_2}, \text{ and}$$

$$S(b, \vec{g}) = f \cdot S_{fat}(\rho_{fat}, T_{1,fat}, T_{2,fat}, TR, TE) \cdot e^{-b\vec{g}\boldsymbol{D}_{fat}\vec{g}^T} + (1 - f) \cdot S_{mus}(\rho_{mus}, T_{1,mus}, T_{2,mus}, TR, TE) \cdot e^{-b\vec{g}\boldsymbol{D}_{mus}\vec{g}^T} + \varepsilon$$

where $S(b, \vec{g})$ is the noisy diffusion signal for b-value b and gradient direction $\vec{g}$, f is the fat fraction, ρ the proton density, $T_1$and T_2 the longitudinal and transvers magnetization, ε the Rician noise signal and $\boldsymbol{D}_{fat}$ and $\boldsymbol{D}_{mus}$the diffusion tensors for fat and muscle respectively. The simulated signal was then used to calculate the distribution of diffusion parameters as a function of SNR and fat.

Statistical Analysis

The Pearson correlation coefficient was used to evaluate the correlation between SNR, %fat and muscle T_2 value and the estimation of the individual DTI parameters. The evaluation of SNR involved datasets of healthy controls only. The evaluation of the effect of %fat on the DTI estimation involved data-sets of DMD patients with an SNR>20 only, so as to evaluate better the separate effects of SNR and %fat. To determine the effect of mean water T_2 on the DTI parameters and SNR, datasets of both groups were evaluated individually, as DMD patients are known to have an elevated T_2. A general linear model was used to assess differences in DTI-parameters and mean water T_2 between patients with DMD and healthy controls. The water T_2 was included as a covariate for the DTI parameters and a Fischer least significant difference (LSD) model was used to correct for multiple comparisons. The between-group analysis was performed twice, once with only datasets with an SNR>20 and once with all data-sets taking into account the effect of confounders. The significance level was set at $p<0.05$. All statistical analyses were performed using SPSS version 20 for Windows (SPSS Inc., Chicago).

Results

All scans were successfully performed in DMD patients and healthy controls. Example multi-contrast images are illustrated in Figure 1.

The effect of SNR

Mean SNR values averaged over all muscles were 27.9±9.8 in healthy controls (HC) and 20.9± 9.7 in DMD patients. The associations between DTI parameters and SNR are visualized in Figure 2(A-E). In the low SNR ranges, MD and the eigenvalues are underestimated and FA is overestimated. Values of FA ($r=-0.35$, $p<0.001$), λ_1 ($r=-0.52$, $p<0.001$) and λ_2 ($r=-0.28$, $p<0.049$) were negatively correlated with SNR; no significant correlation was observed for λ_3. For the majority of the DTI-parameters stabilization of the values occurred at SNR levels above 20. Eliminating data points below this threshold would result in exclusion of 18% (13/72) of the total healthy control ROI's and an exclusion of 47% (93/198) of the total ROIs. Twelve of the excluded HC ROIs belonged to two subjects. However, it should also be noted that correlations between MD ($r=-0.38$, $p=0.029$), λ_1 ($r=-0.54$, $p<0.0001$) and λ_2 ($r=-0.19$, $p=0.0175$) and SNR remained even when ROIs with an SNR<20 were excluded. Furthermore, similar behaviour is visualized with the simulation experiment, describing the diffusion parameters as a function of SNR, in which almost all *in-vivo* obtained data points fall within one standard deviation of the simulated signal, see Figure 2(A-E).

The effect of fat fraction

The mean %fat of all lower leg muscles was 17.4% ± 14.4% in DMD patients and 4.3% ± 0.8% in healthy controls. Only datasets of DMD patients with an SNR above 20 were included in this part of the analysis, as healthy controls normally do not show fat infiltration. All data points are visualized in Figure 3 (A-E) and show a decrease as was also seen in the simulation experiment, except for the FA which tends to show the opposite behaviour (Fig. 3 A-E). Significant negative correlations were observed for MD ($r=-0.26$, $p=0.04$) and λ_3 ($r=-0.34$, $p=0.02$) and no correlations were present for FA, λ_1 and λ_2 in the *in-vivo* data.

The effect of mean water T_2 relaxation times

In all lower leg muscle, the mean water T_2 was significantly greater in the DMD patients than in the healthy controls ($p<0.001$). Mean water T_2 values, averaged over all the muscles, were 39.5±0.6ms for DMD patients and 35.1±0.5ms for healthy controls. Correlations between mean water T_2 and the DTI parameters were assessed per group individually. For both groups no correlations were observed between the mean water T_2 and the individual DTI-parameters (Figures 4A-E). Additionally,

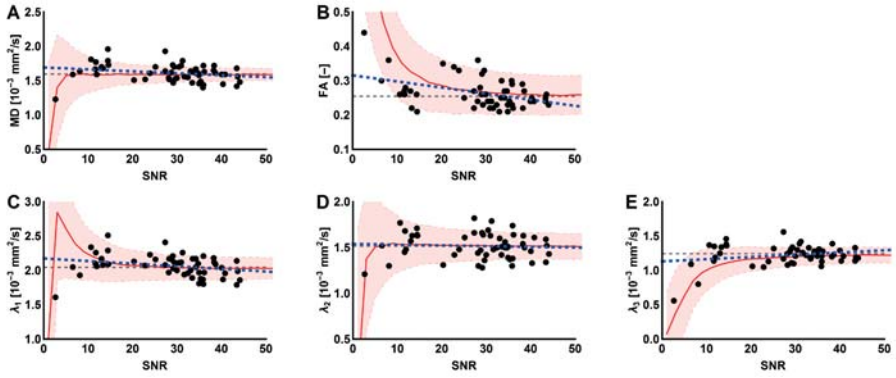

Figure 2. Representation of the confounding effect of SNR. The individual DTI parameters are plotted against the SNR. (A-E) Each dot represents an individual muscle of a healthy control subject (black) with the corresponding fit (blue dashed line). Stabilization starts to occur in the higher SNR ranges and seems to vary between DTI parameters. In the background of the graph, the mean (red line) and standard deviation (shaded area) are shown of the DTI parameters as a function of SNR derived from the simulation experiment using WLLS. The grey dashed line indicates the true values used as input for the simulations. Clearly visible in the low SNR ranges are an overestimation of FA and an underestimation of MD and the eigenvalues.

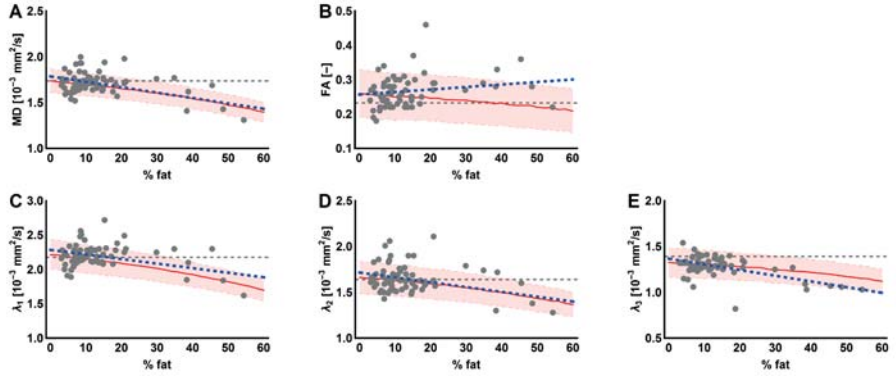

Figure 3. Visualization of the confounding effect of infiltration of adipose tissue on the DTI parameter estimation. The individual DTI parameters are plotted against the fat fraction (%). (A-E) Each dot represents an individual muscle of a DMD patient (grey) with the corresponding fit (blue dashed line). In the background of the graph, the mean (red line) and standard deviation (shaded area) are shown of the DTI parameters as a function of %fat derived from the simulation experiment using WLLS. The grey dashed line indicates the true values used as input for the simulation experiment.

	Only ROIs with a SNR>20		All ROIs	
	DMD	**Controls**	**DMD**	**Controls**
GL	N = 4	N=9	N=16	N =12
λ_1	1.95±0.08	2.01±0.04	1.93±0.07	2.13±0.08
λ_2	1.42±0.07	1.51±0.04	1.50±0.06	1.53±0.07
λ_3	1.31±0.03*(p<0.001)	1.15±0.02	1.13±0.05	1.08±0.05
MD	1.54±0.06	1.56±0.03	1.58±0.05	1.51±0.05
FA	0.25±0.02	0.26±0.01	0.33±0.02*(p=0.04)	0.25±0.02
GM	N=7	N=10	N=16	N =12
λ_1	1.98±0.05	2.07±0.04	2.1±0.06	2.00±0.07
λ_2	1.50±0.04	1.46±0.04	1.49±0.03	1.46±0.04
λ_3	1.28±0.04	1.25±0.04	1.21±0.03	1.23±0.03
MD	1.56±0.05	1.61±0.04	1.60±0.04	1.57±0.04
FA	0.26±0.01	0.24±0.01	0.26±0.01	0.26±0.01
SOL	N=8	N=10	N=16	N =12
λ_1	2.23±0.05	1.99±0.07	2.06±0.05	2.14±0.06
λ_2	1.70±0.05	1.59±0.05	1.69±0.04	1.60±0.05
λ_3	1.31±0.04	1.32±0.03	1.28±0.03	1.32±0.04
MD	1.72±0.05	1.64±0.04	1.65±0.04	1.73±0.05
FA	0.24±0.01	0.22±0.01	0.25±0.01*(p=0.006)	0.22±0.01
TA	N=10	N=10	N=14	N =12
λ_1	2.30±0.05	2.19±0.05	2.31±0.04	2.22±0.04
λ_2	1.66±0.04	1.54±0.04	1.65±0.03	1.56±0.04
λ_3	1.33±0.03*(p<0.007)	1.17±0.03	1.31±0.03*(p=0.024)	1.2±0.03
MD	1.78±0.04*(p<0.009)	1.61±0.04	1.77±0.03*(p=0.020)	1.64±0.03
FA	0.27±0.02	0.32±0.01	0.29±0.01	0.31±0.01
PER	N=5	N=9	N=14	N =12
λ_1	2.18±0.08	2.18±0.06	2.27±0.06	2.19±0.07
λ_2	1.60±0.06	1.59±0.05	1.69±0.05	1.61±0.05
λ_3	1.25±0.05	1.23±0.04	1.12±0.04	1.22±0.05
MD	1.69±0.08	1.66±0.05	1.71±0.04	1.69±0.04
FA	0.27±0.02	0.29±0.02	0.33±0.02*(p=0.049)	0.29±0.02
TP	N=12	N=10	N=14	N =12
λ_1	2.18±0.05	2.18±0.06	2.31±0.04	2.25±0.05
λ_2	1.67±0.04	1.66±0.04	1.7±0.04	1.68±0.04
λ_3	1.35±0.03	1.36±0.03	1.38±0.03	1.37±0.03
MD	1.75±0.03	1.74±0.03	1.79±0.04	1.75±0.05
FA	0.23±0.01	0.28±0.02	0.26±0.01	0.25±0.01

Table 1. Mean values ±SD for the different DTI parameters (FA: fractional anisotropy, MD: mean diffusivity and the eigenvalues (λ_1, λ_2, and λ_3)) using all ROIs and using only ROIs with a SNR>20 in healthy controls and DMD patients of the investigated muscles (medial and lateral head of gastrocnemius (GM, GL), soleus (Sol), anterior tibialis (TA), peroneus (PER) and posterior tibialis (TP)). Significant differences between patients and controls are marked with an asterisk (*).

the correlation between mean water T_2 and SNR was assessed and no significant correlations were found.

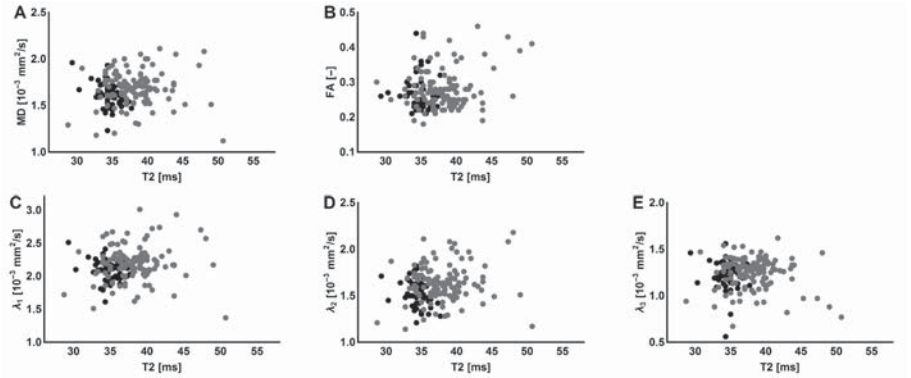

Figure 4. The effect of T_2 changes on the DTI parameter estimation. The individual DTI parameters are plotted against the mean water T_2 values. (A-E) Each dot represents an individual muscle of a DMD patient (grey) or a healthy control subject (black). The small but significant increased mean water T_2 values in DMD patients seem to have a negligible effect on the DTI parameter estimation.

Assessing differences in DTI parameters between groups

Including all ROIs:

Table 1 lists the mean diffusion values per muscle of the DMD patients and healthy controls using all ROIs. Between-group analysis without data selection based on the confounders showed a significant increase in MD (p=0.020, Fig. 5A) and λ_3 (p=0.024) in the TA muscle for DMD patients compared to healthy controls. Also, a significant increase in FA was found in the GL (p=0.04), SOL(p=0.006) and PER (p=0.049) muscles (Fig. 5C, Table. 1). No significant changes in λ_1 and λ_2 were observed between groups.

Including ROIs with SNR>20:

Mean and standard deviations of the DTI parameters per muscle of the DMD patients and healthy controls using only ROIs with SNR>20 are shown in table 1. Taking only ROIs with an SNR>20, a total of 47% (93/198) of the ROIs were excluded from the between-group analysis. Group comparison now showed a significantly increased MD in the TA muscle (p<0.009)(Fig. 5B) together with a significantly higher λ_3 in the GL (p<0.001) and TA muscle (p<0.007) for DMD patients compared to healthy controls (Fig. 5B). No significant changes between groups were detected in λ_1 and λ_2 (Table. 1). These results are in accordance with the group analysis using all images.

However, in contrast to the previous group analysis, no significant changes were detected for FA. Although not significantly different, some trends were observed towards a lower FA in the TA (p=0.059) and TP muscle (p=0.058, Fig. 5D), increased λ_2 in the TA muscle (p=0.063) and an increased λ_1 in the SOL muscle (p=0.084) of DMD patients.

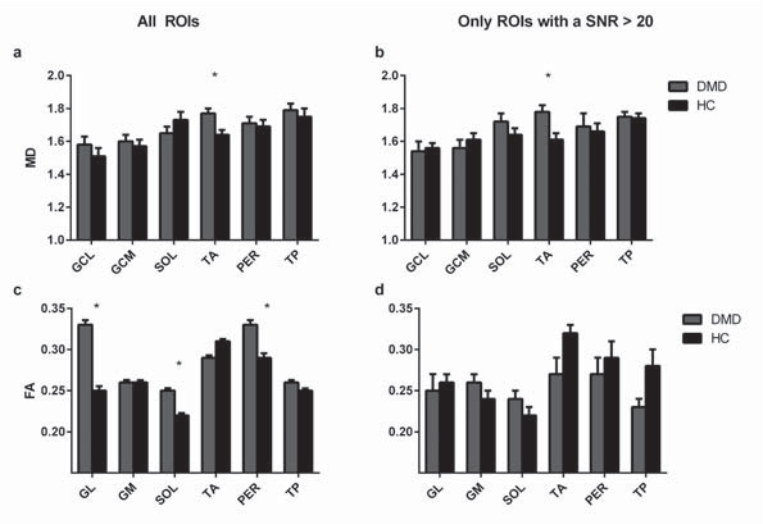

Figure 5. Mean values ±SD of the Mean Diffusivity (A,B) and Fractional Anisotropy (C,D) using all ROIs and using only ROIs with a SNR>20 of the investigated muscles in DMD patients (grey) versus healthy control subjects (black). Muscles with values which were significantly different are marked with an asterisk (*). Remarkable is the increased FA in some of the muscles of the DMD patients using all ROIs (C), which is probably an artificial finding, since the effect disappears when low SNR data is rejected (D). (GM = medial head of gastrocnemius, GL = lateral head of the gastrocnemius, SOL = soleus, TA = anterior tibialis, PER = peroneus and TP = posterior tibialis).

Discussion

In this study we evaluated the effect of individual confounders on the DTI-parameter estimation in patients with DMD and healthy controls. In line with the conclusions of previous simulation-based works [20-22], both SNR and %fat influenced DTI-parameter estimation. In contrast, the significantly elevated mean water T_2 had no effect on the DTI parameter estimation in patients with DMD. When all data-sets were included in the between-group analysis, there were between-group differences in more individual DTI parameters (FA, MD and λ_3) than when only datasets with sufficient SNR (SNR>20) were used (MD and λ_3). Because the number of statistically significant findings is reduced when low SNR data are eliminated, at least some of the between-group differences in DTI parameters are most likely to have been caused by confounding factors. Overall, these findings support the conclusion that

distinguishing between the causes of changes in DTI measures in skeletal muscle requires in vivo measurements of SNR, mean water T_2 and % fat.

SNR as a confounding parameter

The stabilization effect visualized in our distributions in the high SNR ranges, together with the overestimation of FA and the underestimation of MD and the eigenvalues in the low SNR ranges, are in line with our simulation experiment as well as with previous work. [20, 22] In a low SNR condition, an erroneously elevated measurement of anisotropy can occur even in highly isotropic structures. This previously reported phenomenon underlies the behaviour visible in the distributions of the DTI-parameters plotted against SNR. [30] In addition, our data showed significant negative correlations between MD, λ_1 and λ_3 and SNR when data points with an SNR>20 were considered, suggesting a minor influence of SNR even in the higher SNR ranges. This observation is consistent with predictions that for muscle-only regions of interest, an SNR of 20-25 is needed for 5% accuracy in DTI parameter estimation and the required SNR level varies between DTI measures. [20, 22] A feature of Figures 2a-e is the high variation in SNR levels between the various data-points. The low SNR data are localized in particular subjects and could have been caused by movement during scanning, B_0 shifts, and/or less available signal resulting from smaller patient size or higher fat infiltration. Overall these data support the conclusion that SNR, alone or in concert with one of these factors affecting it, influence DTI measurements in skeletal muscle. Since reaching sufficient SNR is already challenging in muscle DTI in healthy controls, this will be even more the case in paediatric populations and patients (who may be more prone to discomfort during imaging or pathological factors such as fat infiltration).

% fat as a confounding parameter

As the influence of fat infiltration and the effect of SNR on the DTI parameter estimation are interrelated, only datasets with SNR greater than 20 are used for this part of the analyses. Significant negative correlations were observed between %fat and MD, and λ_3. As %fat increases with age in patients with DMD, it could be that these correlations are partly reflecting intrinsic diffusion changes occurring with progression of the disease. However, in previous work it has been shown that with the presence of fat tissue, even without any other physiological effect present, causes MD and the eigenvalues to be underestimated and FA to be overestimated. [21, 22] These results are in agreement with our work as well as with the simulation experiment and suggest that the correlations observed here are most likely due to the confounding effect of %fat. However, as the observed correlations are weak and involve a majority of data points from low %fat values, the specific role that %fat has on the DTI measurements in patients with DMD remains unclear.

T2 as a confounding parameter

Despite the significantly increased mean water T_2 found in all the lower leg muscles of the DMD patients compared to healthy controls, we showed no dependence of DTI parameters on water T_2 changes. Taken by itself the increased water T_2 in patients by ~5 ms would increase the SNR by ~15%. However, due to the DMD pathology, this is accompanied by an increase in fat fraction (~20%), which in turn reduces the SNR. Taken combined, this results in no statistical correlation between increased T_2 and SNR, and consequently no correlation with DTI-parameter estimation in patients with DMD. In addition, simulation work has shown that much larger increases in mean water T_2 were necessary to show an effect on the estimation of the DTI measures.[20]

Between-Group Differences Determined by using all ROIs

Without taking into account any of the previously addressed confounders, between-group analysis showed a significantly elevated MD and λ_3 in the TA muscle and elevated mean FA values in the GL, SOL and PER muscles. These apparent differences in DTI parameters between groups could have multiple explanations. First, they could have resulted from changes in the intrinsic diffusion properties of muscle water due to pathology. Second, they could be due to the presence of confounding effects on the DTI measurements. As both low SNR and high %fat datasets are included in this part of the group analysis, it is most likely that the apparent increases in FA simply reflect low SNR, rather than changes in muscle microstructure. This conclusion is supported by previous experimental work that showed that FA is artificially increased in regions with significant fat-muscle partial volume artefacts. [21] However, the significantly increased MD and λ_3 in the TA muscle and the lack of any significant changes in MD or the eigenvalues in the other muscles are inconsistent with the effects predicted by low SNR and high fat levels. [2, 9, 31] One possible explanation for these elevated diffusivities in the TA is that the effect of pathology may be much stronger than the potential effect of confounders. Second, it might be that the estimation of MD and the eigenvalues – particularly when using WLLS for tensor estimation – is slightly less sensitive to the influence of noise. This is consistent with the prediction of simulation-based work. [20] Finally, it could be that MD and the eigenvalues are only affected in the higher fat fractions and that this DMD cohort did not contain many patients with highly fat infiltrated muscles.

Between-Group Differences Determined by using only ROIs with SNR>20

After accounting for SNR as a confounding effect, using only datasets with a SNR cut-off above 20, micro-structural changes are observed between groups. A significant increase in MD in the TA and increases in λ_3 in the TA and GL muscle of DMD patients were found. In contrast to the observations in the between-group

analysis using all datasets, no significant increases in FA were detected between groups when correcting for low SNR. As this between-group analysis is based on a smaller number of subjects than the analysis using all ROIs, this could have resulted in not finding changes in FA. This is in accordance with mouse skeletal muscle work where increases in MD and λ_3 have been reported as an immediate response to muscle injury. [17] At the same time, the observed trend for a decrease in FA combined with the increase in MD in the TA muscle is in agreement with common changes associated with muscle injury and damage. [2, 4, 17, 32, 33] However, as a consequence of not fully correcting for confounders it could be that both %fat and SNR have had a potential effect on the DTI parameter estimation. As the effect of both confounders would result in an underestimation of MD and λ_3, it is likely that the observed changes in these DTI measures, in both between group analysis, are due to changes in the intrinsic diffusion rather than due to confounding effects. Therefore, the increased MD and λ_3 in the TA muscle is most likely reflecting the pathophysiology in patients with DMD.

Previous studies

Besides the agreements found with clinical applications in diseased and damaged human skeletal muscle, there is to our knowledge one other clinical study which focused on skeletal muscle DTI in patients with DMD; that study reported a significantly increased FA and decreased MD with disease progression. [9, 31] These observations are to some extent in line with the results from our group analysis using all ROIs, to be precise with the detected significant increased FA in several muscles, which is likely caused by confounders, as both %fat and low SNR result in an overestimation of FA: no corrections for the confounding effects of SNR, %fat or T_2 changes were made.

Limitations

A few potential limitations of the study should be acknowledged. First of all, no distinction has been made between the six individual muscles during the evaluation of confounding effects on the DTI parameter estimation. All evaluations are based on the assumption that variations in DTI parameters between muscles are negligible. [34] As previous studies have shown that the variations between muscles are minor compared to the changes detected due to confounding effects, we assume that these small variations between muscles will be outweighed by the larger effects of SNR, % fat and T_2 changes. [34] Secondly, as mentioned before a large amount of data has been excluded to retain quality for the between-group analysis using only ROIs with SNR>20. This could potentially have resulted in not finding any differences in some of the DTI measures between the groups. A larger number of

subjects, combined with an even further optimized DTI protocol, will be advisable for future work. Lastly, the tri-exponential T_2 fitting method has not yet been shown to produce equivalent water T_2 estimates to fat-suppressed T_2 methods. In using this method, we are assuming that the effects of the confounding parameters on the DTI estimates are greater than any error or variability produced by using the tri-exponential fitting approach.

Conclusion

In conclusion, experimental evaluation of the effects of SNR, %fat and mean water on the DTI measurements showed that a sufficient SNR is essential for a reliable estimation of the DTI parameters in skeletal muscle and that in vivo measurements of % fat and mean water T_2 are necessary to assess whether detected changes in DTI parameters could be ascribed to pathophysiology or to confounding effects. Overall, our work suggests that reliable DTI measurements in skeletal muscle can be obtained in DMD patients and healthy controls, while accounting for confounding factors.

References

1. Cleveland GG, Chang DC, Hazlewood CF, Rorschach HE. Nuclear magnetic resonance measurement of skeletal muscle: anisotrophy of the diffusion coefficient of the intracellular water. Biophys J 1976;16:1043-1053.
2. Qi J, Olsen NJ, Price RR, Winston JA, Park JH. Diffusion-weighted imaging of inflammatory myopathies: polymyositis and dermatomyositis. J Magn Reson Imaging 2008;27:212-217.
3. Kermarrec E, Budzik JF, Khalil C, Le Thuc V, Hancart-Destee C, Cotten A. In vivo diffusion tensor imaging and tractography of human thigh muscles in healthy subjects. AJR Am J Roentgenol 2010;195:W352-356.
4. Zaraiskaya T, Kumbhare D, Noseworthy MD. Diffusion tensor imaging in evaluation of human skeletal muscle injury. J Magn Reson Imaging 2006;24:402-408.
5. Froeling M, Nederveen AJ, Heijtel DF, et al. Diffusion-tensor MRI reveals the complex muscle architecture of the human forearm. J Magn Reson Imaging 2012;36:237-248.
6. Sinha S, Sinha U, Edgerton VR. In vivo diffusion tensor imaging of the human calf muscle. J Magn Reson Imaging 2006;24:182-190.
7. Budzik JF, Balbi V, Verclytte S, Pansini V, Le Thuc V, Cotten A. Diffusion tensor imaging in musculoskeletal disorders. Radiographics 2014;34:E56-72.
8. Budzik JF, Le Thuc V, Demondion X, Morel M, Chechin D, Cotten A. In vivo MR tractography of thigh muscles using diffusion imaging: initial results. Eur Radiol 2007;17:3079-3085.
9. Ponrartana S, Andrade KE, Wren TA, et al. Repeatability of chemical-shift-encoded water-fat MRI and diffusion-tensor imaging in lower extremity muscles in children. AJR Am J Roentgenol 2014;202:W567-573.
10. Van Donkelaar CC, Kretzers LJ, Bovendeerd PH, et al. Diffusion tensor imaging in biomechanical studies of skeletal muscle function. J Anat 1999;194 (Pt 1):79-88.
11. Sinha U, Csapo R, Malis V, Xue Y, Sinha S. Age-related differences in diffusion tensor indices and fiber architecture in the medial and lateral gastrocnemius. J Magn Reson Imaging 2015;41:941-953.
12. Scheel M, Prokscha T, von Roth P, et al. Diffusion tensor imaging of skeletal muscle--correlation of fractional anisotropy to muscle power. Rofo 2013;185:857-861.
13. Okamoto Y, Kunimatsu A, Kono T, Nasu K, Sonobe J, Minami M. Changes in MR diffusion properties during active muscle contraction in the calf. Magn Reson Med Sci 2010;9:1-8.
14. Galban CJ, Maderwald S, Uffmann K, Ladd ME. A diffusion tensor imaging analysis of gender differences in water diffusivity within human skeletal muscle. Nmr Biomed 2005;18:489-498.
15. Damon BM, Ding Z, Anderson AW, Freyer AS, Gore JC. Validation of diffusion tensor MRI-based muscle fiber tracking. Magn Reson Med 2002;48:97-104.
16. Froeling M, Oudeman J, Strijkers GJ, et al. Muscle changes detected with diffusion-tensor imaging after long-distance running. Radiology 2015;274:548-562.
17. Heemskerk AM, Strijkers GJ, Drost MR, van Bochove GS, Nicolay K. Skeletal muscle degeneration and regeneration after femoral artery ligation in mice: monitoring with diffusion MR imaging. Radiology 2007;243:413-421.
18. Scheel M, von Roth P, Winkler T, et al. Fiber type characterization in skeletal muscle by diffusion tensor imaging. Nmr Biomed 2013;26:1220-1224.
19. Okamoto Y, Mori S, Kujiraoka Y, Nasu K, Hirano Y, Minami M. Diffusion property differences of the lower leg musculature between athletes and non-athletes using 1.5T MRI. MAGMA 2012;25:277-284.
20. Froeling M, Nederveen AJ, Nicolay K, Strijkers GJ. DTI of human skeletal muscle: the effects of diffusion encoding parameters, signal-to-noise ratio and T2 on tensor indices and fiber tracts. Nmr Biomed 2013;26:1339-1352.
21. Williams SE, Heemskerk AM, Welch EB, Li K, Damon BM, Park JH. Quantitative effects of inclusion of fat on muscle diffusion tensor MRI measurements. J Magn Reson Imaging 2013;38:1292-1297.

22. Damon BM. Effects of image noise in muscle diffusion tensor (DT)-MRI assessed using numerical simulations. Magn Reson Med 2008;60:934-944.
23. Hoffman EP, Brown RH, Jr., Kunkel LM. Dystrophin: the protein product of the Duchenne muscular dystrophy locus. Cell 1987;51:919-928.
24. Sarkozy A, Deschauer M, Carlier RY, et al. Muscle MRI findings in limb girdle muscular dystrophy type 2L. Neuromuscul Disord 2012;22 Suppl 2:S122-129.
25. Janssen BH, Voet NBM, Nabuurs CI, et al. Distinct Disease Phases in Muscles of Facioscapulohumeral Dystrophy Patients Identified by MR Detected Fat Infiltration. Plos One 2014;9.
26. Wokke BH, Hooijmans MT, van den Bergen JC, Webb AG, Verschuuren JJ, Kan HE. Muscle MRS detects elevated PDE/ATP ratios prior to fatty infiltration in Becker muscular dystrophy. Nmr Biomed 2014;27:1371-1377.
27. Froeling M, Oudeman J, van den Berg S, et al. Reproducibility of diffusion tensor imaging in human forearm muscles at 3.0 T in a clinical setting. Magn Reson Med 2010;64:1182-1190.
28. Azzabou N, Loureiro de Sousa P, Caldas E, Carlier PG. Validation of a generic approach to muscle water T2 determination at 3T in fat-infiltrated skeletal muscle. J Magn Reson Imaging 2015;41:645-653.
29. Loughran T, Higgins DM, McCallum M, Coombs A, Straub V, Hollingsworth KG. Improving Highly Accelerated Fat Fraction Measurements for Clinical Trials in Muscular Dystrophy: Origin and Quantitative Effect of R2*Changes. Radiology 2015;275:570-578.
30. Basser PJ, Pajevic S. Statistical artifacts in diffusion tensor MRI (DT-MRI) caused by background noise. Magn Reson Med 2000;44:41-50.
31. Ponrartana S, Ramos-Platt L, Wren TA, et al. Effectiveness of diffusion tensor imaging in assessing disease severity in Duchenne muscular dystrophy: preliminary study. Pediatr Radiol 2015;45:582-589.
32. Heemskerk AM, Drost MR, van Bochove GS, van Oosterhout MF, Nicolay K, Strijkers GJ. DTI-based assessment of ischemia-reperfusion in mouse skeletal muscle. Magn Reson Med 2006;56:272-281.
33. Qin EC, Juge L, Lambert SA, Paradis V, Sinkus R, Bilston LE. In vivo anisotropic mechanical properties of dystrophic skeletal muscles measured by anisotropic MR elastographic imaging: the mdx mouse model of muscular dystrophy. Radiology 2014;273:726-735.
34. Li K, Dortch RD, Welch EB, et al. Multi-parametric MRI characterization of healthy human thigh muscles at 3.0 T - relaxation, magnetization transfer, fat/water, and diffusion tensor imaging. Nmr Biomed 2014;27:1070-1084.

3

Chapter 3

Non-uniform muscle fat replacement along the proximodistal axis in Duchenne Muscular Dystrophy

M.T. Hooijmans; E.H. Niks; J. Burakiewicz; C. Anastasopoulos; S.I van den Berg; E.W. van Zwet; A.G. Webb; J.J.G.M Verschuuren; H.E. Kan

Neuromusc. Disor. 2017 Feb; 27:458-464

ABSTRACT

The progressive replacement of muscle tissue by fat in Duchenne muscular dystrophy (DMD) has been studied using quantitative MRI between, but not within individual muscles. We studied fat replacement along the proximodistal muscle axis using the Dixon technique on a 3T MR scanner in 22 DMD patients and 12 healthy controls. Mean fat fractions per muscle per slice for seven lower and upper leg muscles were compared between and within groups assuming a parabolic distribution. Average fat fraction for a small central slice stack and a large coverage slice stack were compared to the value when the stack was shifted one slice (15mm) up or down. Higher fat fractions were observed in distal and proximal muscle segments compared to the muscle belly in all muscles of the DMD subjects (p<0.001). A shift of 15mm resulted in a difference in mean fat fraction which was on average 1-2% ranging up to 12% (p<0.01). The muscle end regions are exposed to higher mechanical strain, which points towards mechanical disruption of the sarcolemma as one of the key factors in the pathophysiology. Overall, this non-uniformity in fat replacement needs to be taken into account to prevent sample bias when applying quantitative MRI as biomarker in clinical trials for DMD.

INTRODUCTION

Duchenne muscular Dystrophy (DMD) is caused by a mutation in the *DMD* gene and is characterized by progressive muscle weakness. [1] Quantitative MRI is becoming increasingly important as a non-invasive method to follow disease progression, and is considered a promising surrogate outcome measure for clinical trials. [2] Assessment of fat replacement in individual muscles and in relation to clinical outcomes has been studied extensively by MRI. [3-17]

The fat fraction of a muscle is normally calculated from the average of several central slices in a muscle, [7, 8, 11] or of a specific region of interest. [17, 18] However, it is unknown if fat is distributed uniformly over the muscle, and thus how robust this type of measurement is with respect to the exact location over which the images are quantified. For example, in Charcot-Marie-Tooth disease and Facio-Scapulo-Humeral muscular dystrophy, it is known that fat replacement varies along the proximodistal axis. [19, 20] In DMD it is plausible that fat distribution is non-uniform, as dystrophin is non-uniformly distributed, [21] and mechanical strain is highest in the muscle end regions. [22-24] This non-uniformity potentially has a major effect on the calculated fat fraction, particularly since in longitudinal studies DMD boys inevitably grow in-between examinations and accurate repositioning is very challenging. In this study, therefore, we 1) assessed the distribution of fat replacement along the proximodistal muscle axis, and 2) determined the effect of a slight shift in spatial localization along the proximodistal muscle axis on the measured mean fat fraction in DMD boys using two commonly used approaches: analysis of a small central slice stack or volume [3, 4, 6, 10, 17] and analysis of a non-contiguous slice stack with a large coverage in feet head direction. [7, 11, 12, 15]

METHODS

2.1 Participants

Twenty-two DMD patients (mean age 9.3±3.1 years, range 5-16 years) and twelve healthy control subjects (9.7± 2.9 years, range: 5-14 years) participated in this study. Patients were recruited from the Dutch Dystrophinopathy database. [25] Exclusion criteria were MRI contraindications and the inability to lie supine for at least 30 minutes. Diagnosis was confirmed by molecular genetic testing. Among the DMD patients, 16 were fully ambulant, 6 patients were wheelchair bound and all patients used corticosteroids with intermittent dosing regimens (varying between 8-10 days

on/off). Healthy controls were recruited from local schools and sport clubs. The study was approved by the local medical ethics committee, and written informed consent was obtained from all subjects and their parents.

2.2 MR methods

MR images were acquired in the right lower and upper leg on a 3T MR system (Ingenia, Philips Healthcare, Best, The Netherlands), using a 16-channel body receive coil array placed on top of the legs in combination with the 12-channel receive coil array located within the patient table. Patients were positioned in a feet first, supine position. The coil was placed on top of the leg in order to cover the full length of the upper and lower leg. In the taller boys, the coil had to be repositioned during scanning to ensure full coverage of the upper leg. The imaging protocol contained a 3D survey scan for localization, transmit field (B_1^+) calibration and 3-Point Gradient Echo Dixon to determine fat replacement (23 slices; voxel size 1x1x10 mm; interslice gap 5 mm; repetition time (TR)/ echo time (TE)/ echo time shift (ΔTE) 210/4.41/0.76 ms; 2 signal averages and a flip angle of 8°). All scans were aligned to the tibia and femur bone, and positioned in such a way as to provide maximal coverage of the muscles in the lower and upper leg.

2.3 Data-analysis

Fat and water images were generated using a multi-peak model based on a six fat peak spectrum coded in Matlab (Mathworks, Natick, MA, USA). Values were not corrected for T_2* relaxation effects. [26, 27] The sequence was optimized with respect to TR and flip angle to avoid T_1 relaxation effects. After reconstruction, visual inspection was used to assess image quality to detect reconstruction failure, Bo artefacts and movement artefacts. Images with clear artefacts were removed from further analysis.

Regions of interest (ROIs) were drawn manually using Medical Image Processing, Analysis and Visualization (MIPAV) software (http://mipav.cit.nih.gov) for seven individual lower and upper leg muscles for which full coverage of the muscle was achieved within the field-of-view of the Dixon scan, namely the soleus (SOL), the tibialis anterior (TA), the peronei (PER), the tibialis posterior (TP), the extensor digitorum longus (EDL), the vastus lateralis (VL) and the biceps femoris long head (BFL) muscle. ROIs were drawn on the reconstructed water images. The boundaries of the ROIs were chosen to always fall within a muscle in order to avoid contamination of subcutaneous fat and fatty intermuscular septa. In the more severely affected patients, both the reconstructed fat and water images were used to ensure that the boundaries of the ROI fell within the muscle. ROIs were only drawn on slices in which

the muscle was visible. Quantitative fat fractions were calculated as signal intensity (SI) fat/ (SI fat+ SI water))*100 from the reconstructed fat and water images and reported as a mean value of all pixels within a ROI. Fat fraction (%) was calculated per ROI and per slice. For visual comparison of fat distribution along the proximodistal muscle axis between subjects of different ages, all datasets were aligned according to their maximal cross-sectional area of the muscle (maxCSA).

2.4 Statistical Analysis

Generalized Estimating Equations (GEE) were used to assess the fat distribution pattern in both groups separately, assuming a parabolic curvature (ax^2+bx+c). GEE was also used to assess differences in fat distribution pattern along the proximodistal muscle axis between DMD patients and healthy controls. GEE takes into account the repeated measurements within the same muscle (individual slices).

Differences in mean fat fraction between measurement locations within an individual muscle were assessed using a paired t-test for a Small Coverage (SC) and Large Coverage (LC) analysis. For the SC analysis, the mean fat fraction was averaged over four central slices. The first location was at the thickest part of the calf or at mid-thigh level. For the second and third location, the selection of slices was shifted one slice in the distal direction or one slice in the proximal direction in relation to the first location. All three locations along the proximodistal muscle axis covered the same distance (5.5 cm) of the calf. For the LC analysis, the mean fat fraction was averaged over 5 non-consecutive slices. The middle slice of the stack was positioned at the thickest part of the leg or at mid-thigh level for the first location. For the second and third location, the selection of slices was shifted one slice proximal and one slice distal in relation to the first location. All three locations along the proximodistal muscle axis covered the same distance (13 cm) of the calf.

Finally, a Bland-Altmann plot was used to assess the difference between the fat fraction calculated at the central slices versus fat fraction calculated over the whole muscle. A Bonferroni correction was applied to correct for multiple comparisons resulting in a significance level set of $p<0.01$ in the paired analysis and a significance level set of $p<0.002$ in the GEE analysis. Statistical analyses were performed using SPSS version 20 for Windows (SPSS Inc., Chicago).

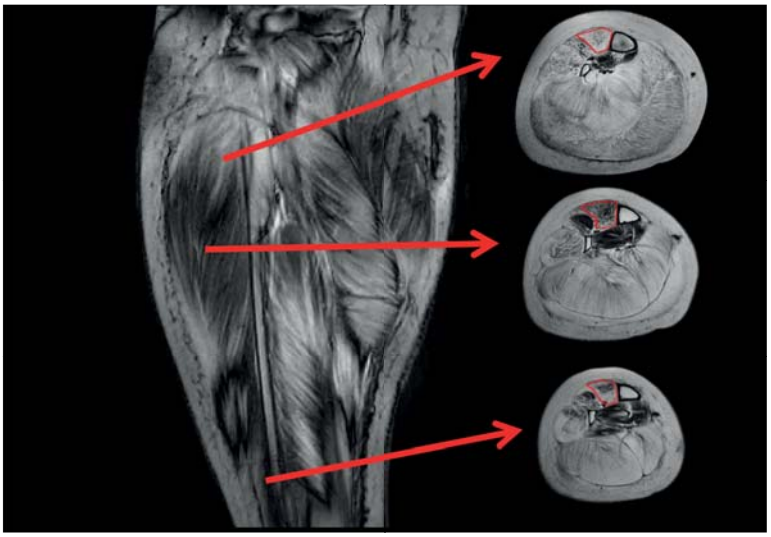

Figure. 1 Fat reconstruction of the right lower leg of a DMD patient in the coronal and axial plane. Note the distribution of fat along the proximodistal muscle axis of the TA muscle (red arrows). Together with three axial fat-only images showing a distal, middle and proximal muscle section of the TA muscle visualized with a manually drawn ROI (red). The middle slice has, already visually, less fat replacement compared to the proximal and distal slice.

RESULTS

Full lower leg datasets were obtained in all DMD patients and healthy controls. Upper leg datasets were acquired in all healthy controls and in 16 DMD patients. In six DMD patients, the protocol could not be completed due to fatigue, patient discomfort in the supine lying position, or anxiety upon entrance into the scanner bore. Five upper leg datasets (two DMD patients and three healthy control subjects) and one lower leg dataset (HC subject) had to be excluded due to movement artefacts. In all cases, the two outer slices on both sides were excluded from the analysis due to reconstruction failure caused by B_0 inhomogeneities.

3.1 Fat distribution over the entire length of the muscle

Within-group analysis showed that the fat distribution pattern along the proximodistal muscle axis was non-uniform in patients and controls. Higher fat fractions were observed in the more proximal and distal muscle parts compared to the maxCSA (Figure. 1; Figure. 2 a-b). The fat distribution pattern could be well described by a parabolic curvature for all the analyzed muscles of the DMD patients (Range in a: 0.133-0.390; $p<0.001$), and healthy controls (range in a: 0.003-0.084; $p<0.001$), with the exception of the PER muscle (a= 0.003; p=0.858). Between-group

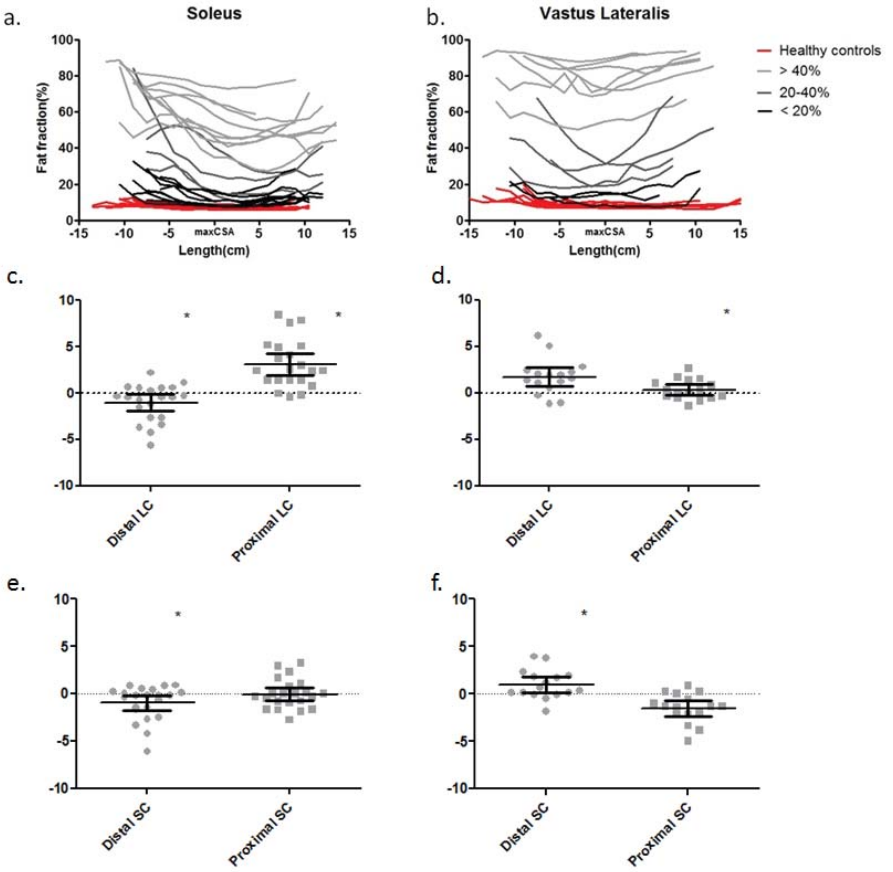

Figure. 2 Fat distribution over the entire length of the muscle and the difference in fat fraction due to a slight shift in positioning. Fat fraction (% fat) as a function of location (cm) along the proximodistal muscle axis (a) for the SOL muscle (b) and the VL muscle. The middle point of the graph is aligned with the maximal Cross Sectional Area (maxCSA) of the muscle in order to facilitate visual comparisons between subjects. The left direction shows the more distal muscle part while the right direction showed the proximal muscle part. Due to natural variation in length, as well as leg and muscle size, the amount of data points plotted on both sides of the maxCSA varied per subject and per muscle. Each line represents one individual subject. To increase the readability of the graphs DMD patients are grouped and colored according to their mean fat fraction. (red = HC subjects, black= %fat <20, dark grey= 20 <%fat>40, light grey=%fat> 40%). This grouping according to mean fat fraction is only for visual support and not part of the statistical analysis. Differences in mean fat fraction (c-e) for the SOL muscle (d-f) and the VL muscle for the small coverage (SC) and large coverage (LC) analysis. SC/LC – Distal: the difference between mean fat fraction obtained at the thickest part of the calf or at mid-thigh level and obtained when shifted one slice in the distal direction. SC/LC – Proximal: the difference between mean fat fraction obtained at the thickest part of the calf or at mid-thigh level and obtained when shifted one slice in the proximal direction. Each grey square/dot represents one individual DMD subject. The black bars represent the mean and 95% CI. Significant differences are indicated with *. Note the more homogenous fat distribution along the proximodistal muscle axis in the higher affected DMD patients in the VL muscle together with the high variation when the analysis window was shifted one slice proximal or distal.

analysis showed a significantly more pronounced parabolic fat distribution pattern in DMD patients compared to healthy controls for all muscles analyzed (p<0.001), with exception of the BFL muscle (DMD a=0.133; HC a=0.084; p=0.176).

3.2 Differences in fat fraction with a slight shift in positioning

Shifting the slices which were analyzed by one slice either in the proximal or distal direction resulted in a significant difference in fat fraction for the majority of the muscles for both the SC and LC analysis. (Table. 1) The difference was on average 1.7% and up to 12% for the SC analysis (Figure.2 c-d) and 1.7% ranging up to 10.7% for the LC analysis (Figure. 2 e-f).The Bland-Altman plot of the central slice fat fraction versus whole muscle fat fraction showed that the largest differences in mean fat fraction (i.e. between 0.13% and 22.24%) occurred in muscles with intermediate fat fractions (Figure. 2a,b; Figure. 3)

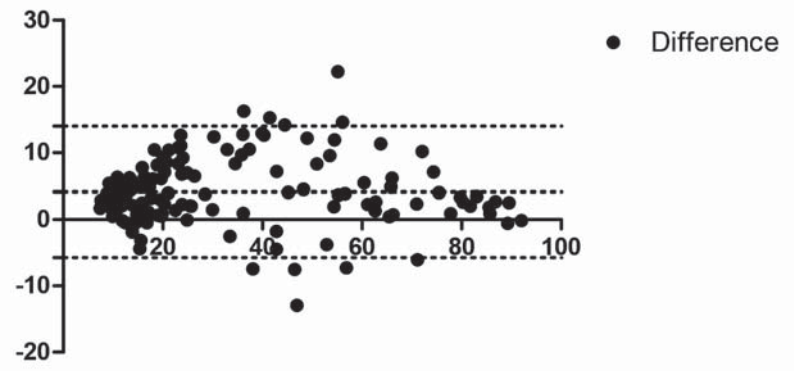

Figure. 3 Difference between whole muscle fat fraction and the averaged fat fraction. Bland-Altman plot of the difference in fat fraction between whole muscle measurement and the averaged fat fraction over the four middle slices. Each square represents one individual muscle of an individual subject. Note the increase in the difference between the two methods in the intermediate fat fractions.

Muscle	LC -- Distal	LC -- Proximal	SC-- distal	SC- proximal
EDL	1.4 ±2.3 (0.04-6.9%) *	2.9±3(0.03-10.7%)	-1.5 ±2.8 (0.06-12%) *	0.4±3.1(0.01-10.7%)
PER	-0.2±2.9(0.17 -4.1%)	2.1±1.9 (0.7-7.8%) *	-2.5±1.9 (0.12 -5.2%) *	1.4±3.6 (0.67-11.3%) *
SOL	-1.0±2(0.03-3.7%) *	3.1±2.6 (0.01-3.26%)*	-1±1.8 (0.03-6.1%) *	-0.06±1.6 (0.01-3.26%)
TA	0.2±2.6 (0.16-9.3%)	2.3.±2.8 (0.4-8.4%)*	-1.3±2.2 (0.16-9.1%) *	-0.02±2.2 (0.02-5.3%)
TP	0.5±0.6(0.04-2.1%)*	0.9±0.8(0.07-3.37%)*	-0.21±0.7 (0.04-2.1%)	-0.2±1.1 (0.07-3.37%)
BFL	0.9±1.4 (0.03-4.4%) *	0.4±1.2 (0.15-3%)	0.7±1.7 (0.21-4.2%) *	-1.6±2.2 (0.32-7%) *
VL	1.7±1.9 (0.25-6.2%)*	0.4±1.1 (0.02-1.7%)	1.0±1.5(0.04-3.96%)	-1.6±1.6 (0.3-5%) *

Table. 1 The mean, standard deviation and the absolute range of the difference in %fat for a slight shift in location along the axis in the DMD patients for the large coverage (LC) and the small coverage (SC) analysis. SC/LC – Distal: the difference between mean fat fraction obtained at the thickest part of the calf or at mid-thigh level and obtained when shifted one slice in the distal direction. SC/LC – Proximal: the difference between mean fat fraction obtained at the thickest part of the calf or at mid-thigh level and obtained when shifted one slice in the proximal direction. Significant differences are indicated with *. Abbreviations: tibialis anterior (TA) and posterior (TP) extensor digitorum longus (EDL), peroneal muscles (PER), soleus (SOL), vastus lateralis (VL) and biceps femoris long head (BFL)

DISCUSSION

Our results show that in DMD patients all analyzed leg muscles have a non-uniform fat distribution pattern along the proximodistal muscle axis, showing higher fat replacement near the origin and insertion of the muscle compared to the muscle belly. This specific pattern is also found in the muscles of the healthy control subjects, although significantly less prominent.

The non-uniform fat fraction has important implications for the use of quantitative MRI or MR spectroscopy of fat replacement or muscle biopsies as biomarkers in clinical trials. [2] Our study has shown that a slight shift of 1.5cm along the proximodistal muscle axis results in significant differences in estimated mean fat fraction. Importantly, these differences are in the same range (SC analysis average: 1.7% up to 12%; LC analysis average: 1.2% up to 11%) as changes found in fat fraction in longitudinal studies over an 12 or 18 month time period. [8, 11, 13-15, 17] Due to the parabolic shape of the fat distribution along the proximodistal muscle axis, a shift in slice spacing to either the proximal or the distal side of the muscle will result in an artificial increase of the measured fat fraction when the slice stack is positioned at the lowest point of the parabola. As a result, this sample bias is independent of the shift direction and cannot be averaged out. However, this is not always the case since usually slice stacks are positioned at a specific distance from a bony landmark. As this will not directly match to the lowest point of the parabola for each muscle,

it is possible that the difference will be averaged out on a group level. Overall, this greatly diminishes the discriminant power of the technique and stresses the need for extreme accurate and reproducible spatial localization over time.

Fat replacement is commonly assessed using MR by 2D or 3D imaging or MR spectroscopy. [7, 8, 11, 18] The intrinsic parameters involved in this methodology, i.e. slice gaps, slice thickness, field-of-view and restricted voxel size could result in limited and location-specific information on the fat fraction. In addition, due to the age of DMD boys in current clinical trials, boys will inevitably grow during the trial. Both aspects complicate spatial localization in a longitudinal study set up. Using a combination of bony landmarks, internal muscle references, and external references such as fish oil capsules placed on the skin is recommended to increase accuracy. [28, 29] Ultimately, a 3D acquisition that covers the whole limb will be the most robust method to acquire data in a longitudinal follow-up. The full coverage allows accurate offline matching of datasets.

Another implication of the non-uniform distribution of fat with respect to the use of MRI in clinical trials is the less prominent parabolic curvature in muscles with either high or low fat fractions compared to intermediately affected muscles. These differences in parabolic curvature are most likely caused by evolution of the fat distribution pattern over time from a homogeneous initial phase (unaffected muscle) through a heterogeneous middle state (intermediate affected muscle) to a homogeneous end stage (highly affected muscle). This effect can also be visualized in the Bland-Altman plot, where more prominent differences in mean fat fraction between the central four slices versus the whole muscle fat fraction were observed in the intermediate affected muscles compared to the un-affected and highly affected muscles. Therefore, the highest bias due to sampling errors occurs in these intermediate affected muscles. However, these muscles in particular are the ones which are most likely to be useful as a surrogate endpoint in clinical trials, as they have the highest potential of showing a response to treatment via a decrease in the rate of progression of fat replacement.

In addition to the clinical implications of measuring the non-uniform nature of the fat distribution, this type of measurement could help in the understanding of the underlying pathophysiology in DMD. In healthy skeletal muscle, mechanical strain is non-uniformly distributed along the proximodistal muscle axis, where higher strain is observed in the muscle end regions compared to the muscle belly. [23, 24, 30] In healthy mice, dystrophin has been shown to be particularly concentrated near these end regions [31] in contrast to other proteins associated with mechanical stability such as

connectin and nebulin. [32] In addition, dystrophin-deficient muscles are especially susceptible to stretch-induced muscle injury.[33, 34] It therefore seems logical that mechanical disruption of the membrane might be one of the key causative factors for muscle degeneration, and for fat replacement in DMD to evolve more prominently in the end regions compared to the muscle belly.

Our study had some limitations. In the reconstruction of the three-point Dixon images, no T_2* correction was applied which could result in an overestimation of the fat fractions in the low fat ranges. [27] However, as this will result in artificially high fat fractions in the low fat range, correcting for T_2* would only result in an even more pronounced parabolic curvature. Secondly, in this work only the seven lower and upper leg muscles of which full coverage could be ensured have been analyzed. In the upper leg in particular the field-of-view was not large enough to cover entire muscles and the Bo artefacts near the joints prevented analysis of bi-articular muscles. This could have resulted in a selection bias towards shorter mono-articular muscles in which strain might be distributed differently than in longer muscles. Thirdly, the relatively young study population resulted in a majority of less and intermediate affected muscles which has an influence on the average parabolic curvature used as an outcome measure.

To conclude, we have shown a clear non-uniform fat replacement pattern along the proximodistal muscle axis in DMD within individual lower and upper leg muscles. This non-uniformity in fat fraction within an individual muscle has a major influence on quantitative MR measurements and biopsy parameters that are currently considered as outcome measures in clinical trials, and highlights the need for accurate repositioning in longitudinal studies. A slight shift along the proximodistal muscle axis results in a difference in fat fraction which is on average 1-2% ranging up to 12%. These differences are most prevalent in the muscles with intermediate fat fractions. In addition, these findings seem to point to mechanical disruption of the membrane as one of the key factors in the pathophysiology of DMD.

REFERENCES

1. Mendell JR, Shilling C, Leslie ND, et al. A two-tiered approach to newborn screening for Duchenne muscular dystrophy (DMD) using dried blood spots for sequential CK and DNA analysis. Neuromuscular Disord 2012;22:805-805.
2. Straub V, Balabanov P, Bushby K, et al. Stakeholder cooperation to overcome challenges in orphan medicine development: the example of Duchenne muscular dystrophy. Lancet Neurol 2016;15:882-890.
3. Akima H, Lott D, Senesac C, et al. Relationships of thigh muscle contractile and non-contractile tissue with function, strength, and age in boys with Duchenne muscular dystrophy. Neuromuscular Disord 2012;22:16-25.
4. Arpan I, Willcocks RJ, Forbes SC, et al. Examination of effects of corticosteroids on skeletal muscles of boys with DMD using MRI and MRS. Neurology 2014;83:974-980.
5. Willcocks RJ, Forbes SC, Finanger EL, et al. Magnetic resonance imaging and spectroscopy detect changes with age, corticosteroid treatment, and functional progression in DMD. Neuromuscular Disord 2013;23:810-810.
6. Willcocks RJ, Arpan IA, Forbes SC, et al. Longitudinal measurements of MRI-T-2 in boys with Duchenne muscular dystrophy: Effects of age and disease progression. Neuromuscular Disord 2014;24:393-401.
7. Wokke BH, van den Bergen JC, Versluis MJ, et al. Quantitative MRI and strength measurements in the assessment of muscle quality in Duchenne muscular dystrophy. Neuromuscular Disord 2014;24:409-416.
8. Hollingsworth KG, Garrood P, Eagle M, Bushby K, Straub V. Magnetic Resonance Imaging in Duchenne Muscular Dystrophy: Longitudinal Assessment of Natural History over 18 Months. Muscle Nerve 2013;48:586-588.
9. Garrood P, Hollingsworth KG, Eagle M, et al. MR Imaging in Duchenne Muscular Dystrophy: Quantification of T-1-Weighted Signal, Contrast Uptake, and the Effects of Exercise. J Magn Reson Imaging 2009;30:1130-1138.
10. Kinali M, Arechavala-Gomeza V, Cirak S, et al. Muscle histology vs MRI in Duchenne muscular dystrophy. Neurology 2011;76:346-353.
11. Hogrel JY, Wary C, Moraux A, et al. Longitudinal functional and NMR assessment of upper limbs in Duchenne muscular dystrophy. Neurology 2016;86:1022-1030.
12. Wary C, Azzabou N, Giraudeau C, et al. Quantitative NMRI and NMRS identify augmented disease progression after loss of ambulation in forearms of boys with Duchenne muscular dystrophy. Nmr Biomed 2015;28:1150-1162.
13. Wary C, Azzabou N, Zehrouni K, et al. One year follow-up of Duchenne muscle dystrophy with nuclear magnetic resonance imaging and spectroscopy indices. Neuromuscular Disord 2014;24:853-853.
14. Bonati U, Hafner P, Schadelin S, et al. Quantitative muscle MRI: A powerful surrogate outcome measure in Duchenne muscular dystrophy. Neuromuscul Disord 2015;25:679-685.
15. Ricotti V, Evans MR, Sinclair CD, et al. Upper Limb Evaluation in Duchenne Muscular Dystrophy: Fat-Water Quantification by MRI, Muscle Force and Function Define Endpoints for Clinical Trials. Plos One 2016;11:e0162542.
16. Fischmann A, Hafner P, Gloor M, et al. Quantitative MRI and loss of free ambulation in Duchenne muscular dystrophy. J Neurol 2013;260:969-974.
17. Willcocks RJ, Rooney WD, Triplett WT, et al. Multicenter prospective longitudinal study of magnetic resonance biomarkers in a large duchenne muscular dystrophy cohort. Ann Neurol 2016;79:535-547.
18. Forbes SC, Walter GA, Rooney WD, et al. Skeletal Muscles of Ambulant Children with Duchenne Muscular Dystrophy: Validation of Multicenter Study of Evaluation with MR Imaging and MR Spectroscopy. Radiology 2013;269:198-207.
19. Janssen BH, Voet NBM, Nabuurs CI, et al. Distinct Disease Phases in Muscles of Facioscapulohumeral Dystrophy Patients Identified by MR Detected Fat Infiltration. Plos One 2014;9.

20. Gaeta M, Mileto A, Mazzeo A, et al. MRI findings, patterns of disease distribution, and muscle fat fraction calculation in five patients with Charcot-Marie-Tooth type 2 F disease. Skeletal Radiol 2012;41:515-524.
21. Rybakova IN, Patel JR, Ervasti JM. The dystrophin complex forms a mechanically strong link between the sarcolemma and costameric actin. J Cell Biol 2000;150:1209-1214.
22. Lieber RL, Friden J. Muscle Damage Is Not a Function of Muscle Force but Active Muscle Strain. J Appl Physiol 1993;74:520-526.
23. Morgan DL, Proske U. Popping sarcomere hypothesis explains stretch-induced muscle damage. Clin Exp Pharmacol P 2004;31:541-545.
24. Shin DD, Hodgson JA, Edgerton VR, Sinha S. In vivo intramuscular fascicle-aponeuroses dynamics of the human medial gastrocnemius during plantarflexion and dorsiflexion of the foot. J Appl Physiol 2009;107:1276-1284.
25. Zijnen; JCvdBHBGAJvERPIJMdGPJWMP. Forty-Five years of Duchenne muscular dystrophy in the Netherlands. Journal of Neuromuscular Diseases 2014:99-109.
26. Yu HZ, Shimakawa A, McKenzie CA, Brodsky E, Brittain JH, Reeder SB. Multiecho Water-Fat Separation and Simultaneous R-2* Estimation With Multifrequency Fat Spectrum Modeling. Magn Reson Med 2008;60:1122-1134.
27. Loughran T, Higgins DM, McCallum M, Coombs A, Straub V, Hollingsworth KG. Improving Highly Accelerated Fat Fraction Measurements for Clinical Trials in Muscular Dystrophy: Origin and Quantitative Effect of R2*Changes. Radiology 2015;275:570-578.
28. Fischmann A, Gloor M, Fasler S, et al. Muscular involvement assessed by MRI correlates to motor function measurement values in oculopharyngeal muscular dystrophy. J Neurol 2011;258:1333-1340.
29. Sinclair CDJ, Morrow JM, Miranda MA, et al. Skeletal muscle MRI magnetisation transfer ratio reflects clinical severity in peripheral neuropathies. J Neurol Neurosur Ps 2012;83:29-32.
30. Hafner P, Bonati U, Erne B, et al. Improved Muscle Function in Duchenne Muscular Dystrophy through L-Arginine and Metformin: An Investigator-Initiated, Open-Label, Single-Center, Proof-Of-Concept-Study. Plos One 2016;11.
31. Samitt CE, Bonilla E. Immunocytochemical Study of Dystrophin at the Myotendinous Junction. Muscle Nerve 1990;13:493-500.
32. Atsuta F, Sato K, Maruyama K, Shimada Y. Distribution of Connectin (Titin), Nebulin and Alpha-Actinin at Myotendinous Junctions of Chicken Pectoralis-Muscles - an Immunofluorescence and Immunoelectron Microscopic Study. J Muscle Res Cell M 1993;14:511-517.
33. Moens P, Baatsen PHWW, Marechal G. Increased Susceptibility of Edl Muscles from Mdx Mice to Damage-Induced by Contractions with Stretch. J Muscle Res Cell M 1993;14:446-451.
34. Hu X, Blemker SS. Musculoskeletal simulation can help explain selective muscle degeneration in Duchenne muscular dystrophy. Muscle Nerve 2015;52:174-182.

Chapter 4

Elevated phosphodiester and T2 levels can be measured in the absence of fat infiltration in Duchenne muscular dystrophy patients

M.T. Hooijmans, E.H. Niks, J. Burakiewicz, J.J.G.M Verschuuren, A.G. Webb, H.E. Kan

NMR Biomed. 2017 Jan;30(1). doi: 10.1002/nbm.3667.

Abstract

Quantitative MRI and MRS are increasingly important as non-invasive outcome measures in therapy development for Duchenne muscular dystrophy (DMD). Many studies have focussed on individual measures such as fat fraction and metabolite levels in relation to age and functionality, but much less attention has been given to how these indices relate to each other. Here, we assessed spatially-resolved metabolic changes in leg muscles of DMD patients, and classified muscles according to the degree of fat replacement compared to healthy controls. Quantitative MRI (3-point Dixon and multi-spin echo without fat suppression and a tri-exponential fit) and 2D-CSI ^{31}P MRS scans were obtained from eighteen DMD patients and twelve healthy controls using a 3T and a 7T MR scanner. Metabolite levels, T_2 values and fat fraction were individually assessed for five lower leg muscles. In muscles with extensive fat replacement, phosphodiester over ATP (PDE/ATP) inorganic phosphate over phosphocreatine (Pi/PCr), intracellular tissue pH and T_2 were significantly increased compared to healthy controls. In contrast, in muscles without extensive fat replacement, only PDE/ATP and T_2 values were significantly elevated. Overall, our results show that PDE levels and T_2 values increase prior to the occurrence of fat replacement and remain elevated in later stages of the disease. This suggests that these individual measures could not only function as early markers for muscle damage but also reflect potentially reversible pathology in the more advanced stages.

Introduction

Duchenne Muscular Dystrophy (DMD) is an X-linked disease caused by a mutation in the DMD-gene, affecting approximately 1 in 3500 male new-borns. [1] The absence of a functional dystrophin protein in the muscle cells of DMD patients manifests itself in progressive muscle weakness, functional loss, and cardiac and respiratory failure. [2] Within muscle tissue different pathophysiological events, such as changes in energy metabolism, fat infiltration, oedema and fibrosis, take place simultaneously. [3] The time course of these various processes is not fully understood but it appears that initial inflammation, and changes in energy metabolism, are eventually followed by the replacement of muscle tissue by fat and fibrotic tissue. It is generally thought that fat replacement of muscle tissue is irreversible while other processes may be at least partially reversible.

Both MRI and MRS have been used to non-invasively map these individual pathophysiological processes in DMD. [4-7] Muscle replacement by fat is commonly determined by chemical shift based methods such as Dixon. This replacement correlates well with age, disease progression and functional measures. [8-11] Another MR parameter which is frequently used in DMD is the T_2, which reflects both fat replacement and inflammation/edema. If used without correcting for the presence of fat, these relaxation times are referred to as global T_2 values and display the same progressive course as the fat fraction. [12-14] In addition, it is possible to assess the individual T_2 relaxation times of fat and water. The water T_2 is thought to represent the inflammation component, and is elevated compared to healthy controls. [4, 15-17] In contrast to global T_2 values, water T_2 values decrease with age and disease progression, most likely inversely related to the increase of fibrotic tissue. [18] Finally, metabolic changes in the muscles of DMD patients can be detected by using phosphorous spectroscopy (^{31}P-MRS). Reduced phosphocreatine (PCr) levels which have been associated with loss of metabolic activity, elevated phosphodiester levels (PDE) which might be directed related to membrane anomalies and a more alkaline pH associated with leaky myocytes have been detected in DMD patients compared to healthy controls. [6, 19-22] Furthermore, the PCr over inorganic phosphate (Pi) ratio has been shown to decline with age while the PDE/ATP ratio increased with age. [22, 23] Until now most MR studies have focussed on individual MR parameters, and little attention has been given to how these indices relate to each other. In particular, the temporal relation between changes in metabolic parameters, obtained from ^{31}P MRS, and changes in fat fraction and water T_2 assessed with quantitative MRI is unclear. In Becker Muscular Dystrophy (BMD) structural changes such as the replacement of muscle tissue by fat and fibrosis are predominantly present in later stages of

the disease, while metabolic changes occur earlier. [24] This suggests that metabolic changes precede fat replacement. In contrast, work in facioscapulohumeral dystrophy (FSHD) patients showed that metabolic changes were only present in muscles with extensive fat replacement, which suggests that in this muscular dystrophy, metabolic changes and fat replacement occur simultaneously. [25] Finally, recent work in the arm muscles of DMD patients indicated a linear relation between fat fraction and disease progression, while metabolic changes most likely show non-linear behaviour. [26] Taken together, this body of work highlights the fact that it is important to assess more than just one aspect of muscle damage in DMD for a better understanding of the time course of the pathophysiology. In order to do this, it is essential that different measures be spatially co-localized in order to compare the results. However, ^{31}P MRS in DMD is commonly performed using surface coil localization, which makes it difficult to combine the results from spatially-resolved proton imaging and non-spatially-resolved MRS. The availability of higher field strength magnets creates the possibility to obtain high quality and muscle specific ^{31}P MRS data within reasonable measuring times.

In this work, we present combined quantitative MRI and spatially-resolved (2D-CSI) ^{31}P MRS data of the leg muscles in DMD patients to determine metabolic changes and inflammation in muscles with and without fat infiltration to assess if metabolic changes and inflammation vary in different stages of the disease process.

Methods

Study population

Eighteen DMD patients (Age: 9.2± 3.7 yrs.; range: 5-16 yrs) and twelve age matched healthy control subjects (Age: 9.7± 2.9 yrs.; range: 5-14 yrs) participated in this study. All healthy subjects were recruited from local schools and sport clubs, while all patients were recruited from the Dutch Dystrophinopathy Database. [27] All DMD diagnoses were confirmed by genetic testing. Fourteen DMD patients were ambulant, and four patients were wheelchair-bound. All patients used corticosteroids with intermittent dosing regimens, which varied between 8-10 days on/off. The local medical ethical committee approved the study and all subjects and/or their parents signed informed consent.

MR Examination

All ^{31}P datasets were acquired on a Philips 7T Achieva MR system (Philips Healthcare, The Netherlands) with a custom-built double-tuned birdcage coil. Patients were

positioned in a supine position, feet first in the scanner. The coil was positioned around the left lower leg, at the thickest part of the calf directly distal to the patella. The imaging protocol contained a gradient echo FISP sequence for anatomical imaging (15 slices; slice thickness 7mm; interslice gap 0.5 mm; repetition time (TR) 10 ms; echo time (TE) 3.0 ms; flip angle (FA) 30°; FOV 180x200 mm), a B0-map for shimming (14 slices; slice thickness 8 mm, no slice gap; TR/TE 30/3.11ms; FA 20°; FOV 160x180 mm) and a 2D phosphorous MRS Chemical Shift Imaging (CSI) dataset to assess skeletal muscle energy metabolism (FOV 200x200/150x150 mm; matrix size 10 x 10; TR 2000 ms; samples 2048; FA 45°; Hamming weighted acquisition with 12 signal averages at the central k-lines). No slice selection was applied. ^{31}P data were measured over the entire length of the coil which covered 12 cm of the leg in the feet/head direction. Second order shimming was applied with an image based shimming routine. The 2D-CSI positioning was guided by the anatomical images. As the diameter of the lower leg and the boundaries between the different muscle groups change along the length of the leg, the 2D-CSI sequence was planned in such a way that within the volume of the coil a specific voxel was located within one individual lower-leg muscle. [24]

On the same day, quantitative imaging datasets were acquired at 3 Tesla. A 3-point gradient echo Dixon sequence was acquired of the same leg on a Philips 3T Ingenia MR system for fat quantification in the lower leg (23 slices; slice thickness 10 mm; interslice gap 5 mm; TR/TE/ΔTE 210/4.41/0.76 ms; NSA 2; FA 8°; FOV 180x180 mm). In addition, a multi turbo spin echo sequence (MSE) was acquired to determine the T2 (17 echoes; TR/TE/ΔTE 3000/8/8 ms; echo train (8-136ms); voxel size 1.4x1.8x10 mm; gap 20 mm; slice thickness 10 mm; 5 slices, no fat suppression, refocussing pulse shape: central part of a sinc function , CPMG condition). The middle of the slice stack was positioned on the thickest part of the calf directly distal to the patella, to ensure accurate co-localisation with the ^{31}P data set.

Data-analysis

All phosphorous data sets were visualized with the 3D Chemical shift imaging package (3DiCSI). Individual spectra were identified in 5 lower leg muscles; the lateral (GL) and medial (GM) head of the gastrocnemius muscle, the soleus muscle (SOL), tibial anterior muscle (TA) and peroneus (PER) muscle with a grid overlay on the anatomical image. Voxels were carefully positioned to avoid overlap with adjoining muscles. All individual free induction decays were exported and processed with AMARES in jMRUI software package (version 5, http://sermn02.uab.es/mrui/). [28] Signals of Pi, PDE, PCr and γ-, α- and β-ATP were fitted with Gaussian line shapes. All metabolites are presented as a ratio over γ-ATP signal. Metabolite ratios were

corrected for partial saturation using literature values. [29] In addition, prior knowledge on the line width, as described previously, was used for PDE and β-ATP.[24] To calculate intracellular tissue pH, the shift in resonance between the Pi peak and PCr peak was used: pH=6.75 + log((3.27-S)/(S-5.69)). [30] As the disease progression in DMD patients is characterized by replacement of muscle tissue with fat, spectra of several patients suffered from a low signal-to-noise ratio (SNR) due to the low amount of muscle tissue in the voxel. To ensure spectral quality, SNR values were determined for each spectrum. Noise was defined as the standard deviation of the residual signal after the fitting procedure. Only spectra with SNR greater than 10 for the PCr peak in combination with the ability to properly fit all other metabolites were accepted.

Quantitative fat fractions were generated from 3-point Dixon images using (SI) fat/(SI fat+ SI proton))*100 according to a multi peak model containing six peaks. [31] As the sequence was optimized with respect to TR and FA for minimization of T1 relaxation effects, no correction for different T1 values was needed.[32] The sequence was not corrected for T_2* relaxation. [33, 34]

T2 values were calculated from the MSE images according a tri-exponential fitting routine written in Matlab (Mathworks, Natick, MA, USA) based on a previously described method. [35] The assumed T_2 fat values part of the tri-exponential fitting model were individually determined for each of the datasets. No B_1^+ sorting was applied, as $B1^+$ maps were analysed and almost all voxels fell within the general rejection criteria set for T_2 quantification ($B1^+$ lies in the range of 80-130% of the nominal $B1^+$ set by the scanner) Regions of interest (ROI) were drawn for the five individual lower leg muscles on all the slices within the coverage of the 2D-CSI using Medical Image Processing Analysis and Visualization (MIPAV) software (http://mipav.cit.nih.gov). T2 and fat fraction are presented as a mean value of all pixels within a ROI over multiple slices. All muscles of DMD patients were classified into two groups according to their fat fractions: Non-fat-infiltrated (NFI) DMD patients and fat-infiltrated DMD patients (FI DMD). Cut-off levels were determined for each muscle individually, using the mean fat fraction + 2* SD of that specific muscle in HC subjects.

Statistical analysis

A general linear model was used to compare Pi, PCr, PDE, ATP and pH and T2 levels between groups for the five lower leg muscles. Age was entered as a covariate. Statistical analyses were performed in SPSS version 20 for Windows (SPSS Inc., Chicago) and the level of statistical significance was corrected for multiple testing and set at ($p<0.002$). After which a post-hoc analysis was used to assess which groups

(HC subjects, NFI and FI DMD patients) were different. Fischer's Least Significant Difference (LSD) model was used to correct for multiple comparisons during post-hoc analysis, significance level was set at ($p<0.05$).

Results

Reconstructed T2 maps and corresponding fit of one of the voxel of the three analysed slices are visualized in Figure 1. Examples of 3T images and ^{31}P spectra of a non-fat infiltrated DMD patient, a fat infiltrated DMD patient and a healthy control subject are depicted in Figure 2. For the healthy controls, all the spectra reached the quality control criteria. For the DMD patients, 16 out of 90 spectra had to be excluded due to lack of sufficient quality (GL=6/18; GM 4/18; SOL= 1/18; TA=3/22; PER=2/18).

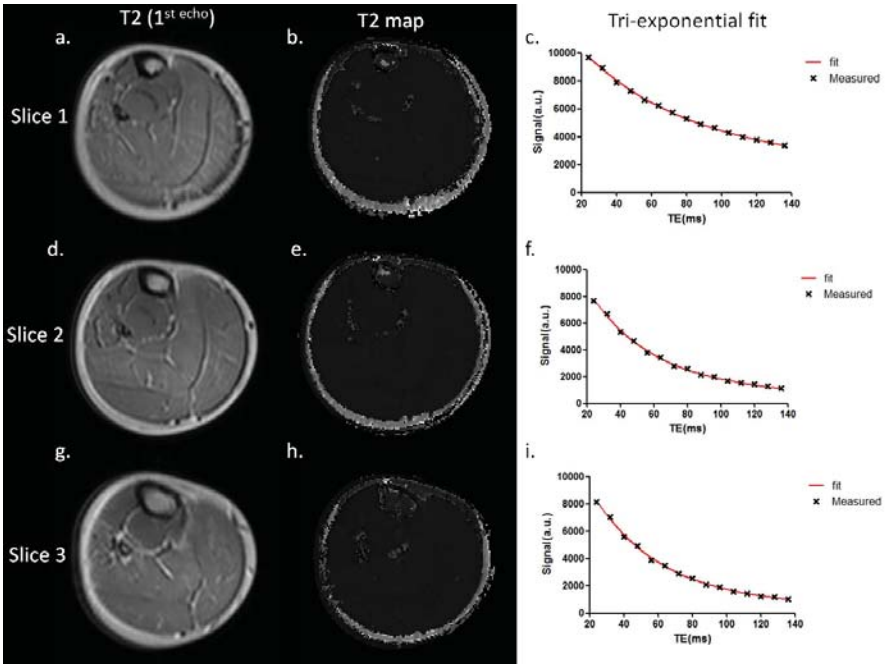

Figure 1. Axial multi-spin echo images of the right lower leg of a non-fat infiltrated DMD patient showing the 1st echo (TE: 8ms) of the three inner slices (a,d,g); the reconstructed T2 map of those three slices (b,e,h); and the corresponding fit of a single point located in the Soleus muscle for those three slices (c,f,i). the measured signal is shown using black crosses and the fitted signal using the red line. The first two echoes (not shown) were not used for the fit to eliminate potential influence of stimulated echoes. TE = echo timo (ms) and a.u. are arbitrary units.

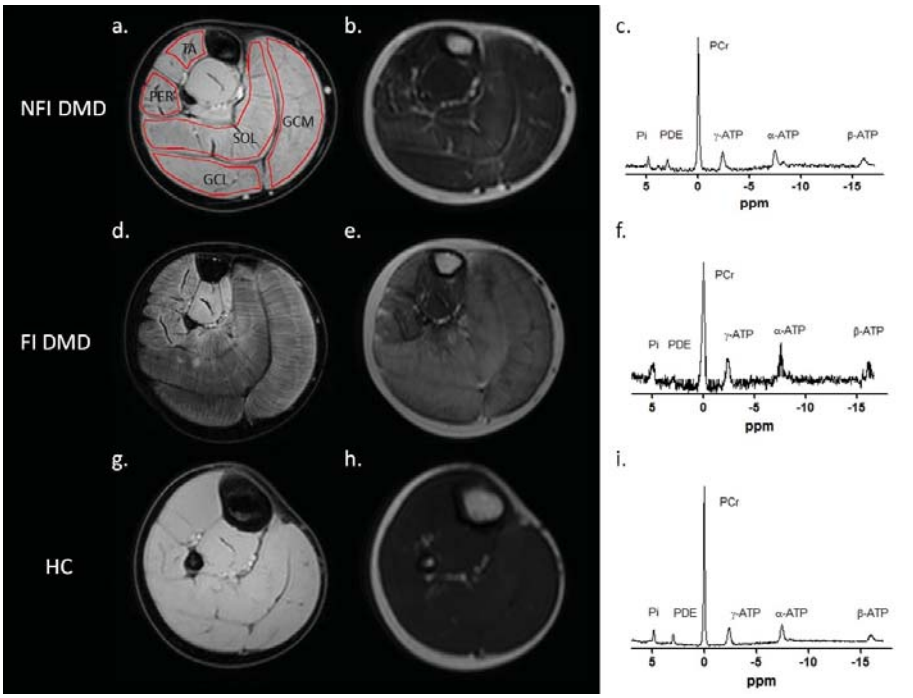

Figure 2. Axial images of the right lower leg of a FI DMD patient (a-c), NFI DMD patient (d-f) and a HC subject(g-i): (a, d, g);(a) proton images with a representation of the manually drawn ROIs for the five lower leg muscles - medial and lateral head of gastrocnemius (GM, GL), soleus (SOL), anterior tibialis (TA) and the peroneus (PER) muscles. (b, e, h); the 7th echo of a multi-spin-echo image (TE: 56 ms);(c, f, i) a representative ^{31}P spectrum for a FI DMD patient [c] NFI DMD patient [f] and a healthy control subject [i]. Note the reduction in SNR in the phosphorous spectrum of the DMD patient.

Metabolite ratios classified according to fat fraction

For the analysed muscles the NFI/FI DMD subgroups were divided as follows; GL NFI n=5/ FI n=7 (cut-off fat fraction 11.37%), GM NFI n=6/ FI n=8 (cut-off 10.05%), PER NFI n=4/ FI n=12 (cut-off 12.62%), SOL NFI n=7/ FI n=11 (cut-off 9.64%), TA NFI n=7/ FI n=8 (cut-off 10.81%). Metabolite ratios, T_2 values and fat fractions for the healthy controls and NFI and FI DMD patients are shown in the supplemental data (Table.1). Compared to healthy controls, PDE/ATP levels were significantly increased in the NFI and FI DMD group for all lower leg muscles ($p<0.05$), except for the PER muscle in the NFI DMD group ($p=0.19$)(Figure 3a). T_2 values were significantly increased in both the NFI and FI group in all muscles compared to healthy controls, except for the TA muscle in the NFI group (Figure 3b). In addition, intracellular tissue pH was significantly increased in the FI DMD group compared to healthy controls for all muscles ($p<0.01$), while in the NFI group the PER and TA muscle showed significantly increased pH levels. (Figure 4b) Pi/PCR was significantly elevated in the GL, SOL

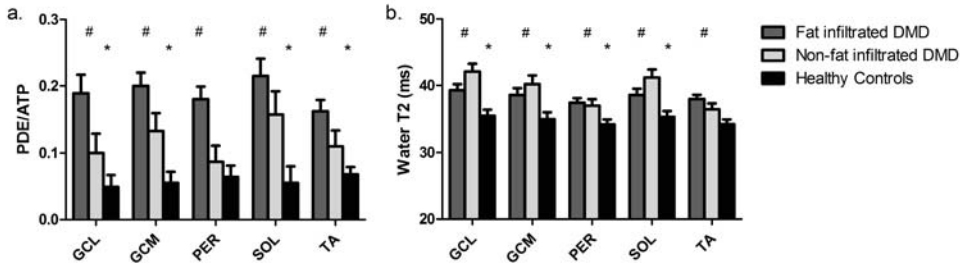

Figure 3. Mean values ±SD for PDE/ATP (a) and T_2 (b) in healthy controls (black) non-fat infiltrated DMD patients (light grey) and fat infiltrated DMD patients (dark grey) are shown per muscle. Significant differences between NFI DMD patients and controls are marked with an asterisk (*) and significant differences between FI DMD patients and controls are marked with an number sign (#). (PDE = phosphodiester, ATP=adenosine triphosphate, GL/GM= lateral and medial head gastrocnemius, PER= peroneus, SOL=soleus, TA=anterior tibialis)

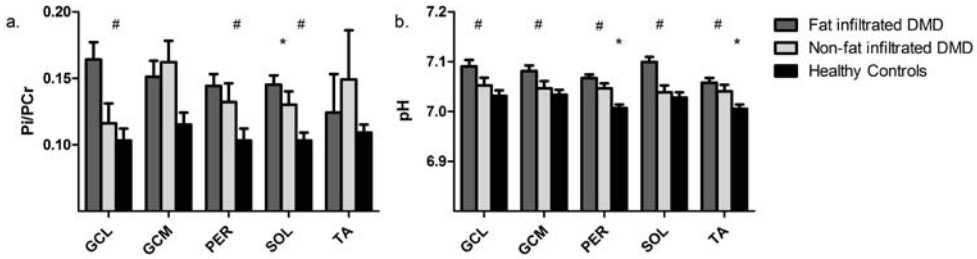

Figure 4. Mean values +/- SD for Pi/PCr (a) and pH (b) in healthy controls (black) non-fat infiltrated DMD patients (light grey) and fat infiltrated DMD patients (dark grey) are shown per muscle. Significant differences between NFI DMD patients and controls are marked with an asterisk (*) and significant differences between FI DMD patients and controls are marked with an number sign (#). (Pi = inorganic phosphate, PCr = phosphocreatine, GL/GM= lateral and medial head gastrocnemius, PER= peroneus, SOL=soleus, TA=anterior tibialis)

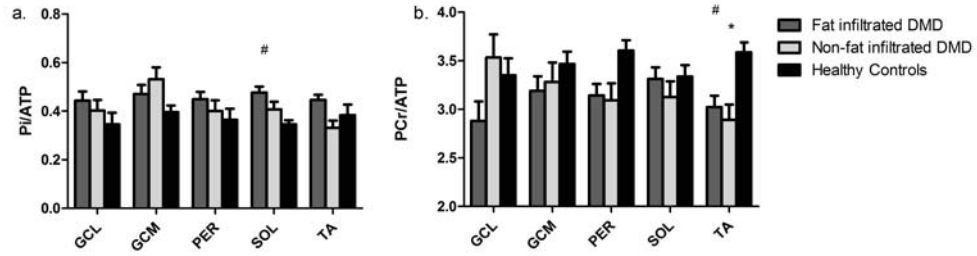

Figure 5. Mean values ±SD for Pi/ATP (a) and PCr/ATP (b) in healthy controls (black) non-fat infiltrated DMD patients (light grey) and fat infiltrated DMD patients (dark grey) are shown per muscle. Significant differences between NFI DMD patients and controls are marked with an asterisk (*) and significant differences between FI DMD patients and controls are marked with an number sign (#). (Pi = inorganic phosphate, PCr = phosphocreatine, ATP=adenosine triphosphate, GL/GM= lateral and medial head gastrocnemius, PER= peroneus, SOL=soleus, TA=anterior tibialis)

and PER muscle in the FI DMD group and in the SOL muscle in the NFI DMD group compared to healthy controls (Figure 4a). Pi/ATP was elevated in the SOL muscle for the FI group compared to healthy controls (Figure 5a). PCr/ATP was reduced in both the NFI and FI DMD group for the TA muscle compared to healthy controls. No changes were found for the other muscles (Figure 5b).

In the comparison of the FI groups versus the NFI group, only PDE/ATP was significantly elevated in all muscles, with exception of the SOL muscle. ($p<0.05$) In addition, T_2 values tended to be higher in NFI group compared to the FI group, although not significantly. ($p\geq0.074$) No consistent changes were found between NFI and FI DMD group for the other metabolites.

Discussion

In this study we used a combination of quantitative proton MRI and localized ^{31}P MR spectroscopy to evaluate high-energy phosphate levels and T_2 in DMD patients in muscles with and without fat replacement. By assessing ^{31}P metabolites at 7 tesla, we were able to localize the metabolic changes within individual muscles. Since in DMD (and many other muscular dystrophies muscles) tissue is replaced with fat at different rates and at different time points, the muscle specific multi parametric datasets obtained allows the evaluation of these pathophysiological processes in different disease stages.

Metabolic changes in the absence of fat

In DMD, it is thought that persistent inflammation due to muscle damage eventually results in replacement of muscle tissue with fat and fibrosis. [36] Consequently, indices which are sensitive to changes before fat replacement occurs are very valuable. Our results showed that PDE levels and T_2 values are already elevated compared to controls in muscles without increased fat levels. PDE levels have been hypothesized to reflect phospholipid membrane degradation products which in some situations proved to be reversible, while elevated T_2 values are attributed to changes in the extracellular and vascular spaces and are generally thought to reflect inflammation. [18, 37-39] Together these results suggest that these individual measures can reflect muscle damage prior to the more apparent structural changes. This is in accordance with previous work in DMD and BMD patients where elevated PDE levels were detected prior to structural changes. [17, 24] In addition, higher PDE/ATP levels were observed for all muscles in the FI DMD group compared to the NFI DMD group, with exception of the SOL muscle. This suggests that it might reflect the progressive

behaviour of the disease. This is in agreement with previous work which compared metabolic changes between patient groups and showed even higher PDE levels in DMD patients compared to BMD patients and DMD carriers. [19, 40] Interestingly, PDE showed to be one of the most responsive ^{31}P indices to AVV exon skipping treatment in the forelimb of GRMD dogs, changing towards more healthy values. [41] Subsequently, the elevated T_2 values in the absence of fat detected here are in agreement with previous work in DMD patients, showing increased water T_2 levels in combination with low fat fractions in the Vastus Lateralis and Soleus muscle. [42] To monitor potential therapeutic effects, the ability to distinguish between affected and less affected muscle tissue in combination with the ability to revert back to normal values are important features of a surrogate biomarker.

In addition to the metabolic changes, T_2 values were lower in all muscles with fat infiltration compared to the muscles without fat infiltration, although not significantly. This phenomenon is often mentioned in the MR literature and has mainly been attributed to the increase in fibrotic tissue in later stages of the disease. [17, 43] Recent histological work confirmed the presence of connective and fibrotic fibers which gradually start to increase after the age of 6. [44] Interestingly, T_2 values have been shown to decrease in response to three months of corticosteroid therapy in DMD patients.[15] In combination with the natural course of T_2 in DMD this indicates that T_2 as potential outcome measure is primarily valuable in the early phases of the disease.

Metabolic changes in the presence of fat

In muscles with increased fat infiltration, greater metabolic changes were present; in addition to PDE/ATP and T2 values, both Pi/PCr and intracellular tissue pH were significantly increased in majority of muscles with increased fat levels. The exact cause for the often-reported more alkaline intracellular tissue pH in muscular dystrophies is unclear. Two processes have been suggested to be involved; i.e. an altered proton sarcolemma membrane efflux mechanism due to a misbalance in Ca^+ and increased mitogenesis due to continuous muscle regeneration in DMD. The increase in Pi/PCr most likely is linked to elevated ADP concentrations due to poor coupling of the oxidative phosphorylation in resting muscle. [19, 22, 40] Interestingly, no consistent changes were found for Pi/ATP and PCr/ATP compared to controls. Up to now, all work in DMD found significantly reduced PCr/ATP levels and increased Pi/ATP levels. This contrast could be related to the studied DMD study populations. Most previous MR data have been obtained in older non-steroid treated DMD populations by using surface coil localization, resulting in more severely affected muscles, while here data was obtained relatively early in the disease course. [6, 17, 21, 22, 26, 40]

Almost no differences were detected between NFI and FI DMD group for Pi/PCr, Pi/ATP, PCr/ATP and pH which suggest non-progressive behaviour of these metabolic changes. This finding is partly in agreement with recently published longitudinal ^{31}P MRS data in the arm muscles of DMD patients which showed that none of the metabolic indices changed linearly with age. [26] The fact that Pi, PCr and intracellular tissue pH are predominantly changed in the presence of fat points out that these various processes might occur simultaneously. Fat fraction reflects loss of muscle tissue whereas metabolic changes, as they are solely detected in muscle tissue, are thought to reflect the quality of the remaining muscle tissue. These simultaneous processes yield complementary information and stress the importance of assessing multiple aspects of muscle damage in both early and later stages of the disease.

Taken combined, our results provide more insight in the time relation between the various pathophysiological processes which take place in muscle; as PDE/ATP and T_2 are elevated in the absence of fat, these might be the first signs of damage detectable with MR. Thereafter, apparently intracellular tissue pH and Pi/PCr become altered, as they are predominantly found in muscles with fat infiltration. Simultaneously with these metabolic changes, muscle tissue is replaced by fat and fibrotic tissue which is reflected by increased fat levels compared to controls and an apparent decrease in T_2 values. Finally, we showed only minor changes in muscle Pi/ATP and PCr/ATP. Suggesting that these metabolites remain relatively well preserved in the early disease stages. Based on previous work it seems that in later disease stages, muscle energy metabolism becomes increasingly misbalanced after which Pi/ATP and PCr/ATP also show changes. [6, 19, 22, 26] It is highly probable that this imbalance in energy metabolism will increase until all muscle tissue is replaced by fat and fibrotic tissue.

Limitations

Some limitations of the study should be acknowledged. First of all, a large number of spectra (16 out of 90) had to be discarded due to insufficient quality as a result of a low SNR in muscles with extensive fat replacement. This could have resulted in some bias in regards to the less severely affected muscles. However, as metabolic changes which were present in muscles without fat replacement were even more pronounced in muscles with fat replacement, we do not think that any changes that were present went undetected. Secondly, the identification of voxel solely in an individual muscle is somewhat complicated using a 2D-CSI sequence as the diameters of the muscle change along the length of the leg. To circumvent this problem, the anatomical images used to plan the 2D-CSI sequence were carefully checked to ensure that one voxel was located within one individual muscle over the full length of the coil prior to starting the scan. Thirdly, no B_1^+ correction was used for the tri-exponential T2 fitting

method applied here, which could have resulted in some bias in the determination of the T_2 values in areas with low $B1^+$. However, this seems to be particularly the case for the upper leg, [45] whereas due to the smaller dimensions the problem seems to be less pronounced in the lower leg. [46] Lastly, quantitative imaging datasets were acquired at 3T, while MRS data were acquired at 7T. To minimize localization errors as much as possible, the FISP sequence used for carefully positioning the 2D-CSI at the 7T was also assessed to select the corresponding slices on the 3-Point Gradient Echo Dixon and T2 MSE acquired at the 3T system.

Conclusion

In conclusion, our results show that with the combination of quantitative proton MRI and localized ^{31}P MR spectroscopy we were able to distinguish between early and late pathophysiological changes in DMD patients. Both PDE levels and T2 values are not only already changed prior to the presence of fat infiltration, but remain elevated in more severely affected muscles. This suggest that these measures could not only function as early markers for muscle damage, but could also reflect a potentially reversible pathology in more advanced stages of the disease. Future work will aim to assess spatially localized longitudinal multimodal MR measures in DMD to be able to evaluate these processes over time.

References

1. Bushby KMD, Gardnermedwin D. The Clinical, Genetic and Dystrophin Characteristics of Becker Muscular-Dystrophy .1. Natural-History (Vol 240, Pg 98, 1993). J Neurol 1993;240:453-453.
2. Hoffman EP, Brown RH, Kunkel LM. Dystrophin - the Protein Product of the Duchenne Muscular-Dystrophy Locus. Cell 1987;51:919-928.
3. Rosenberg AS, Puig M, Nagaraju K, et al. Immune-mediated pathology in Duchenne muscular dystrophy. Sci Transl Med 2015;7.
4. Willcocks RJ, Arpan IA, Forbes SC, et al. Longitudinal measurements of MRI-T-2 in boys with Duchenne muscular dystrophy: Effects of age and disease progression. Neuromuscular Disord 2014;24:393-401.
5. Arpan I, Forbes SC, Lott DJ, et al. T-2 mapping provides multiple approaches for the characterization of muscle involvement in neuromuscular diseases: a cross-sectional study of lower leg muscles in 5-15-year-old boys with Duchenne muscular dystrophy. Nmr Biomed 2013;26:320-328.
6. Newman RJ, Bore PJ, Chan L, et al. Nuclear Magnetic-Resonance Studies of Forearm Muscle in Duchenne Dystrophy. Brit Med J 1982;284:1072-1074.
7. Fischmann A, Hafner P, Fasler S, et al. Quantitative MRI can detect subclinical disease progression in muscular dystrophy. J Neurol 2012;259:1648-1654.
8. Fischmann A, Hafner P, Gloor M, et al. Quantitative MRI and loss of free ambulation in Duchenne muscular dystrophy. J Neurol 2013;260:969-974.
9. Hollingsworth KG, Garrood P, Eagle M, Bushby K, Straub V. Magnetic Resonance Imaging in Duchenne Muscular Dystrophy: Longitudinal Assessment of Natural History over 18 Months. Muscle Nerve 2013;48:586-588.
10. Wokke BH, van den Bergen JC, Versluis MJ, et al. Quantitative MRI and strength measurements in the assessment of muscle quality in Duchenne muscular dystrophy. Neuromuscular Disord 2014;24:409-416.
11. Akima H, Lott D, Senesac C, et al. Relationships of thigh muscle contractile and non-contractile tissue with function, strength, and age in boys with Duchenne muscular dystrophy. Neuromuscular Disord 2012;22:16-25.
12. Kim HK. T2 Mapping in Duchenne Muscular Dystrophy: Distribution of Disease Activity and Correlation with Clinical Assessments (vol 255, pg 899, 2010). Radiology 2010;256:1016-1016.
13. Kim HK, Laor T, Horn PS, Wong B. Quantitative Assessment of the T2 Relaxation Time of the Gluteus Muscles in Children with Duchenne Muscular Dystrophy: a Comparative Study Before and After Steroid Treatment. Korean J Radiol 2010;11:304-311.
14. Forbes SC, Walter GA, Rooney WD, et al. Skeletal Muscles of Ambulant Children with Duchenne Muscular Dystrophy: Validation of Multicenter Study of Evaluation with MR Imaging and MR Spectroscopy. Radiology 2013;269:198-207.
15. Arpan I, Willcocks RJ, Forbes SC, et al. Examination of effects of corticosteroids on skeletal muscles of boys with DMD using MRI and MRS. Neurology 2014;83:974-980.
16. Carlier PG. Global T2 versus water T2 in NMR imaging of fatty infiltrated muscles: Different methodology, different information and different implications. Neuromuscular Disord 2014;24:390-392.
17. Wary C, Azzabou N, Giraudeau C, et al. Quantitative NMRI and NMRS identify augmented disease progression after loss of ambulation in forearms of boys with Duchenne muscular dystrophy. Nmr Biomed 2015;28:1150-1162.
18. Araujo ECA, Fromes Y, Carlier PG. New Insights on Human Skeletal Muscle Tissue Compartments Revealed by In Vivo T2 NMR Relaxometry. Biophys J 2014;106:2267-2274.
19. Kemp GJ, Taylor DJ, Dunn JF, Frostick SP, Radda GK. Cellular Energetics of Dystrophic Muscle. J Neurol Sci 1993;116:201-206.

20. Newman RJ, Radda G. Phosphorus Nuclear Magnetic-Resonance Studies in Duchenne and Becker Dystrophy. Clin Sci 1982;63:P36-P36.
21. Griffiths RD, Cady EB, Edwards RHT, Wilkie DR. Muscle Energy-Metabolism in Duchenne Dystrophy Studied by P-31-Nmr - Controlled Trials Show No Effect of Allopurinol or Ribose. Muscle Nerve 1985;8:760-767.
22. Younkin DP, Berman P, Sladky J, Chee C, Bank W, Chance B. P-31 Nmr-Studies in Duchenne Muscular-Dystrophy - Age-Related Metabolic Changes. Neurology 1987;37:165-169.
23. Wary C, Azzabou N, Zehrouni K, et al. One year follow-up of Duchenne muscle dystrophy with nuclear magnetic resonance imaging and spectroscopy indices. Neuromuscular Disord 2014;24:853-853.
24. Wokke BH, Hooijmans MT, van den Bergen JC, Webb AG, Verschuuren JJ, Kan HE. Muscle MRS detects elevated PDE/ATP ratios prior to fatty infiltration in Becker muscular dystrophy. Nmr Biomed 2014;27:1371-1377.
25. Kan HE, Klomp DWJ, Wohlgemuth M, et al. Only fat infiltrated muscles in resting lower leg of FSHD patients show disturbed energy metabolism. Nmr Biomed 2010;23:563-568.
26. Hogrel JY, Wary C, Moraux A, et al. Longitudinal functional and NMR assessment of upper limbs in Duchenne muscular dystrophy. Neurology 2016;86:1022-1030.
27. Zijnen; JCvdBHBGAJvERPIJMdGPJWMP. Forty-Five years of Duchenne muscular dystrophy in the Netherlands. Journal of Neuromuscular Diseases 2014:99-109.
28. Naressi A, Couturier C, Devos JM, et al. Java-based graphical user interface for the MRUI quantitation package. Magn Reson Mater Phy 2001;12:141-152.
29. Bogner W, Chmelik M, Schmid AI, Moser E, Trattnig S, Gruber S. Assessment of (31)P Relaxation Times in the Human Calf Muscle: A Comparison between 3 T and 7 T In Vivo. Magn Reson Med 2009;62:574-582.
30. Taylor DJ, Kemp GJ, Woods CG, Edwards JH, Radda GK. Skeletal-Muscle Bioenergetics in Myotonic-Dystrophy. J Neurol Sci 1993;116:193-200.
31. Hamilton G, Yokoo T, Bydder M, et al. In vivo characterization of the liver fat H-1 MR spectrum. Nmr Biomed 2011;24:784-790.
32. Reeder SB, Hu HH, Sirlin CB. Proton density fat-fraction: a standardized MR-based biomarker of tissue fat concentration. J Magn Reson Imaging 2012;36:1011-1014.
33. Yu HZ, Shimakawa A, McKenzie CA, Brodsky E, Brittain JH, Reeder SB. Multiecho Water-Fat Separation and Simultaneous R-2* Estimation With Multifrequency Fat Spectrum Modeling. Magn Reson Med 2008;60:1122-1134.
34. Loughran T, Higgins DM, McCallum M, Coombs A, Straub V, Hollingsworth KG. Improving Highly Accelerated Fat Fraction Measurements for Clinical Trials in Muscular Dystrophy: Origin and Quantitative Effect of R2*Changes. Radiology 2015;275:570-578.
35. Azzabou N, Loureiro de Sousa P, Caldas E, Carlier PG. Validation of a generic approach to muscle water T2 determination at 3T in fat-infiltrated skeletal muscle. J Magn Reson Imaging 2015;41:645-653.
36. Azzabou N, Carlier PG. Fat quantification and T2 measurement. Pediatr Radiol 2014;44:1620-1621.
37. Sterin M, Cohen JS, Mardor Y, Berman E, Ringel I. Levels of phospholipid metabolites in breast cancer cells treated with antimitotic drugs: A P-31-magnetic resonance spectroscopy study. Cancer Res 2001;61:7536-7543.
38. Argov Z, Maris J, Damico L. Invivo Phosphorus Nuclear Magnetic-Resonance (P-31-Nmr) Study of Dystrophic Hamster Muscle. J Neurol Sci 1988;86:185-193.
39. Damon BM, Gregory CD, Hall KL, Stark HJ, Gulani V, Dawson MJ. Intracellular acidification and volume increases explain R-2 decreases in exercising muscle. Magn Reson Med 2002;47:14-23.

40. Barbiroli B, Funicello R, Iotti S, Montagna P, Ferlini A, Zaniol P. P-31-Nmr Spectroscopy of Skeletal-Muscle in Becker Dystrophy and Dmd Bmd Carriers - Altered Rate of Phosphate-Transport. J Neurol Sci 1992;109:188-195.
41. Le Guiner C, Montus M, Servais L, et al. Forelimb Treatment in a Large Cohort of Dystrophic Dogs Supports Delivery of a Recombinant AAV for Exon Skipping in Duchenne Patients. Mol Ther 2014;22:1923-1935.
42. Forbes SC, Willcocks RJ, Triplett WT, Rooney WD, Lott DJ. Magnetic Resonance Imaging and Spectroscopy Assessment of Lower Extremity Skeletal Muscles in Boys with Duchenne Muscular Dystrophy: A Multicenter Cross Sectional Study (vol 9, e106435, 2014). Plos One 2014;9.
43. Willcocks RJ, Rooney WD, Triplett WT, et al. Multicenter prospective longitudinal study of magnetic resonance biomarkers in a large duchenne muscular dystrophy cohort. Ann Neurol 2016;79:535-547.
44. Peverelli L, Testolin S, Villa L, et al. Histologic muscular history in steroid-treated and untreated patients with Duchenne dystrophy. Neurology 2015;85:1886-1893.
45. Brink WMV, M.J. ¡Peeters, J.M. ; Boernert, P. ; Webb, A.G.; . Passive radiofrequency shimming in the thighs at 3 Tesla using high permittivity materials and body coil receive uniformity correction. Magn Reson Med 2015:00:00.
46. Hooijmans MT, Dzyubachyk O, Nehrke K, et al. Fast multistation water/fat imaging at 3T using DREAM-based RF shimming. J Magn Reson Imaging 2015;42:217-223.

Supplementary data

	Controls	NFI DMD	FI DMD
GL	n=12	n= 5	n= 7
Pi/ATP	0.35±0.05	0.4±0.04	0.44±0.04
Pi/PCr	0.1±0.01	0.12±0.02	0.16±0.01*$
PCr/ATP	3.35±0.17	3.5±0.2	2.9±0.2
PDE/ATP	0.05±0.02	0.1±0.03*	0.19±0.03*$
pH	7.03±0.01	7.05±0.02	7.09±0.013*
T2 (ms)	35.5±0.9	42.1±1.2*	39.3±0.9*
Fat fraction(%)	8.4±1.5	11.7±1.7	46.8±19.7
GM	n=12	n= 6	n= 8
Pi/ATP	0.396±0.047	0.53±0.05	0.47±0.04
Pi/PCr	0.12±0.009	0.16±0.02	0.15±0.012
PCr/ATP	3.47±0.13	3.29±0.2	3.19±0.15
PDE/ATP	0.06±0.02	0.13±0.03*	0.2±0.02*$
pH	7.03±0.01	7.05±0.02	7.08±0.01*
T2 (ms)	34.9±1.02	40.2±1.3*	38.6±1*
Fat fraction(%)	7.6±1.2	9.7±1.1	50.1 ±21.8
PER	n= 12	n= 4	n= 12
Pi/ATP	0.37±0.05	0.4±0.05	0.45±0.03
Pi/PCr	0.1±0.01	0.13±0.01	0.14±0.01*
PCr/ATP	3.6±0.11	3.1±0.17	3.2±0.12
PDE/ATP	0.06±0.02	0.09±0.02	0.18±0.02*$

table continued

pH	7.01±0.01	7.05±0.01*	7.07±0.01*
T2 (ms)	34.2±0.7	36.9±0.97*	37.4±0.7*
Fat fraction(%)	10.2±1.2	12.2±0.6	38.7±21.2
SOL	n= 12	n= 7	n= 11
Pi/ATP	0.35±0.02	0.41±0.03	0.48±0.02*
Pi/PCr	0.1±0.01	0.13±0.01*	0.15±0.01*
PCr/ATP	3.34±0.12	3.13±0.16	3.3±0.12
PDE/ATP	0.06±0.02	0.16±0.04*	0.22±0.03*
pH	7.03±0.01	7.04±0.01	7.09±0.01*$
T2 (ms)	35.3±0.9	41.2±1.2*	38.6±0.9*
Fat fraction(%)	7.8±1.9	10.7±1.5	43.5±16.3
TA	n= 12	n= 7	n= 8
Pi/ATP	0.28±0.04	0.33±0.03	0.45±0.02
Pi/PCr	0.12±0.01	0.15±0.04	0.12±0.03
PCr/ATP	3.59±0.10	2.9±0.16*	3.02±0.12*
PDE/ATP	0.07±0.01	0.11±0.02*	0.16±0.02*$
pH	7.01±0.01	7.04±0.01*	7.06±0.01*
T2 (ms)	34.1±0.7	36.4±0.9	37.9±0.7*
Fat fraction(%)	8.2±1.3	8.9±1.2	30.1±8.9

Table 1. Mean values ±SD for the different metabolites, T2 and %fat in healthy controls, DMD patients with no fat infiltration (NFI) and DMD patients with fat infiltration (FI). Significant differences between patients and controls are marked with an asterisk (*). Significant differences between NFI and FI DMD patients are marked with a dollar sign ($). (Pi = inorganic phosphate, PDE = phosphodiester, PCr = phosphocreatine, ATP=adenosine triphosphate GL/GM= lateral and medial head gastrocnemius, PER= peroneus, SOL=soleus, TA=anterior tibialis)

5

Chapter 5

Spatially localized phosphorous metabolism of skeletal muscle in Duchenne Muscular Dystrophy patients: 24 –month follow-up

M.T. Hooijmans, N. Doorenweerd, C. Baligand, J.J.G.M. Verschuuren, I. Ronen, E.H. Niks, A.G. Webb, H.E. Kan

PLoS One. 2017 Aug 1;12(8): e0182086

Abstract

Objectives: To assess the changes in phosphodiester (PDE)-levels, detected by ^{31}P magnetic resonance spectroscopy (MRS), over 24-months to determine the potential of PDE as marker for muscle tissue changes in Duchenne Muscular Dystrophy (DMD) patients.

Methods: Spatially resolved phosphorous datasets were acquired in the right lower leg of 18 DMD patients (range: 5-15.4 years) and 12 age-matched healthy controls (range: 5-14 years) at three time-points (baseline, 12-months, and 24-months) using a 7T MR-System (Philips Achieva). 3-point Dixon images were acquired at 3T (Philips Ingenia) to determine muscle fat fraction. Analyses were done for six muscles that represent different stages of muscle wasting. Differences between groups and time-points were assessed with non-parametric tests with correction for multiple comparisons. Coefficient of variance (CV) were determined for PDE in four healthy adult volunteers in high and low signal-to-noise ratio (SNR) datasets.

Results: PDE-levels were significantly higher (two-fold) in DMD patients compared to controls in all analyzed muscles at almost every time point and did not change over the study period. Fat fraction was significantly elevated in all muscles at all timepoints compared to healthy controls, and increased significantly over time, except in the tibialis posterior muscle. The mean within subject CV for PDE-levels was 4.3% in datasets with high SNR (>10:1) and 5.7% in datasets with low SNR.

Discussion and Conclusion: The stable two-fold increase in PDE-levels found in DMD patients in muscles with different levels of muscle wasting over 2-year time, including DMD patients as young as 5.5 years-old, suggests that PDE-levels may increase very rapidly early in the disease process and remain elevated thereafter. The low CV values in high and low SNR datasets show that PDE-levels can be accurately and reproducibly quantified in all conditions. Our data confirms the great potential of PDE as a marker for muscle tissue changes in DMD patients.

Introduction

Duchenne Muscular Dystrophy (DMD) is an X-linked disease caused by a mutation in the *DMD* gene which codes for the protein dystrophin. The absence of dystrophin in the muscle cells results in progressive muscle weakness and muscle damage which is reflected by changes in energy metabolism, inflammation, fibrosis and eventually by progressive replacement of muscle tissue by fat. [1] Although numerous clinical trials have so far led to conditional approval of a few compounds by the Food and Drug Administration (FDA) and European Medical Association (EMA), there is still an urgent need for more effective therapies and outcome measures in DMD. [2]

Quantitative magnetic resonance imaging (MRI) and spectroscopy (MRS) of muscle are becoming increasingly important as potential outcome measures for therapeutic evaluations in DMD, with both fat fraction (%fat) and water T_2 being commonly used. [3] Therapy development aims to improve or preserve the quality of the muscle tissue. In order to inform about muscle tissue itself, a marker should reflect changes within the muscle and should have sufficient discriminative power. Unfortunately, neither %fat nor water T_2 fulfill these criteria. While %fat correlates well with function, it reflects the replacement of muscle by fat and therefore does not allow any statement on muscle tissue itself. [4-6] Water T2 has a closer relation with muscle, as it reflects inflammation and/or edema-like processes in this tissue. However, it has a low discriminative ability in DMD due to the use of corticosteroids – the difference in water T2 from a corticosteroid-treated boy with DMD and a healthy control is close to the detection limit of any difference. [7]

Assessment of energy metabolism in muscle using phosphorous (^{31}P) spectroscopy (MRS) has shown differences between healthy controls and DMD patients. [8-11] As the concentration of the metabolites visible with ^{31}P MRS is negligible in fat, this measurement almost exclusively measures muscle tissue. A broad variety of metabolic changes have been shown in DMD muscles, of which phosphodiesters (PDE) are especially interesting as a marker. PDE-levels are generally associated with membrane degradation products, and they are thought to reflect muscle membrane damage. [12] PDE levels have been shown to be elevated in the absence of increased fat%, and to remain elevated in more severely affected muscles in DMD. [13-15] They also revert back to normal after adeno-associated virus (AVV) vector therapy in Golden Retriever Muscular Dystrophy (GRMD) dogs, a canine model for DMD. [16] However, longitudinal assessments using ^{31}P MRS in DMD are very limited and hence it is unknown how PDE changes over time in the same individual muscle.[14] Since muscles in DMD patients become

affected at different time-points and at different rates it is essential to perform muscle specific measurements. [17, 18]

The overall aim of this work was to assess the time course of changes in phosphodiester (PDE)-levels detected by ^{31}P MRS in individual muscles over a 2-year time period, using spatially resolved ^{31}P MRS and quantitative Magnetic Resonance Imaging (qMRI) of lower leg muscles that represent different levels of muscle wasting. Because in DMD and many other muscular dystrophies muscle tissue is progressively replaced with fat, which directly reduces the SNR, we also aimed to assess the variability and accuracy of PDE-level quantification between two measurements. In addition, the effect of SNR on quantifying PDE-levels was assessed. Finally, the course of the Pi, PCr, ATP concentrations and intracellular tissue pH over two-year time-period were assessed with a post-hoc analysis. Our results show that PDE-levels were increased two-fold compared to healthy controls in muscles with different disease stages at virtually all time-points and did not change over a two-year period. The low CV and coefficient of reproducibility (CR) values in high and lower SNR datasets showed that PDE-levels can be accurately and reliably quantified in all conditions, which confirms the potential of PDE as an outcome measure.

Methods

Participants

DMD patients were recruited from the Dutch Dystrophinopathy Database [19] and all diagnoses were confirmed by genetic testing. A total of 18 DMD patients (mean: 9.8±2.6; range:5.5-15.4yrs.) and 12 healthy age-matched controls (mean:10.3±2.8; range:5-14yrs.) completed the baseline visit, 15 DMD patients (mean:10.2±2.9; range:6.5-16.4yrs.) and 10 healthy controls (mean:10.8±2.7; range:5-15yrs.) completed the 12-month follow-up, and 12 DMD patients (mean:9.85±2; range:7.5-17.7yrs.) and 10 healthy controls (mean:12.1±2.6; range:5-16yrs.) completed the 24-month follow-up. Among the DMD patients, 13 were ambulant throughout the entire study, and 5 were wheelchair bound at baseline. All used corticosteroids with intermittent dosing regimens (varying between 8-10 days on/off). One of the DMD patients lost ambulation between the baseline and 12-month follow-up visit. The study was approved by the local medical ethical committee of Leiden University Medical Center and written informed consent was obtained from all patients and parents. Participant recruitment started June 2013.

In addition, for quality control purposes only, a total of 4 male healthy control subjects (age range: 33-82yrs.) were included in the study and scanned twice on the same day to assess reproducibility. All subjects gave written informed consent.

MR Examination

^{31}P MRS datasets were obtained from the right lower leg using a 7T MR scanner (Philips, Achieva, Best, The Netherlands) with a custom-built double (^{31}P and ^{1}H) tuned volume coil. The subjects were positioned in a supine position with feet first into the scanner. The coil was placed at the thickest part of the calf directly distal to the patella, and scans were aligned with the tibia bone. The imaging protocol contained a 2D-Chemical Shift Imaging (CSI) dataset to assess energy metabolism (FOV 200x200/150x150 mm; matrix size 10 x 10; TR 2000 ms; samples 2048 ; FA 45°; Hamming weighted acquisition with 12 signal averages at the central k-lines), a B0 map as input for an image based shimming routine shimming (14 slices; slice thickness 8 mm, no slice gap; Repitition Time (TR)/ echo time (TE) 3000/3.11ms; FA 20°; FOV 160x180 mm) and a T1-weighted sequence for anatomical localization (15 slices; slice thickness 7mm; interslice gap 0.5 mm; TR 10 ms; TE 3.0 ms; flip angle (FA) 30°; FOV 180x200 mm). No slice selection was applied in feet/head direction for the 2D-CSI. As a result, ^{31}P signal was measured over the full length of the coil, which covered 12 cm of the lower leg. The T1-weighted sequence was used to plan the 2D-CSI in such a way that one individual voxel was located within one muscle over the entire length of the coil, taking into account that the diameter and boundaries between individual muscles and muscle groups change along the length of the lower leg. The survey and the T1-weighted sequence were used as a reference to position the subject, and to plan the imaging stack as accurately as possible between the three subsequent time-points. On the same day, 3-point DIXON images (23 slices; slice thickness/gap 10/5mm; TR/TE/ΔTE 210/4.41/0.76 ms; 2 number of signal averages (NSA); flip angle 8°; 1x1x10mm) were acquired on a 3T MR system (Philips Ingenia, Best the Netherlands) with an anterior 16-element receive array and 12-element posterior receive coils built into the patient table to quantify muscle fat fraction. The middle of the slice stack was positioned at the thickest part of the calf, to ensure accurate co-localization with the ^{31}P dataset.

Finally, four HC subjects were scanned twice on the same day with the same imaging protocol and settings as described above for the ^{31}P 2D-CSI datasets. Subjects were repositioned in the scanner, as accurately as possible, in between the two measurements and the survey and T1w sequence were used as reference to plan the 2D-CSI. CSI datasets were acquired as dynamic scans and retrospectively averaged to obtain datasets with 1 signal average for low SNR and one with 12 signal averages for high SNR.

Data-analysis

All phosphorous datasets were visualized with 3D chemical shift image package (3DCSi). Individual spectra were identified for six lower leg muscles: the lateral and medial head of the gastrocnemius (GCL and GCM), the peroneus (PER), the soleus (SOL), the tibialis anterior (TA) and tibialis posterior (TP) muscle, and exported as free induction decays. The FIDs were processed in the time domain using AMARES in the JMRUI software package (version 5, http://sermn02.uab.es/mrui/). [20] All metabolite signals were fitted with Gaussian line shapes, presented as a ratio over the γ-ATP or PCr signal, and corrected for T1 saturation effects using literature values.[21] In addition, the linewidth for PDE and β-ATP was set as described previously. [22] The shift in resonance between the Pi peak and PCr peak was used to calculate the intracellular tissue pH (pH=6.75+log((3.27-S)/(S-5.69))). [23] Since muscles become progressively replaced by fat in DMD, several spectra in the DMD patients suffered from low SNR. SNR values were determined for each individual spectrum and noise was calculated as the standard deviation of the residual signal after fitting. Spectra with a SNR lower than 10:1 for PCr and the inability to identify all metabolite signals were excluded.

Datasets from the four healthy volunteers were used to calculate the CV and CR to assess the repeatability and accuracy of quantifying PDE-levels between the two repeated measurements in high SNR (HH) condition, low SNR (LL) condition, and between the high and low SNR condition of the first scan (HL): this latter comparison is to mimic the loss in SNR over time due to increased fatty infiltration. The CV was calculated by dividing the standard deviation of the repeated measures by the mean of the repeated measures. In addition, a Bland-Altman plot was computed to show the CR, which is defined as 1.96 times the standard deviation of the paired differences, for the same conditions (HH, LL and HL) as the CV values. The mean within-subject CV values and CR values are reported for all three conditions. In addition, PDE-levels were quantified from spectra acquired in the TA muscle of a single healthy subject with different number of averages (NSA= 1, 2, 3, 4, 6 and 12), resulting in varying SNR. Results were plotted as a function of the SNR of the PCr peak. The voxel was placed partly outside the leg in order to reach sufficiently low SNR. Similar analysis for other muscles was not feasible in practice because of the intrinsically higher SNR and the inability to place the voxel partly outside the leg. The 95% confidence interval of the plateau of the exponential fit was assessed to determine a SNR cut-off.

Fat and water images were reconstructed from 3-point Dixon images according to a six-peak fat model and used to calculate muscle fat fractions (SI) fat/(SI fat+ SI

water))*. [100] (Hu et al 2008) The protocol was optimized to minimize T1 relaxation effects. The reconstruction did not account for T2* relaxation times. Regions of interest (ROI) were manually drawn for the six individual lower leg muscles on all the slices within the coverage of the 2D-CSI using Medical Image Processing Analysis and Visualization (MIPAV) software (http://mipav.cit.nih.gov). %Fat is presented as the mean value of all pixels within a ROI over multiple slices covering the same region as the 2D CSI.

Statistical Analysis

For the reproducibility assessment in healthy volunteers, a Spearman correlation was used to show the between-measurement reproducibility of PDE-levels for the three SNR comparisons. Subsequently, a Bland-Altman plot was used to assess the agreement between the two repeated measurements for HH, LL, HL conditions.

For the primary analysis, differences in PDE-levels and %fat between healthy controls and DMD patients at baseline, 12-month follow-up and 24-month follow-up were assessed with a Mann-Whitney U test with correction for multiple comparisons ($p<0.001$). Thereafter, a Friedman test was used to assess differences in PDE-levels and %fat in DMD patients between the subsequent time-points. Here, the level of significance was set at $p<0.01$.

Post-hoc analyses were done to determine the relationship between PDE-levels and age in the TP muscle in DMD patients at baseline, using a Spearman correlation and for the difference in Pi, PCr, ATP and intracellular pH between patients and controls, as well as for the patients over time. We focused the analysis on the TP muscle as it was the only muscle which did not show differences in PDE-levels and %fat at baseline. The between-group analyses were done with a Mann-Whitney U test, and within the DMD group over time with a Friedman test ($p<0.05$). All statistical analyses were performed in SPSS version 20 for Windows (SPSS Inc., Chicago)

Results

Phosphorous MR spectra and reconstructed water maps for a representative DMD patient for all three time points are shown in Figure 1. All spectra reached the quality control criteria for the healthy controls at baseline, five out of 60 spectra were excluded at 12-month follow-up and all spectra reached quality control at 24-month follow-up. For the DMD subjects 19 out of 108 spectra had to be excluded at baseline, 11 out of 90 at 12-month follow-up, and 4 out of 72 at 24-month follow-up. All of the

spectra of the HC datasets obtained for the reproducibility assessment reached the quality control criteria.

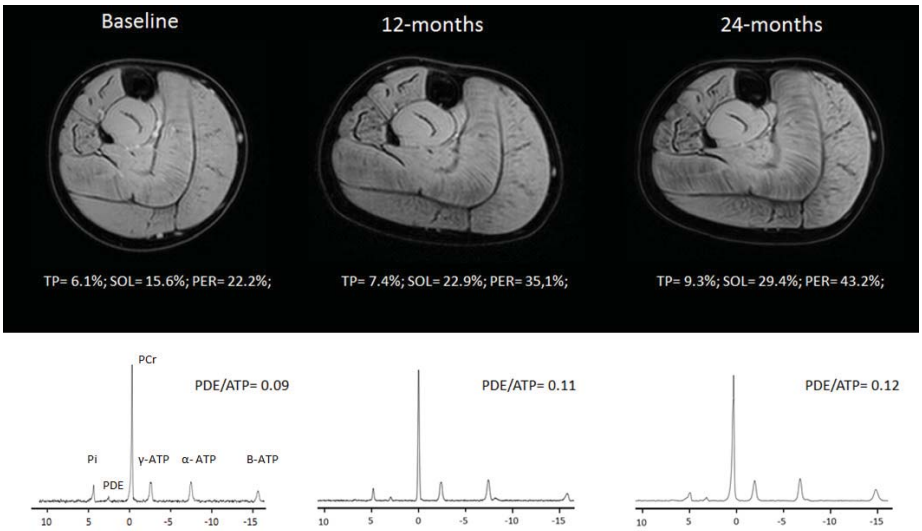

Figure 1. Representative reconstructed water images of the right lower leg and phosphorous spectra of the TP muscle of a DMD patient at baseline, 12-months and 24-months. PDE-levels in TP muscles are presented in the graph and %fat for the all analyzed muscle for all three time points are stated here: (Baseline GCL:5.6%;GCM:7.3%; SOL: 7.1%; PER:14,4%; TA: 6.24%; TP: 4.2%; 12-months: GCL: 6,6%; GCM:8.8%; SOL: 5.2%; PER:20.6%; TA: 5.71%; TP: 4.3%; 24-months: GCL:10.1%; GCM:11.3% SOL: 5.9%; PER:24.7%; TA: 7.3%; TP: 4.3%)

Repeated measures and effect of SNR

To simulate intermediate fat infiltrated muscles, we generated low SNR datasets (NSA=1, SNR=15.2±4.1), and compared them to high SNR datasets (NSA=12, SNR=22.1 ±0.7). Quantification of PDE-levels proved to be highly reproducible in all three conditions with a mean within-subject CV of 4.3% (range:0.29-19%) in the HH condition (mean SNR: 22.1; range: 20.8-23.1), a mean within-subject CV of 5.7% (range:0.03-17.5%) in the LL condition (mean SNR: 15.2; range: 7.5-21.3), and a mean within-subject CV of 7.3% (range:0.73-26.3%) in the HL condition. This high reproducibility was also confirmed by intra-class correlation coefficients of 0.98 for the HH condition, 0.97 in LL condition and 0.93 in HL condition and good agreement in the Bland Altman plots. (Figure 4) In addition, we found that PDE-levels were overestimated at lower SNR levels of the PCr peak in the TA muscle (Figure 5). Based on the exponential fit, it seems that PDE-levels can be quantified within 95% of the confidence interval above SNR levels of 10.4:1 for the PCr peak in the TA muscle.

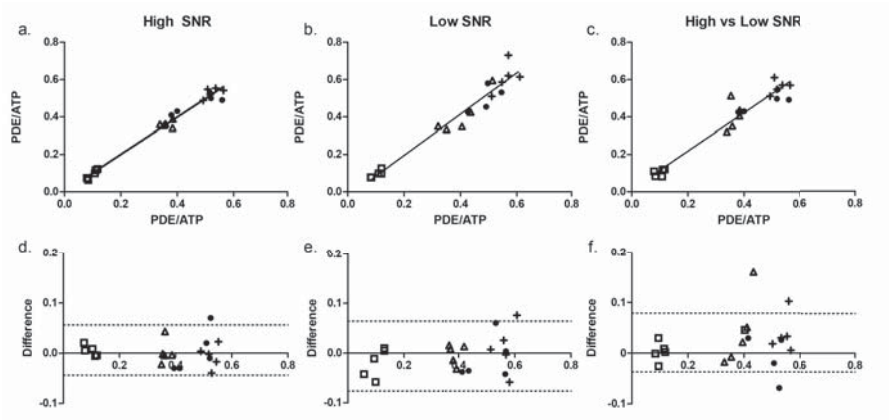

Figure 2. Intra-class correlation coefficient between PDE-levels from the two repeated measurements and Bland-Altman plots of the difference in PDE-levels between the two repeated measurements for HH condition (a&d), the LL condition (b&e) and the HL condition (c&f). The five individual subjects are labelled with different symbols. Each symbol represents one individual muscle of an individual subject. The black line is the line of identity.

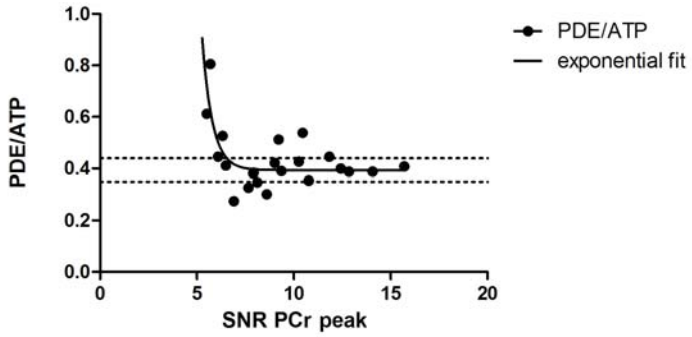

Figure 3. PDE/ATP as a function of SNR of the PCr peak. Each data point represents PDE/ATP assessed from the tibialis anterior muscle of the same subject under different SNR conditions. The black line represents the exponential fit and the dashed lines the 95% confidence interval of the estimated plateau.

%fat and PDE-levels

PDE-levels were significantly elevated compared to healthy controls at all time-points for all individual leg muscles ($p<0.001$), with the exception of the TP muscle at baseline ($p=0.004$). No differences were found in PDE-levels between baseline, 12-month follow-up and 24-month follow-up for the individual muscles ($p>0.01$).

(Figure 2.) However, post-hoc analysis showed a significant positive correlation with age in the TP muscle at baseline (R=0.79 p=0.01). This was also the only muscle in which fat fraction was not significantly elevated. In addition, %fat significantly increased over time for the GCM, GCL, SOL and PER muscle. No differences in %fat were detected between time-points for the TA (p =0.061) and the TP muscle (p=0.097) (Figure 5).

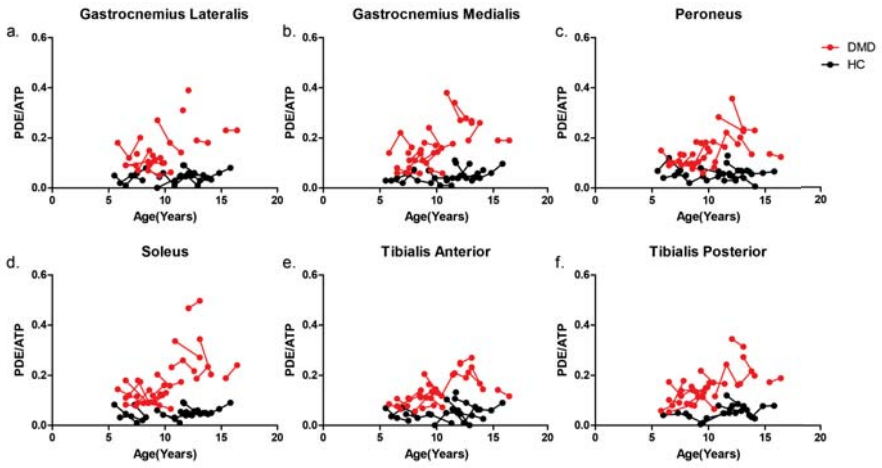

Figure 4. Individual trajectories of PDE-levels plotted as a function of age in DMD patients (Red) and HC subjects (Black) for the GCL (a), GCM (b), PER (c), SOL (d), TA (e) and TP (f) muscle. The dots with a connecting line represent an individual subject. PDE-levels were significantly different between groups but did not change over a two-year time period.

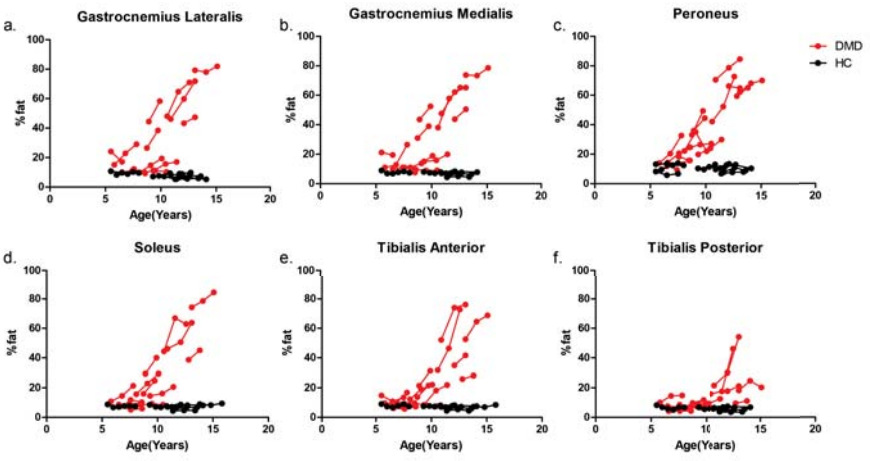

Figure 5. Individual trajectories of fat fraction plotted as a function of age in DMD patients (Red) and HC subjects (Black) for the GCL (a), GCM (b), PER (c), SOL (d), TA (e) and TP (f) muscle. The dots with a connecting line represent an individual subject. Fat fractions were significantly increased compared to controls in all muscles and all time points with the exception of the TP and TA muscle.

Post-hoc analysis for the other metabolic indices

Mean and standard deviation of the metabolic indices in the DMD patients and HC subjects at the three time points are shown in Table 1. The individual trajectories of the metabolic indices and pH as a function of age in the TP muscle are shown in Figure 6. Intracellular tissue pH was significantly elevated compared to controls in all analyzed muscles at baseline, 12-month follow-up and 24-month follow-up, with the exception of the TP muscle at 12-month and 24-month follow-up. Pi/PCr was significantly increased compared to healthy controls in all muscles at baseline, in the SOL and PER muscle at 12-month follow-up and in the SOL, PER, TP and GCL muscle at 24-month follow-up. In addition, elevated Pi/ATP was found in the SOL and PER muscle at baseline, in the SOL and GCM at 12-month follow-up and in all muscles except the TA muscle at 24-month follow-up. Finally, PCr/ATP was significantly decreased compared to controls in the PER, TP, and TA muscle at baseline. No differences were found between groups at the subsequent time points. None of the metabolic indices changed over the three time points. However, more pronounced changes, although not at a statistically significant level, were visible at 24-month follow-up compared to the other time-points.

	DMD			HC		
	Baseline	**12months**	**24months**	**Baseline**	**12months**	**24months**
pH						
GCL	7,07±0,04*	7,06±0,04*	7,06±0,02**	7,03±0,03	7,02±0,02	7,01±0,01
GCM	7,07±0,04*	7,07± 0,05*	7,08±0,04**	7,03±0,03	7,02±0,02	7,01±0,02
PER	7,06±0,03**	7,05±0,04*	7,05±0,03**	7,01±0,02	7,02±0,03	7,00±0,01
SOL	7,08±0,05*	7,06±0,05*	7,07±0,03**	7,03±0,02	7,02±0,02	7,01±0,01
TA	7,05±0,03**	7,05±0,03*	7,04±0,03**	7,003±0,02	7,001±0,03	6,97±0,02
TP	7,06±0,03**	7,05±0,04	7,05±0,03	7,008±0,02	7,02±0,02	7,01±0,02
Pi/PCr						
GCL	0,14±0,05*	0,12 ±0,05	0,11±0,02*	0,11±0,02	0,09±0,02	0,09±0,02
GCM	0,16±0,04*	0,13±0,02	0,13±0,05	0,12±0,03	0,11±0,02	0,11±0,02
PER	0,14±0,03*	0,14±0,02*	0,14±0,04*	0,10±0,03	0,11±0,02	0,09±0,02
SOL	0,14±0,03**	0,13±0,04**	0,13±0,03*	0,10±0,016	0,11±0,02	0,10±0,02
TA	0,15±0,04*	0,13±0,03	0,12±0,02	0,11±0,02	0,12±0,03	0,10±0,02
TP	0,13±0,03*	0,13±0,02	0,14±0,03*	0,09±0,03	0,10±0,02	0,09±0,04
Pi/ATP						
GCL	0,43±0,09	0,36±0,11	0,36±0,07*	0,35±0,09	0,30±0,06	0,31±0,06
GCM	0,46±0,08	0,38 ±0,07*	0,44±0,13*	0,4±0,11	0,32±0,06	0,34±0,06
PER	0,43±0,11*	0,39±0,08	0,42±0,09*	0,38±0,07	0,34±0,08	0,30±0,05
SOL	0,46±0,09**	0,37±0,09**	0,42±0,09*	0,35±0,07	0,32±0,06	0,32±0,06
TA	0,43±0,09	0,37±0,06	0,38±0,09	0,38±0,07	0,37±0,12	0,34±0,06
TP	0,39±0,07	0,39±0,06	0,39±0,06*	0,35±0,10	0,33±0,07	0,27±0,11

Table 1. Continued

PCr/ATP						
GCL	3,15±07	3,0±0,56	3,37±0,2	3,35±0,33	3,09±0,38	3,3±0,31
GCM	3,22±0,45	2,89±0,44	3,38±0,35	3,47±0,42	2,96±0,37	3,36±0,24
PER	3,13±0,37*	2,82±0,31	3,21±0,41	3,6±0,39	3,18±0,48	3,34±0,26
SOL	3,23±0,4	2,87±0,45	3,28±0,28	3,34±0,39	2,98±0,41	3,4±0,22
TA	2,97±0,38*	2,86±0,3	3,23±0,3	3,56±0,29	3,16±0,36	3,36±0,41
TP	3,02±0,37*	3,09±0,31	2,94±0,27	3,68±0,34	3,27±0,26	3,21±0,47
PDE/ATP						
GCL	0,17±0,09#	0,13±0,07#	0,13±0,04#	0,05±0,03	0,05±0,02	0,04±0,02
GCM	0,17±0,09#	0,17±0,09#	0,16±0,07#	0,06±0,03	0,04±0,01	0,06±0,03
PER	0,16±0,08#	0,13±0,06#	0,14±0,04#	0,06±0,03	0,05±0,03	0,06±0,02
SOL	0,17±0,11#	0,15±0,11#	0,14±0,07#	0,06±0,02	0,05±0,01	0,04±0,03
TA	0,14±0,0⁶#	0,12±0,06#	0,14±0,05#	0,06±0,03	0,05±0,02	0,03±0,03
TP	0,14±0,08	0,16±0,06#	0,15±0,11#	0,07±0,03	0,07±0,02	0,05±0,02

Table 1. Mean values ±SD for the Pi/PCr, Pi/ATP, PCr/ATP and intracellular tissue pH in healthy controls and DMD. Significant differences between patients and controls are marked with an asterisk (*) for p<0.05,with a double asterisk (**) for p<0.0005 and with a hashtag (#) for p<0.001. Pi = inorganic phosphate, PDE = phosphodiester, PCr = phosphocreatine, ATP=adenosine triphosphate GCL/GCM= lateral and medial head gastrocnemius, PER= peroneus, SOL=soleus, TA=anterior tibialis, TP = posterior tibialis

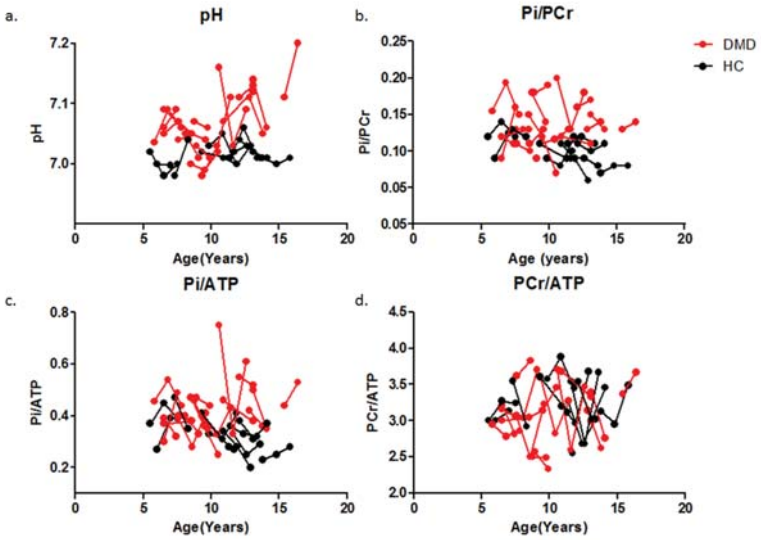

Figure 6. Individual trajectories of Pi/PCr (a), pH (b), PI/ATP (c) and PCr/ATP (d) plotted as a function of age in DMD patients (Red) and HC subjects (Black) for the TP muscle. The dots with a connecting line represent an individual subject. Note the inconsistent changes in PCr/ATP and the more pronounced changes above the age of 10 years.

Discussion

Repeatability assessment

In this study, we assessed the accuracy and reproducibility of quantifying PDE-levels by using spatially resolved ^{31}P MRS data in low and high SNR conditions in healthy volunteers. Our data proved that quantification of PDE-levels is highly reproducible between measurements in both the HL, LL and HH conditions, which is reflected by low CV values, high intra-class correlations, and good levels of agreement. As the number of studies assessing the reproducibility of resting energy metabolites in muscle is limited, comparison to literature values is challenging. However, they are in line with the reproducibility values of different metabolic markers and exchange rate constants using dynamic ^{31}P MRS in healthy controls, where CV values ranged between 8-11% for phosphate concentrations, between 4 and 12% for PCr recovery and between 3.4 and 20% for exchange rate constants of PCr-to-ATP [24-26]. Generally, CV values of 10% or less are considered to be an acceptable level of agreement between measurements [27]. Previous studies assessed the reproducibility of %fat, cross-sectional area (CSA) and water T2 measurements, commonly used MR imaging measures in DMD, in both HC subjects and DMD patients within and between centers. CV values ranging from 0.8-8% were reported within centers with a mean CV of 4.9%, 3.1% and 3.7% for %fat, CSA and T2 relaxation times [28-30]. CV values of 1.8-7.2% were reported across centers with a mean CV of 7.2, 3.4 and 1.8 for %fat, CSA and water T2 relaxation times (^{1}H-MRS). [28] The CV values found in the present work, for the high, low and high versus low SNR conditions, are similar to those of %fat and (water) T2 relaxation times found in literature and below the general acceptable level of agreement (<10%). This indicates that even in more severely affected patients, simulated by the reduced SNR datasets, one can accurately quantify PDE-levels. However, the question remains whether this would be sufficient discriminative power to be able to detect potential treatment effects.

PDE-levels

Longitudinal and spatially resolved ^{31}P MRS and qMRI data was used to assess the time course of changes in phosphodiester (PDE)-levels over 2-years in DMD patients, in muscles with different levels of muscle wasting. Our results showed that PDE-levels were significantly elevated in DMD patients compared to controls regardless of the level of muscle wasting at virtually all time-points, and did not change over a two-year time period. This indicates that, although DMD boys were recruited as early as 5.5-year-old, PDE levels were elevated prior to the inclusion of the study. The only muscle that did not show abnormal PDE-levels was the TP muscle at baseline. Interestingly, this muscle is known to be affected relatively late in the

course of the disease, which was confirmed in our data by normal %fat at baseline. At later time points, PDE levels became significantly elevated in the TP muscle. This suggests that PDE-levels may increase very early in the disease process, after which they apparently become more stable. This is in agreement with previous work in which PDE-levels of the forearm muscles did not correlate with age in ambulant DMD patients and did not show an increase over one year time. [13, 14] This hypothesis is also strengthened by our own results in the other muscles which did not show a change in PDE-levels over a two-year time period and by the significant correlation with age in the TP muscle at baseline. However, previous work also showed that PDE-levels did correlate with disease progression in non-ambulant patients as well as that PDE-levels showed to be higher in more severely affected patients. [15] Visual inspection of our graphs also suggests a non-linear relation between PDE-levels and age. Consequently, it is likely that PDE-levels do increase with disease progression but much slower than %fat and that a much longer timeframe is needed in order to measure this progression.

PDE-levels in DMD are generally associated with membrane degradation products of the preferentially affected glycolytic Type II fibers. [31] However, the precise origin of this elevation in PDE is not fully understood. Many other diseases have displayed altered intra-cellular PDE-levels in muscle. For instance, in spinal cord injury and congenital lipodystrophy, it has been associated with oxidative stress. [32, 33] In obesity and diabetes altered PDE-levels have been related to reduced mitochondrial capacity. [34] After statin use, in fibromyalgia, Becker muscular dystrophy and facioscapulohumeral muscular dystrophy (FSHD), these alterations have been ascribed to abnormal membrane metabolism associated with muscle dysfunction. [11, 22, 35] In addition, PDE-levels have been shown to be related to a higher content of oxidative type I fibers, to reflect impaired oxidative muscle metabolism, and to increase with respect to age, physical activity level and BMI. [36-38] The total PDE signal measured with ^{31}P MRS originates from glycerol 3-phosphocholine (GPC) and glycerol 3-phosphoethanolamine (GPE), which are both related to membrane phospholipid metabolism. [12, 39-41] Recent work showed that GPC, rather than a combination of GPE and GPC, was the main contributor to the changes observed in muscular PDE-levels in obesity and diabetes.[25] GPC has been shown to accumulate due to inhibition of oxidative phosphorylation, which strengthens the relationship with impaired oxidative capacity. [42] Unfortunately, the SNR of our data was too low to ascribe the changes found in myocellular PDE to either GPC or GPE. Although, the exact underlying cause for the elevation in PDE remains unclear and might be multifactorial, this work points out that myocellular PDE-levels detected with ^{31}P MRS are extremely interesting in DMD

Longitudinal evaluation of the other metabolic indices

The majority of the results from the between-group analysis at the three different time-points were in agreement with prior cross-sectional work and have been discussed previously. [10, 15, 43-46] The longitudinal analysis showed that none of the metabolic indices differed between the subsequent time points, which suggests that all metabolic alterations remain stable over a two-year time period. These findings are in agreement with a one year follow-up study in the forearm muscles of DMD patients.[14] In contrast, the majority of the previous cross-sectional ^{31}P MRS studies in more severely affected DMD patients, did show more pronounced metabolic alterations. [10, 15, 44, 45] Similar behavior was visible above the age of 10 in our data, although not reaching statistical significance. Therefore, our results and those of others together suggest that the metabolic indices most likely show a very slow potentially non-linear progression over time after the initial increase. Even though none of the metabolic indices changed over the two-year time period in our study, those metabolic alterations do reflect status of muscle tissue and could therefore provide important insights into the underlying pathophysiology.

Limitations

Some limitations of the study should be acknowledged. Firstly, some of the MR spectra had to be discarded due to insufficient quality. This could have resulted in some bias towards less severely affected muscles and could possibly explain that no significant abnormalities were found in PCr/ATP ratios. Secondly, the number of patients in the DMD group at 24-month follow-up was relatively low compared to the other time-points. The DMD patients who were unable to participate at 24-month follow-up were generally of older age. Therefore, the results could be biased towards less severely affected muscles and this might have resulted in smaller differences in metabolic indices over the time-points. However, all patients were able to participate in the 12-month follow-up and no changes were detected between baseline and 12-month follow-up. Therefore it seems unlikely that this had a major influence on our results. Thirdly, as the diameter of the muscles changes along the length of the lower leg, it is somewhat difficult to position an individual voxel of the 2D-CSI within an individual muscle over the full length of the coil. The T1-weighted images, obtained as anatomical reference, were carefully used in order to ensure that one individual voxel was located within one individual muscle over the full length of the coil in order to minimize this problem. Fourthly, the fact that DMD boys and HC boys inevitably grow during a 2-year longitudinal study complicates accurate repositioning between subsequent time-points. To circumvent this problem, the T1-weighted images from the previous time-point were used as a visual reference to ensure that 2D-CSI was located at a similar position along the proximo-distal

muscle axis. However, the fact that the size of the leg could have increased between the subsequent time points makes it impossible to cover the exact same region. In addition, the SNR of the ^{31}P MRS datasets in this work was insufficient to separate GPC and GPE. Previous work showed that, in order to reach sufficient SNR, surface coil localized measurements are necessary. However, with those measurements it is impossible to obtain muscle specific measurements, which is essential in DMD as muscles become affected at different time points and with different rates. Lastly, the relation between SNR and quantification of PDE-levels was only assessed for the TA muscle and in one of the subjects. Therefore, it is possible that this relation is different in the other lower leg muscles. However, this is highly unlikely as accuracy of quantification depends on data-quality and not muscle-type.

Conclusion

The two-fold elevation in PDE-levels compared to controls detected prior to structural changes and the high reproducibility of the measurements in low and high SNR conditions confirm the potential of PDE as a marker for muscle tissue changes in DMD patients.

References

1. Rosenberg AS, Puig M, Nagaraju K, et al. Immune-mediated pathology in Duchenne muscular dystrophy. Sci Transl Med 2015;7.
2. Willcocks RJ, Rooney WD, Triplett WT, et al. Multicenter prospective longitudinal study of magnetic resonance biomarkers in a large duchenne muscular dystrophy cohort. Ann Neurol 2016;79:535-547.
3. Straub V, Balabanov P, Bushby K, et al. Stakeholder cooperation to overcome challenges in orphan medicine development: the example of Duchenne muscular dystrophy. Lancet Neurol 2016;15:882-890.
4. Wokke BH, van den Bergen JC, Versluis MJ, et al. Quantitative MRI and strength measurements in the assessment of muscle quality in Duchenne muscular dystrophy. Neuromuscular Disord 2014;24:409-416.
5. Fischmann A, Hafner P, Fasler S, et al. Quantitative MRI can detect subclinical disease progression in muscular dystrophy. J Neurol 2012;259:1648-1654.
6. Hollingsworth KG, Garrood P, Eagle M, Bushby K, Straub V. Magnetic Resonance Imaging in Duchenne Muscular Dystrophy: Longitudinal Assessment of Natural History over 18 Months. Muscle Nerve 2013;48:586-588.
7. Arpan I, Willcocks RJ, Forbes SC, et al. Examination of effects of corticosteroids on skeletal muscles of boys with DMD using MRI and MRS. Neurology 2014;83:974-980.
8. Newman RJ, Bore PJ, Chan L, et al. Nuclear Magnetic-Resonance Studies of Forearm Muscle in Duchenne Dystrophy. Brit Med J 1982;284:1072-1074.
9. Kemp GJ, Taylor DJ, Dunn JF, Frostick SP, Radda GK. Cellular Energetics of Dystrophic Muscle. J Neurol Sci 1993;116:201-206.
10. Griffiths RD, Cady EB, Edwards RHT, Wilkie DR. Muscle Energy-Metabolism in Duchenne Dystrophy Studied by P-31-Nmr - Controlled Trials Show No Effect of Allopurinol or Ribose. Muscle Nerve 1985;8:760-767.
11. Younkin DP, Berman P, Sladky J, Chee C, Bank W, Chance B. P-31 Nmr-Studies in Duchenne Muscular-Dystrophy - Age-Related Metabolic Changes. Neurology 1987;37:165-169.
12. Burt CT, Glonek T, Barany M. P-31 Nuclear Magnetic-Resonance Detection of Unexpected Phosphodiesters in Muscle. Biochemistry-Us 1976;15:4850-4853.
13. Wary C, Azzabou N, Giraudeau C, et al. Quantitative NMRI and NMRS identify augmented disease progression after loss of ambulation in forearms of boys with Duchenne muscular dystrophy. Nmr Biomed 2015;28:1150-1162.
14. Hogrel JY, Wary C, Moraux A, et al. Longitudinal functional and NMR assessment of upper limbs in Duchenne muscular dystrophy. Neurology 2016;86:1022-1030.
15. Hooijmans MT, Niks EH, Burakiewicz J, Verschuuren JJ, Webb AG, Kan HE. Elevated phosphodiester and T2 levels can be measured in the absence of fat infiltration in Duchenne muscular dystrophy patients. Nmr Biomed 2017;30.
16. Le Guiner C, Montus M, Servais L, et al. Forelimb Treatment in a Large Cohort of Dystrophic Dogs Supports Delivery of a Recombinant AAV for Exon Skipping in Duchenne Patients. Mol Ther 2014;22:1923-1935.
17. Kinali M, Arechavala-Gomeza V, Cirak S, et al. Muscle histology vs MRI in Duchenne muscular dystrophy. Neurology 2011;76:346-353.
18. Akima H, Lott D, Senesac C, et al. Relationships of thigh muscle contractile and non-contractile tissue with function, strength, and age in boys with Duchenne muscular dystrophy. Neuromuscular Disord 2012;22:16-25.
19. Zijnen; JCvdBHBGAJvERPIJMdGPJWMP. Forty-Five years of Duchenne muscular dystrophy in the Netherlands. Journal of Neuromuscular Diseases 2014:99-109.
20. Naressi A, Couturier C, Devos JM, et al. Java-based graphical user interface for the MRUI quantitation package. Magn Reson Mater Phy 2001;12:141-152.
21. Bogner W, Chmelik M, Schmid AI, Moser E, Trattnig S, Gruber S. Assessment of (31)P Relaxation Times in the Human Calf Muscle: A Comparison between 3 T and 7 T In Vivo. Magn Reson Med 2009;62:574-582.

22. Wokke BH, Hooijmans MT, van den Bergen JC, Webb AG, Verschuuren JJ, Kan HE. Muscle MRS detects elevated PDE/ATP ratios prior to fatty infiltration in Becker muscular dystrophy. Nmr Biomed 2014;27:1371-1377.
23. Taylor DJ, Bore PJ, Styles P, Gadian DG, Radda GK. Bioenergetics of intact human muscle. A 31P nuclear magnetic resonance study. Mol Biol Med 1983;1:77-94.
24. Lanza IR, Bhagra S, Nair KS, Port JD. Measurement of human skeletal muscle oxidative capacity by 31P-MR spectroscopy: a cross-validation with in vitro measurements. J Magn Reson Imaging 2011;34:1143-1150.
25. Tusek Jelenc M, Chmelik M, Bogner W, Krssak M, Trattnig S, Valkovic L. Feasibility and repeatability of localized (31) P-MRS four-angle saturation transfer (FAST) of the human gastrocnemius muscle using a surface coil at 7 T. Nmr Biomed 2016;29:57-65.
26. Rzanny R, Stutzig N, Hiepe P, Gussew A, Thorhauer HA, Reichenbach JR. The reproducibility of different metabolic markers for muscle fiber type distributions investigated by functional 31P-MRS during dynamic exercise. Z Med Phys 2016;26:323-338.
27. Atkinson G, Nevill AM. Statistical methods for assessing measurement error (reliability) in variables relevant to sports medicine. Sports Med 1998;26:217-238.
28. Forbes SC, Walter GA, Rooney WD, et al. Skeletal Muscles of Ambulant Children with Duchenne Muscular Dystrophy: Validation of Multicenter Study of Evaluation with MR Imaging and MR Spectroscopy. Radiology 2013;269:198-207.
29. Smeulders MJ, van den Berg S, Oudeman J, Nederveen AJ, Kreulen M, Maas M. Reliability of in vivo determination of forearm muscle volume using 3.0 T magnetic resonance imaging. J Magn Reson Imaging 2010;31:1252-1255.
30. Deoni SC, Williams SC, Jezzard P, Suckling J, Murphy DG, Jones DK. Standardized structural magnetic resonance imaging in multicentre studies using quantitative T1 and T2 imaging at 1.5 T. Neuroimage 2008;40:662-671.
31. Webster C, Silberstein L, Hays AP, Blau HM. Fast Muscle-Fibers Are Preferentially Affected in Duchenne Muscular-Dystrophy. Cell 1988;52:503-513.
32. McCully KK, Mulcahy TK, Ryan TE, Zhao Q. Skeletal muscle metabolism in individuals with spinal cord injury. J Appl Physiol (1985) 2011;111:143-148.
33. Sleigh A, Stears A, Thackray K, et al. Mitochondrial oxidative phosphorylation is impaired in patients with congenital lipodystrophy. J Clin Endocrinol Metab 2012;97:E438-442.
34. Szendroedi J, Schmid AI, Chmelik M, et al. Muscle mitochondrial ATP synthesis and glucose transport/phosphorylation in type 2 diabetes. PLoS Med 2007;4:e154.
35. Kan HE, Klomp DWJ, Wohlgemuth M, et al. Only fat infiltrated muscles in resting lower leg of FSHD patients show disturbed energy metabolism. Nmr Biomed 2010;23:563-568.
36. Satrustegui J, Berkowitz H, Boden B, et al. An in vivo phosphorus nuclear magnetic resonance study of the variations with age in the phosphodiester content of human muscle. Mech Ageing Dev 1988;42:105-114.
37. Szendroedi J, Schmid AI, Chmelik M, et al. Skeletal muscle phosphodiester content relates to body mass and glycemic control. Plos One 2011;6:e21846.
38. Valkovic L, Chmelik M, Ukropcova B, et al. Skeletal muscle alkaline Pi pool is decreased in overweight-to-obese sedentary subjects and relates to mitochondrial capacity and phosphodiester content. Sci Rep 2016;6:20087.
39. Sterin M, Cohen JS, Mardor Y, Berman E, Ringel I. Levels of phospholipid metabolites in breast cancer cells treated with antimitotic drugs: A P-31-magnetic resonance spectroscopy study. Cancer Res 2001;61:7536-7543.
40. Ruiz-Cabello J, Cohen JS. Phospholipid metabolites as indicators of cancer cell function. Nmr Biomed 1992;5:226-233.
41. Fallbrook A, Turenne SD, Mamalias N, Kish SJ, Ross BM. Phosphatidylcholine and phosphatidylethanolamine metabolites may regulate brain phospholipid catabolism via inhibition of lysophospholipase activity. Brain Res 1999;834:207-210.

42. Farber SA, Slack BE, Blusztajn JK. Acceleration of phosphatidylcholine synthesis and breakdown by inhibitors of mitochondrial function in neuronal cells: a model of the membrane defect of Alzheimer's disease. FASEB J 2000;14:2198-2206.
43. Newman RJ, Radda G. Phosphorus Nuclear Magnetic-Resonance Studies in Duchenne and Becker Dystrophy. Clin Sci 1982;63:P36-P36.
44. Younkin DP, Berman P, Sladky J, Chee C, Bank W, Chance B. 31P NMR studies in Duchenne muscular dystrophy: age-related metabolic changes. Neurology 1987;37:165-169.
45. Kemp GJ, Taylor DJ, Dunn JF, Frostick SP, Radda GK. Cellular energetics of dystrophic muscle. J Neurol Sci 1993;116:201-206.
46. Banerjee B, Sharma U, Balasubramanian K, Kalaivani M, Kalra V, Jagannathan NR. Effect of creatine monohydrate in improving cellular energetics and muscle strength in ambulatory Duchenne muscular dystrophy patients: a randomized, placebo-controlled P-31 MRS study. Magn Reson Imaging 2010;28:698-707.

Supplementary data

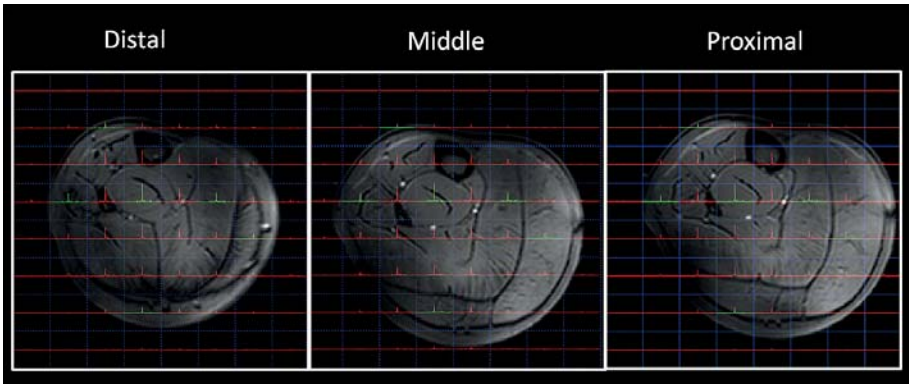

Figure 1. Example of the planning of the 31P 2D-CSI dataset superimposed on an axial T1-weighted image. The spectroscopy grid was positioned so that a specific voxel was located within one individual lower-leg muscle over the entire length of the coil: shown for the most distal, middle and proximal slice of the T1-weighted image.

5

6

Chapter 6

Fast Multi-Station Water/Fat Imaging at 3T using DREAM-based RF Shimming

M.T. Hooijmans, O. Dzyubachyk, K. Nehrke, P. Koken, M.J.Versluis, H.E. Kan, P. Bornert

J. Magn. Reson. Imaging. 2015 Jul;42(1):217-23.

ABSTRACT

Purpose: To show the effect, efficiency and image quality improvements achievable by Dual Refocusing Echo Acquisition Mode (DREAM)-based B_1^+ shimming in whole-body MRI at 3T using the example of water/fat imaging.

Materials and methods: 3D multi-station, dual-echo mDixon Gradient Echo imaging was performed in 10 healthy subjects on a clinical 3T dual-transmit MRI system using station-to-station adapted B_1^+ shimming based on fast DREAM B_1^+ mapping. Whole-body data were obtained using conventional quadrature excitation and station-by-station adapted DREAM-based B_1^+ shimmed excitation, along with the corresponding B_1^+ maps for both excitation modes to assess image quality and RF performance.

Results: Station-dependent DREAM-based B_1^+ shimming showed significantly improved image quality in the stations covering the upper legs, pelvis and upper body region for all subjects ($p < 0.02$). This finding is supported by corresponding B_1^+ maps showing an improved B_1^+ homogeneity and a more precise nominal flip angle in the DREAM-based B_1^+ shimmed excitation ($p<0.01$). Furthermore, the very short dual-channel DREAM B_1^+ mapping times of less than 2 seconds facilitate quick B_1^+ shimming.

Conclusion: Station-dependent DREAM-based B_1^+ shimming improved RF performance and image quality and is therefore a promising technique for whole-body multi-station imaging applications.

INTRODUCTION

Whole-body magnetic resonance imaging (WB-MRI) applications are receiving more clinical attention. [1, 2]In clinical practice, many of these whole-body scans are acquired at moderate field strengths (1.5T) attributable to the sufficient image quality acquired in reasonable measuring times. [3, 4] However, due to the gain in signal-to-noise ratio (SNR) that can be traded into increased spatial resolution or scan acceleration, WB-MRI at higher field strength, like 3T, is becoming more popular. However, at these higher field strengths the effective wavelength of the RF transmit field (B_1^+) inside the patient can approach body dimensions, resulting in standing wave-kind effects, which affects the RF-field homogeneity. This can cause spatially varying image contrast and SNR, which may have serious effects on the quality of clinical diagnosis. [5]

Several approaches have been suggested to address this problem. [3, 5-7] One of the most effective emerging options is dual-channel parallel transmission that allows mitigating this problem by an enhanced control of the RF-field for each individual transmit channel. This allows B_1^+/RF shimming in a subject-specific way, adjusting the relative B_1^+ amplitudes and phases of the otherwise identical waveforms in each of the transmit channels to significantly improve B_1^+ uniformity. [5, 8, 9] However, a prerequisite for patient specific RF shimming is the knowledge about the underlying channel-specific B_1^+ maps that have to be measured with the patient in place. Most current B_1^+ mapping approaches are rather time-consuming, requiring a time-period of at least 15 s for mapping without acquiring any diagnostic data.[10-13] Therefore, especially in multi-station whole-body imaging where the RF-field can change continuously from station to station, very fast and appropriate B_1^+ mapping is required to facilitate adaptive RF shimming. Recently, a new approach for B_1^+ mapping, Dual Refocusing Echo Acquisition Mode (DREAM), which allows single shot B_1^+ mapping within a fraction of a second, was introduced. [14] Based on the quickly acquired B_1^+ maps for the individual transmit channels involved, appropriate and fast B_1^+ shimming can be performed for each individual station during multi-station imaging with the potential to meet the needs for the clinical practice. Therefore, the purpose of this study is to evaluate the effect, efficiency and image quality improvements achievable with DREAM-based B_1^+ shimming in whole-body MRI at a clinical dual-channel 3T MR system using the example of water/fat imaging.

MATERIALS AND METHODS

Study population

Ten healthy subjects (eight male/two female) participated in the study, age: 36.2±8.3 (range: 24–45 years), BMI: 24.25±3.1 kg/m^2 (range: 20.6–29.2 kg/m^2), body size: 1.81±0.09 m (range 1.65–1.92 m), and mass: 80.1±15.4 kg (range: 56–100 kg). The experiments were approved by the local institutional Ethics Committees, and all participants gave written informed consent before their enrolment in the study. Five of the participating subjects were studied at Philips Research Laboratories, Hamburg and five at Leiden University Medical Center, recruited from the LUMC radiology database.

MR technique

Whole-body multi-station data sets were acquired using clinical 3T dual-transmit MRI systems (Ingenia, Philips, Healthcare, Best, the Netherlands). The body coil was used for reception and the subjects were positioned head first in supine position. An identical MRI protocol was used in both centres, starting the data acquisition for each station with a 2D B_1^+ DREAM calibration scan, which is actually a B_1^+ mapping scan for both transmit channels (Figure 1). [14] DREAM is a magnetization prepared single shot sequence. It employs a STEAM preparation module for B_1^+ encoding and a low-angle pulse train to read-out the thus prepared magnetization, acquiring the stimulated echo (STE) and the free-induction decay (FID) signal almost simultaneously on the same readout, as gradient recalled echoes separated in time with appropriate gradient encoding. The true flip angle / B_1^+ map is derived from the ratio between the STE and FID signal, while the phase is derived from the relative transmit phase, directly adopted from one of the source images. In the present work the, the "STE first" DREAM sequence version was used The DREAM scan was centred in the middle of each station to optimize B_1^+ shimming performance. DREAM parameters: field-of-view (FoV): 450×450 mm^2, voxel size: 7×7×15 mm^3, STEAM α: 60°, imaging β: 5°, TE_{FID}/TE_{STE}/TR: 1.06/2.3/3.8 ms, shot duration: 150 ms. This dual-channel DREAM B_1^+ mapping took roughly 1.3 s per station without the use of breath holds, including a waiting time of 1 s between left and right channel transmission. The B_1^+ maps were handed over to the system's RF shim algorithm for estimation of the optimal RF amplitude gains per channel, denoted by their ratio (dB_{ratio}) and phase offsets ($\Delta\varphi$) while ensuring the SAR limits with the patient in place. Subsequently to the B_1^+ calibration scan, B_1^+ maps were obtained for the conventional quadrature transmit mode and the B_1^+ DREAM-shimmed transmit mode with similar sequence parameters as mentioned above facilitating the comparison of dual-channel shimming performance. By "quadrature" we refer to the circular

transmit mode of the unloaded coil (equal amplitudes and fixed 90° phase offset for the two RF channels). Next, two multi-station 3D dual-echo mDixon Gradient Echo acquisitions were measured with the following scan parameters: 24 contiguous axial slices, TR/TE1/TE2: 3.2/1.13/2.0 ms, FA: 5°, FoV: 520×359×120 mm³, voxel size: 1.91´1.91´5 mm³, one with DREAM-based B_1^+ shim sets and the other in quadrature mode. [15] Water/fat separation was performed as the final step after single-echo image reconstruction yielding 3D in-phase (IP), out-of-phase (OP), water, and fat images. The entire acquisition block, comprising 2D B_1^+ DREAM mapping and 3D water/fat resolved scanning (Fig. 1), is embedded in a multi-station acquisition using 16–18 stations with 10 mm station overlap. Breath-holds with duration of 19 s were solely performed for the stations covering the pelvis and chest region. The entire whole-body protocol was performed in a single run starting at the feet and had a total duration of approximately 20 minutes.

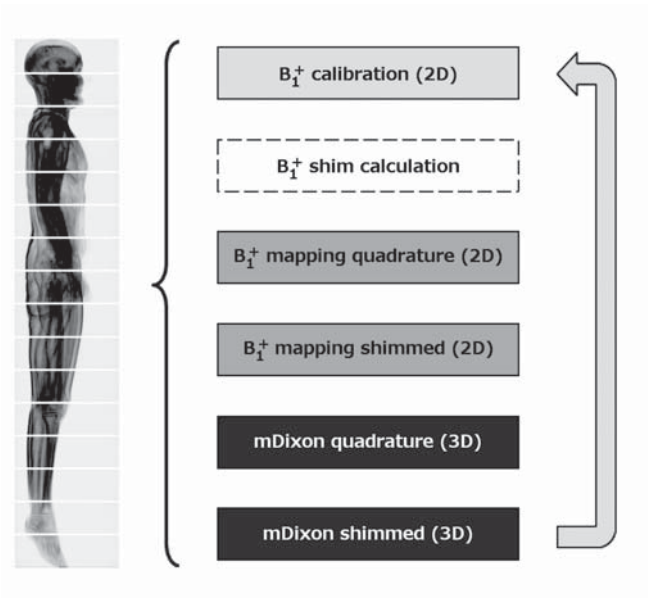

Figure 1. Illustration of the multi-station MR protocol used in this study. For each station, a set of scans was performed starting with a DREAM B_1^+ calibration scan followed by B_1^+ shim calculation. Subsequently, two DREAM B_1^+ maps were acquired to map the conventional quadrature mode RF-field and the DREAM-based B_1^+ -shimmed one, respectively. Finally, two 3D mDixon Gradient Echo scans were performed in both excitation modes. After this acquisition, the systems proceeds to the next station repeating this procedure to acquire the data for the whole multi-station protocol in one run, starting in the feet.

Image and data analysis

Image quality of the two 3D whole-body water/fat resolved scans acquired with the different excitation modes, was independently scored by three MR readers with at least 10 years' experience (MV, HK, KN) without knowledge of the B_1^+ shimming condition during image acquisition using one representative IP slice from five individual stations covering the lower leg (station 3/4), upper leg (station 6/7), pelvis (station 9/10), abdomen (station 12/13) and head (station 15/16/17) region. Scoring was performed solely on image quality using an adjusted five-point grading system [accordingly 1 (very bad) to 5 (excellent)], disregarding the part about their diagnostic value. [5] In addition to this subjective measure, a more objective image quality measure was defined using the entropy H of the normalized image intensity histogram P: $H = -\sum_{p \in P} p \log(p)$. [16] More precisely, the ratio between the histogram entropy H_{shim} for RF shimmed and H_{quad} for quadrature mode data has been used for each individual station and all image types. Values below unity indicate improved image quality on the B_1^+-shimmed volumes and vice versa. Two additional quality measures characterizing the RF field, the coefficient of variation CV, defined as the ratio between the standard deviation σ and the mean of the non-noise values in the B_1^+ map, μ: $CV = \sigma/\mu$, and the $\overline{B_1^+} = \text{mean}(B_1^+)$, were determined for each individual station for the B_1^+ maps acquired in the different excitation modes. [16] Furthermore, the DREAM-based B_1^+ shim settings, the transmit channel amplitude ratio (dB_{ratio}) and the phase offset ($\Delta\varphi$), were recorded for all stations and volunteers. To assess the overall B_1^+ shim performance, the CV, B_1^+, $\Delta\varphi$, and dB_{ratio} were averaged over all subjects and compared for each individual station. This required prior alignment of all the data sets as the subject height varied considerably, resulting in different numbers of stations required to cover the complete body of the individual volunteers. Alignment was achieved by selecting 15 stations that were represented in all the subjects. This, in particular, required disregarding the station covering the feet in all the subjects and additional removal of one station covering the upper thigh region in two of them.

Statistical analysis

The inter-observer agreement was determined with the Kendall τ_B coefficient; values higher than 0.7 were considered to indicate excellent agreement. In the case of excellent inter-observer agreement, the data was pooled for all the observers and the average scores were reported. The Wilcoxon signed-rank test has been used to determine the difference in image quality between the two excitation modes assessed with image grading. After alignment of the data sets, a paired-sample *t*-test was used to assess the difference in mean values for the CV and B_1^+ values for the different excitation modes. After grouping of the individual stations of all

subjects in five zones, classified as: the head, abdomen/chest, pelvis, upper leg and lower leg, the Kolmogorov-Smirnov test was used to test significance of the changes in CV and B_1^+ The significance level was set at $p<0.05$. All statistical analysis was performed using SPSS version 20 for Windows (SPSS Inc., Chicago).

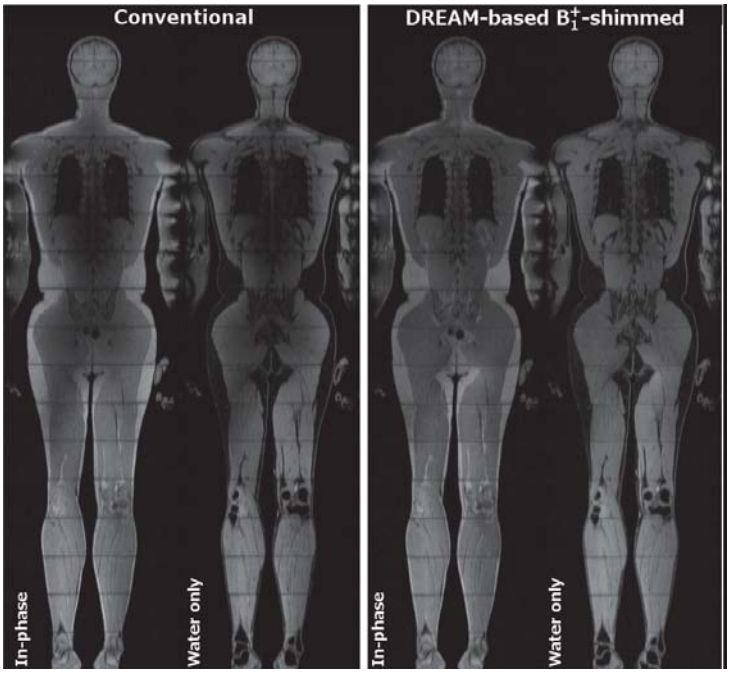

Figure 2. Coronal reformat of the entire reconstructed whole-body volumes. One coronal slice is shown from the gradient echo mDixon images of a representative subject, obtained in the conventional quadrature mode: (a) in-phase, (b) water only; and using DREAM-based B_1^+-shimmed mode: (c) in-phase and (d) water only, respectively. A significant reduction in RF shading artefacts for the DREAM-based B_1^+ shimmed case compared to the conventional quadrature situation is visible in the stations covering the torso and upper legs. The images were not further corrected for the remaining stitching artefacts; those are kept on purpose to illustrate the multi-station nature of the data.

RESULTS

All volunteer scans performed at the two different sites were successfully performed.

Image quality

The comparison of the whole-body data sets obtained with both RF excitation modes revealed a consistent improvement in image quality for all subjects in the images acquired with DREAM-based B_1^+ shimmed excitation (Figs. 2,3). The scoring of the

images showed significant improvements in the stations covering the upper leg, pelvis and upper body region (p=0.014, p<0.0001, p<0.0001), while no improvement in image quality was visible in the stations covering the lower leg and head region (p=0.28, p=0.99) (Table 1). Excellent inter-observer agreement (Kendall τ_B=0.705–0.771, p<0.01) was found between observers' grading of the images. These observer-perception-driven results were supported by the image histogram entropy ratio values of both the IP/OP and fat/water images that confirm the improvement in

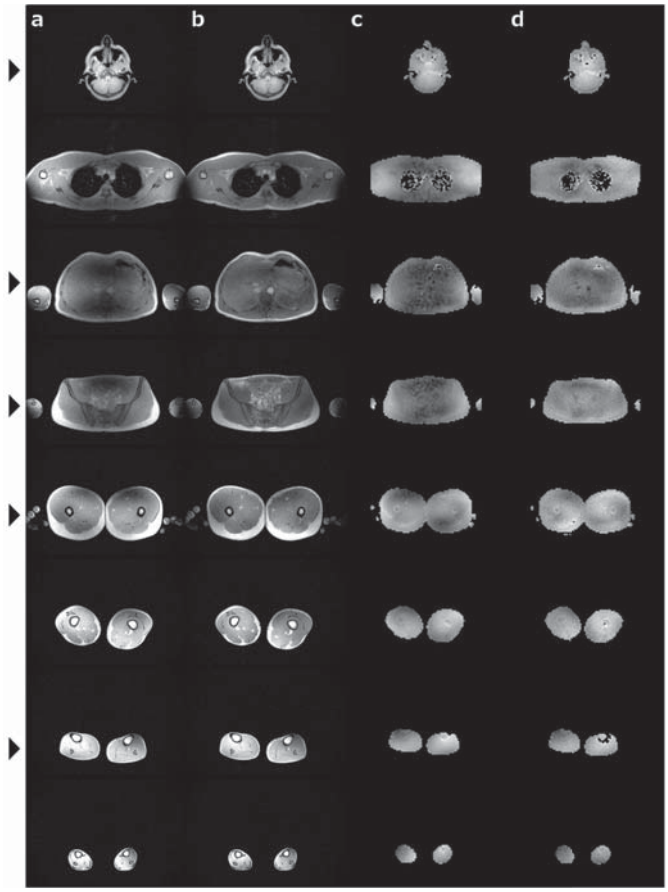

Figure 3. Axial in-phase images and corresponding B_1^+ maps for the two excitation modes. Gradient echo mDixon in-phase images of a representative subject are shown for various stations in (a) for quadrature and (b) for DREAM-based B_1^+-shimmed excitation, along with corresponding DREAM B_1^+ maps: (c) for quadrature and (d) for the B_1^+-shimmed case, respectively. Most pronounced changes consisting of less spatially varying image contrast and RF shading are visible in the upper body region. The stations marked with the arrows (left) are used for the visual grading of the image quality in this particular example; see also Table 1.

image quality (Figures 4b,c). This is especially obvious in the upper body region together with less conclusive results in the head and lower leg region compared to the human observers. In addition, a more obvious effect in image histogram entropy was visible in the water images compared to the fat images (Figures 4b,c).

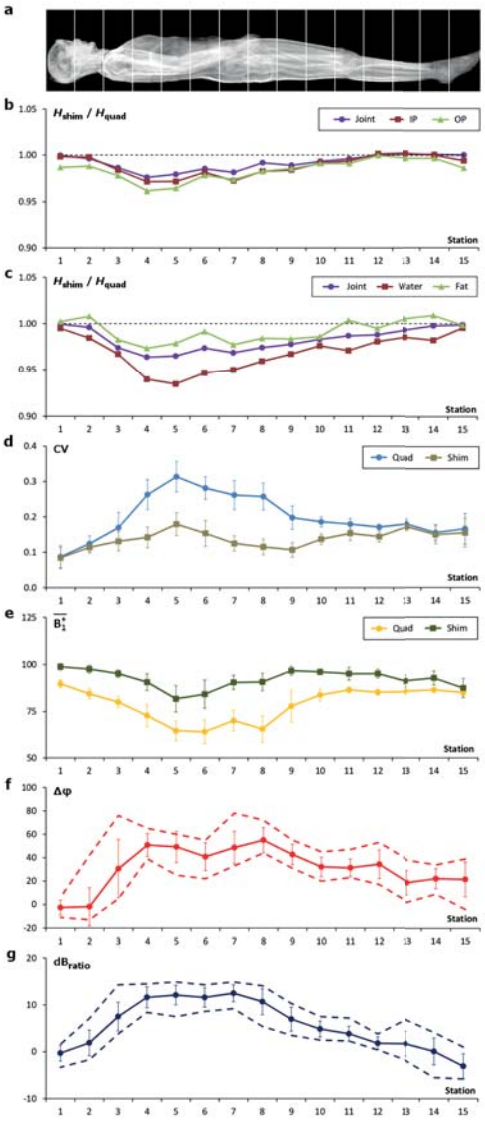

Figure 4. Summarised multi-station results averaged over the entire cohort. (a) Shows the anatomical location of each station. Data have been resampled to 15 stations, with station 1 corresponding to the head and station 15 representing the feet. The average ratio between the histogram entropy for the RF shimmed and quadrature mode excitations were calculated for IP/OP and water/fat mDixon images: (b) Shows the average histogram entropy ratios per individual station for the IP, the OP and both image types together (joint). Values below unity indicate improved image quality for the RF shimmed data. (c) Shows the histogram entropy ratios for the water-only, fat-only data and both image types together (joint), with the water-only showing significantly improved image intensity homogeneity. (d,e) Compare the measured DREAM B_1^+ maps in quadrature ("Quad") and DREAM-based shimmed ("Shim") excitation modes: (d) Shows the coefficient of variation (CV) for both excitation modes, illustrating an improvement in RF homogeneity for DREAM-based shimmed mode; a lower coefficient indicates a better homogeneity. (e) Shows the mean B_1^+, normalised to the desired/expected value (given in %) for both modes, demonstrating the better performance for the RF shimmed case. The station-dependent RF shim values (f,g) show considerable variation. In (f) the phase difference $\Delta\varphi$ (given in degree) and in (g) the amplitude ratio of the two channels (measured in dB) are shown. In subfigures (d–g), the error bars indicate standard deviation, whereas the dashed lines represent the minimum and maximum values of the corresponding variable.

	Excitation mode	Head	Abdomen / chest	Pelvis	Upper leg	Lower leg
Image quality	*Quad*	4.9±0.16	2.2±0.5	2.7±0.47	3.4±0.21	3.6±0.43
	DREAM-based RF shimmed	4.9±0.16	4.3±0.43*	4.3±0.43*	3.7±0.27*	3.7±0.44
CV	*Quad*	0.11±0.03	0.26±0.04	0.23±0.03	0.18±0.01	0.16±0.03
	DREAM-based RF shimmed	0.10±0.02	0.15±0.03*	0.12±0.02*	0.16±0.02*	0.15±0.03
B_1^+, (%)	*Quad*	87.1±2.4	70.5±5.1	74.4±6.0	85.8±1.7	85.5±1.4
	DREAM-based RF shimmed	98.1±1.9*	87.9±5.2*	93.5±3.1*	93.8±3.0*	89.9±4.4*

Table 1. Overview of the results. The mean and standard deviation for image quality according to image grading [score accordingly 1 (very bad) to 5 (excellent)], the CV, and the B_1^+ for DREAM-based RF shimmed and quadrature excitation respectively are presented for the head, abdomen, pelvis, upper leg and lower leg region. Significant differences between excitation modes are marked with an asterisk (*).

B_1^+ maps

The evaluation of the B_1^+ maps to asses overall shimming performance in both excitation modes showed an improvement in the homogeneity of the transmit RF-field using DREAM-based B_1^+ shimming, represented by a significant reduction in the CV compared to the conventional quadrature excitation: quadrature=0.20±0.03, shimmed=0.14±0.02, p<0.001 (Figs. 3,4d). This reduction is mainly found in the upper legs, pelvis and abdomen; see Table 1. In addition to the increase in B_1^+ homogeneity, a more accurate B_1^+ level was obtained with DREAM-based B_1^+ shimming: quadrature=79±4 %, shimmed=92±4 %, p<0.001; (Fig. 4e). Similar improvements were visible for all the defined zones (Table 1). Furthermore, the determined and applied B_1^+ shim sets (dB_{ratio}, $\Delta\varphi$) varied continuously throughout the stations, which is shown in Figs. 4f,g. Most pronounced changes of the shim settings were visible in the stations acquired in the shoulder-neck region, the pelvis and upper legs.

DISCUSSION

This study aimed at evaluating the effect, efficiency, and image quality improvements achievable using DREAM-based B_1^+ shimming to mitigate wave-propagation effects in whole-body imaging at 3T. Compared to conventional quadrature excitation, significant and consistent improvements in B_1^+ homogeneity and image quality are shown for multi-station water/fat imaging according to DREAM-based B_1^+ shimming per station. These improvements were obvious in stations covering the

region from the upper body to the upper legs and were consistently confirmed by three independent measures: visual subjective grading, objective evaluation of the entropy of the image histogram and reduced coefficient of variation and better nominal flip angle derived from the RF shimmed B_1^+ maps. Histogram entropy ratios were measured for the IP/OP and the water/fat volumes. For the IP/OP images, all three plots (including the joint entropy ratio estimation) clearly show improved and similar behaviour achieved due to RF shimming. However, the improvements for the water images are more obvious compared to the fat. This could be due to two reasons. First of all, fat does not show significant wave propagation effects at 3T, whereas water does. [17, 18] Having both separated can make this effect more obvious. Second, water-rich tissue is located in the body core, where wave propagation effects predominantly occur, whereas fat is often more present in the periphery and thus less affected by the field inhomogeneity.

Nevertheless, no significant improvements in image quality and RF homogeneity were found in stations covering the lower leg and head region, which suggests some station dependency in the effectiveness of RF shimming. This fact is not surprising, as the effective wavelength at 3T might not approach object dimensions in the lower legs and the head, in contradistinction to other parts of the body. However, also in those regions were no improvement in image quality and RF homogeneity was found, as well as in all the other regions in general, a more precise flip angle was measured after applying B_1^+ shimming. This indicates that the flip angle necessary to generate the correct image contrast during acquisition, is better maintained as a result of the applied B_1^+ shimming procedure per station.

It is furthermore interesting to review some of the station-dependent RF shim settings. Significant changes in the RF shim settings (dB_{ratio}, $\Delta\varphi$) with respect to quadrature mode were visible in both the shoulder/neck and leg region for all subjects. This could be explained by the asymmetrical loading of the body coil in the feed-head direction, emphasising the need for station-specific adjustments of the RF-field. Nevertheless, within consecutive stations covering the upper body region, less variation in the optimized B_1^+ shim settings was revealed, although quite substantial fluctuation between thorax and abdomen was found in some individuals. Hence, we question if region- instead of station-specific RF shimming could be sufficient for such multi-station whole-body applications. However, given that already small changes to the driving conditions of the channels can have impact on the RF performance, together with the major improvement shown in the mapping efficiency using DREAM, one could suggest that station-specific RF shimming could be recommended just as precaution.

The improvements shown with DREAM-based dual-channel RF shimming shown in this work are in line with findings of several other investigators applying RF shimming methods in the abdomen or other anatomical regions at 3T. [7, 19] However, the greatest benefit of this recently introduced DREAM B_1^+ mapping method is the time-efficiency, accelerating dual-channel B_1^+ mapping for RF shimming by an order of magnitude compared to other, rather time-consuming, B_1^+ mapping approaches. [10, 20] This allows RF transmit performance to be optimized per station during multi-station imaging applications without significant loss of scan efficiency regarding the acquisition of the desired diagnostic data. Furthermore, DREAM has the potential to be applied during very shallow or free breathing in comparison to other methods, where at least 15 seconds breath-holds are necessary to make proper adjustments to the RF-field. Apart from the gain in efficiency, this also eases system workflow, because the operator does not need to instruct the patient about potential breath-holding constraints.

One potential limitation of this study is that it solely compares DREAM-based B_1^+ shimming with the conventional quadrature excitation instead of comparing it to other RF shimming approaches. [21] However, the performance of RF shimming depending on the employed B_1^+ calibration has been recently studied by comparing DREAM to two other B_1^+ mapping approaches at a clinical dual-channel 3T MR system. [21] It was found that the RF shim results achieved with DREAM-based RF shimming were equivalent to those currently achieved with the other RF shimming methods in healthy controls. This implies that the positive effects with DREAM-based RF shimming shown in this study do not overestimate the effectiveness of this method. Secondly, only a small number of subjects participated in the study. As an improvement in image quality, flip angle accuracy and B_1^+ homogeneity due to RF shimming is not unexpected, it might has influenced some of the minor, non-significant findings in the lower leg region. The whole-body application used in this study is focussed on water/fat resolved volumetric imaging. This is of great importance in obesity-related research, where the amount and distribution of body fat are important diagnostic parameters, as well as in other systemic diseases, where the water fat distribution throughout the body is of interest. [22, 23] However, it is important to note that the effective multi-station DREAM B_1^+ mapping and shimming approach can easily be generalized to other whole-body imaging applications addressing different MR contrasts. Thereby this DREAM-based RF shimming approach could be even more beneficial in whole body imaging applications based on the more B_1^+ sensitive Spin Echo or fast Spin-Echo sequences or in imaging techniques where precise magnetization preparation is crucial as in fat suppression for example.

In conclusion, DREAM-based multi-station B_1^+ shimming showed to be very fast and effective compared to standard approaches currently available. Thereby, it achieves the desired improvements in transmit RF-field homogeneity, flip angle accuracy, image quality and workflow, suggesting that DREAM B_1^+ mapping could be of importance in clinical practice.

References

1. Nielsen YJW. Whole-body MR angiography in patients with peripheral arterial disease. Dan Med Bull 2010;57.
2. Siegel MJ, Acharyya S, Hoffer FA, et al. Whole-Body MR Imaging for Staging of Malignant Tumors in Pediatric Patients: Results of the American College of Radiology Imaging Network 6660 Trial. Radiology 2013;266:599-609.
3. Schick F. Whole-body MRI at high field: technical limits and clinical potential. Eur Radiol 2005;15:946-959.
4. Machan JS, H.; Shick, F. . Technical challenges and opportunities of whole-body magnetic resonance imaging at 3T. Physica Medica 2008: 63:70
5. Willinek WA, Gieseke J, Kukuk GM, et al. Dual-source parallel radiofrequency excitation body MR imaging compared with standard MR imaging at 3.0 T: initial clinical experience. Radiology 2010;256:966-975.
6. Kuhl CK, Traber F, Gieseke J, et al. Whole-body high-field-strength (3.0-T) MR imaging in clinical practice. Part II. Technical considerations and clinical applications. Radiology 2008;247:16-35.
7. Franklin KM, Dale BM, Merkle EM. Improvement in B1-inhomogeneity artifacts in the abdomen at 3T MR imaging using a radiofrequency cushion. J Magn Reson Imaging 2008;27:1443-1447.
8. Hoult DI, Phil D. Sensitivity and power deposition in a high-field imaging experiment. J Magn Reson Imaging 2000;12:46-67.
9. Ibrahim TS, Lee R, Abduljalil AM, Baertlein BA, Robitaille PM. Dielectric resonances and B(1) field inhomogeneity in UHFMRI: computational analysis and experimental findings. Magn Reson Imaging 2001;19:219-226.
10. Yarnykh VL. Actual flip-angle imaging in the pulsed steady state: a method for rapid three-dimensional mapping of the transmitted radiofrequency field. Magn Reson Med 2007;57:192-200.
11. Cunningham CH, Pauly JM, Nayak KS. Saturated double-angle method for rapid B1+ mapping. Magn Reson Med 2006;55:1326-1333.
12. Stollberger R, Wach P. Imaging of the active B1 field in vivo. Magn Reson Med 1996;35:246-251.
13. Sacolick LI, Wiesinger F, Hancu I, Vogel MW. B1 mapping by Bloch-Siegert shift. Magn Reson Med 2010;63:1315-1322.
14. Nehrke K, Bornert P. DREAM--a novel approach for robust, ultrafast, multislice B(1) mapping. Magn Reson Med 2012;68:1517-1526.
15. Eggers H, Brendel B, Duijndam A, Herigault G. Dual-echo Dixon imaging with flexible choice of echo times. Magn Reson Med 2011;65:96-107.
16. Belaroussi B, Milles J, Carme S, ZhuYM, Benoit-Cattin H. Intensity non-uniformity correction in MRI: existing methods and their validation. Med Image Anal 2006;10:234-246.
17. Tofts PS. Standing Waves in Uniform Water Phantoms. J Magn Reson Ser B 1994;104:143-147.
18. Dietrich O, Reiser MF, Schoenberg SO. Artifacts in 3-T MRI: physical background and reduction strategies. Eur J Radiol 2008;65:29-35.
19. Childs AS, Malik SJ, O'Regan DP, Hajnal JV. Impact of number of channels on RF shimming at 3T. MAGMA 2013;26:401-410.
20. Welch EBG, A.; berglund, J. . Quantitative whole-body fat-water MRI with R2* estimation at 3 Tesla a Custom table top for multi-station parallel imaging with a single 16-channel surface coil. Proceedings of the 20th annaul meeting of the ISMRM, Salt lake City 2013 (abstract 1524) 2013.
21. Nehrke K, Sprinkart AM, Bornert P. An in vivo comparison of the DREAM sequence with current RF shim technology. Magn Reson Mater Phy 2015;28:185-194.
22. Stranges S, Trevisan M, Dorn JM, Dmochowski J, Donahue RP. Body fat distribution, liver enzymes, and risk of hypertension: evidence from the Western New York Study. Hypertension 2005;46:1186-1193.
23. Kullberg J, Johansson L, Ahlstrom H, et al. Automated assessment of whole-body adipose tissue depots from continuously moving bed MRI: a feasibility study. J Magn Reson Imaging 2009;30:185-193.

6

Chapter 7

7

Summary and general discussion

7.1 Summary

The overall aim of this thesis was to combine various quantitative MR measurements and compare these combined measurements between DMD patients and healthy age-matched controls both on a cross-sectional and longitudinal level, in order to generate a better understanding of the underlying pathophysiology of the disease and ideally to determine the potential of these MRI outcome parameters for monitoring muscle tissue changes in a clinical setting. In order to achieve this aim, we assessed the effect of spatial localization, data quality and confounding effects on the quantification process for various MR outcome parameters. We used a combination of quantitative MRI and spatially resolved ^{31}P MRS to contribute to the understanding of the pathophysiology in DMD.

In **chapter 2** we explored the effect of %fat, SNR and T_2 relaxation time changes on quantitative DTI measurements in skeletal muscle of DMD patients. We showed that sufficient SNR is essential for a reliable estimation of the DTI parameters, and that in vivo measurements of % fat and mean water T_2 are necessary to assess whether detected changes in DTI parameters could be ascribed to pathophysiology or to confounding effects related to low SNR. Overall, we showed that reliable DTI measurements in skeletal muscle can be obtained in DMD patients and healthy controls, if confounding factors are accounted for.

In **chapter 3** we studied fat replacement along the proximodistal muscle axis in DMD patients by using the Dixon technique. We showed that muscle fat fractions were non-uniformly distributed along the proximodistal muscle axis, with higher fat fractions in the muscle end-regions compared to the muscle belly. In addition, we showed the importance of accurate spatial localization along the proximodistal muscle axis when quantifying muscle fat fractions. A slight shift of the slice stack along the proximodistal muscle axis resulted in a difference in mean fat fraction which was on average 1-2%, but with values measured up to 12%. This non-uniformity in fat fraction within an individual muscle has a major influence on quantitative MR measurements that are currently being considered as outcome measures in clinical trials, and highlights the need for accurate repositioning in longitudinal MR studies. In addition, these findings pointed to mechanical disruption of the membrane as one of the key factors in the pathophysiology of DMD.

Chapter 4 presented a combination of quantitative MRI and spatially-resolved (2D-CSI) ^{31}P MRS data in the leg muscles of DMD patients to determine metabolic changes and inflammation in muscles with and without fat infiltration, in order to assess if metabolic changes and inflammation vary at different stages of the disease

process. Both PDE-levels and water T_2 values were significantly increased prior to the occurrence of fat infiltration, and remained elevated in muscles with fat infiltration; whereas Pi/ATP and intracellular tissue pH only changed in muscles that showed fat infiltration. This indicates that we were able to distinguish between early and late pathophysiological changes in DMD patients. More specifically, this suggested that PDE-levels and water T2 values could not only function as early markers for muscle tissue change, but could also reflect potentially reversible pathology in more advanced stages of the disease.

In **chapter 5** we assessed the time course of changes in PDE-levels detected by ^{31}P MRS and the potential value of PDE-levels to monitor muscle tissue changes in DMD patients, using longitudinal and spatially resolved ^{31}P MRS and qMRI data of lower leg muscles that display varying levels of muscle wasting. PDE-levels were significantly higher (two-fold) compared to controls in all analyzed muscles at almost all time points, and did not change over a 2 year time period. Muscle fat fraction significantly increased between the subsequent time points in all analyzed muscles of the DMD patients. In addition, we also assessed the reproducibility of quantifying PDE-levels between two subsequent measurements and the effect of SNR on the accuracy of such quantification. We showed that PDE-levels can reliably and reproducibly be quantified with ^{31}P 2D-CSI in both high and low SNR data sets. The two-fold increase in PDE-levels compared to controls, the stabilization over a two-year time period, its detection prior to structural changes, and its high reproducibility in low and high SNR data confirm the potential of PDE-levels as a marker to monitor muscle tissue changes in DMD patients.

Chapter 6 evaluated the implementation of a fast DREAM-based B_1^+ shimming approach in a whole-body fat/water separation application at 3T. Multi-station DREAM-based B_1^+ shimming showed significantly improved data quality in the stations covering the region from the upper leg to upper body compared to a conventional single shim approach. These improvements were supported by the corresponding B_1^+ maps which showed a more precise flip angle and a more homogeneous B_1^+ field. DREAM-based B_1^+ shimming was shown to be very fast and effective compared to currently available methods, achieving the desired improvements in the transmit RF-field homogeneity, the flip angle accuracy and the image quality while accelerating the calibration process by a factor of ten. This suggests that DREAM-based B_1^+ shimming is a very promising technique for multi-station whole-body imaging applications.

7.2 General discussion

In this thesis, a wide variety of individual MR techniques have been used to assess various pathophysiological changes in healthy and diseased skeletal muscle, on both a cross-sectional and longitudinal level. However, instead of only focussing on individual techniques, this thesis aimed to combine these techniques in a multi-parametric MR approach in order to: 1) assess the effects that methodological aspects can have on quantification, 2) generate a better understanding of the underlying pathophysiology in DMD, and 3) determine the value of these MR outcome parameters to monitor muscle tissue changes. (Figure 7.1) In this chapter, the key findings of the results will be discussed and put into the context of the existing scientific literature. The first part of this chapter will focus on the effect of methodological factors such as data quality, spatial localization and confounding factors on quantification in skeletal muscle applications. The second part of the discussion will focus on how this thesis contributed to new insights in the pathophysiology of DMD, and how these insights can form the foundation for future work.

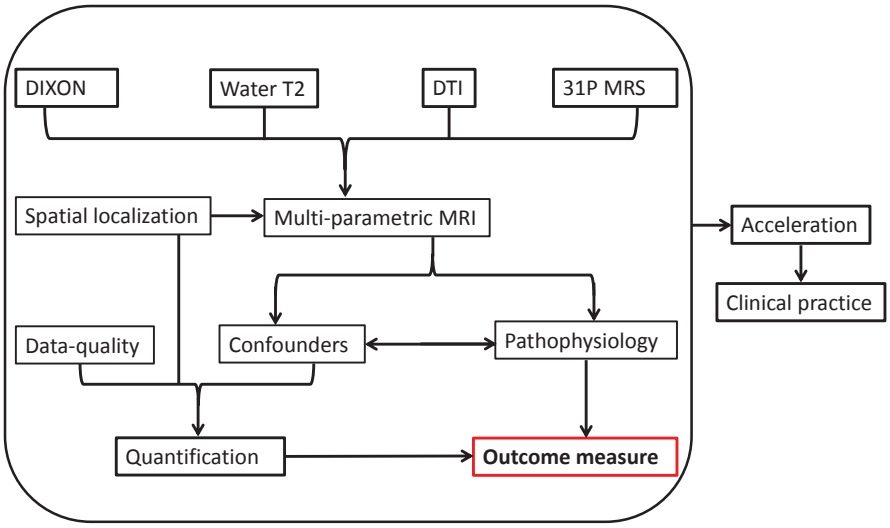

Figure 1. A schematic overview of the inter-connection of all topics in the discussion.

7.2.1 Quantification: Data-quality, Confounders and Spatial localization

In this thesis, ^{31}P 2D CSI and two advanced quantitative imaging techniques have been evaluated with regards to **data quality**, **confounding effects** and **accuracy of spatial localization between measurements,** in order to assess the effect of these factors on **quantification of MR outcome parameters** and **data interpretation**.

7.2.2 Data quality

One of the most common measures used to support a statement about data quality in quantitative MRI is the SNR, where high SNR levels are important to ensure good-quality data. SNR is usually defined as the mean signal divided by the standard deviation of the noise. Previous simulation-based studies from other groups have shown that the reliability of estimating DTI based parameters in skeletal muscle is highly sensitive to changes in SNR, muscle fat fraction and edema/inflammation-like processes. [1, 2] **Chapter 2** of this thesis evaluated the effect of SNR on the DTI parameter estimation in an in-vivo situation, and showed that high-quality data was a prerequisite for a correct DTI parameter estimation in skeletal muscle. To ensure a robust estimation of DTI-based parameters, one could try to fully exclude the effect of data quality on quantification, by acquisition of only high SNR data sets. This can be generalized by reducing spatial resolution or by averaging of more data sets. However, neither "solution" is optimal in a clinical setting, as more averaging is inextricably linked with long measurement times, and a lower resolution results in reduced specificity of the measurements. Moreover, accurate quantification of MR outcome parameters usually involves sufficient levels of SNR rather than maximizing SNR. More specifically, this means that above a certain threshold the robustness of the estimation is relatively stable. The same holds for our data; all five DTI-based parameters (three eigenvalues, MD and FA) can be estimated properly in skeletal muscle with SNR levels above 20, while MD itself can already be estimated properly with SNR levels above 15. Similar findings have been reported in other muscle applications such as STE DTI and BOLD imaging. [3, 4] The influence of data-quality on the quantification process has been evaluated in more detail in **chapter 5** of this thesis by assessing the relation between SNR and PDE-levels and showed that above a certain threshold (SNR PCr peak > 10) PDE-levels could reliably be quantified. Consequently, our recommendation is that the MR protocol needs to be optimized in order to eliminate the effect of SNR on quantification, by reaching sufficient levels to ensure a robust estimation of the desired MR outcome parameter, rather than being aimed at maximizing data quality which may take an impractical amount of scan time. Eventually, it is important that sufficient data quality is reached to quantify and interpret the results, while also taking into account the scan duration. The optimal situation will vary by technique and by application, but scan

durations that exceed 5 minutes are not desirable, especially not in young children and patients who may be more prone to scan discomfort.

7.2.3 Confounding factors

Accurate spatial co-localization in a multi-parametric MR approach, when executed properly, allows among other things the detection of potential confounding factors which can either overshadow pathology or create the impression of pathology. **Chapter 2** of this thesis evaluated the effect of %fat and water T2 on the DTI parameter estimation in an in-vivo situation, and showed that for a robust implementation of DTI measurements, additional factors such as water T_2 changes and %fat need to be measured to prevent unnecessary sources of error when interpreting the results. In addition, our work and experimental data of others showed that, besides the direct effect that %fat and water T_2 changes had on the SNR in a SE-EPI sequence, both measures could also act as independent confounders on the DTI parameter estimation.[1, 2, 5] However, the exact separate effect that these confounders had on the DTI parameter estimation was difficult to assess in our in-vivo approach. This was due to the low inflammation component of the disease and the direct inverse relation of %fat with SNR. Future work should aim at acquisition of high SNR datasets in more pronounced fatty-infiltrated muscles to evaluate the true confounding effect of fat.

The impact of confounding factors has also been shown in other quantitative MR techniques of skeletal muscle, for example Quantitative Magnetization Transfer (QMT) and BOLD imaging.[4] More specifically, both our work and that of others showed that the presence of adipose tissue (muscle fat replacement), low SNR data, and changes in T_2 (fibrosis and inflammatory processes) are common confounding factors in MR techniques used in skeletal muscle applications. However, these common confounding factors are also considered as inevitable structural changes associated with damage, disease and exercise in skeletal muscle. The precise effect that these specific confounders have on the measurement is technique-dependent. Such technique-specific knowledge is essential in order to be able to ascribe detected changes to either pathology or confounding factors, and to ensure accurate interpretation of the results. In the end, the feasibility of multi-parametric MRI in clinical practice can be questioned, but the impact that accounting for confounding factors has on data interpretation is very clear.

7.2.4 Accuracy of spatial localization between measurements

In skeletal muscle applications, repositioning between measurements is usually done by using a combination of bony landmarks, internal muscle references, and

external references such as fish oil capsules placed on the skin. [6, 7] Up to now, there is very little knowledge about the accuracy of spatial localization between measurements based on these guidelines, and more importantly the impact that slight imperfections in spatial localization can have on quantitative measures in skeletal muscle applications.

In **chapter three** of this thesis we showed that slight errors in spatial localization caused artificial differences in mean fat fraction which were on average 1-2% and ranged up to 12% in DMD patients. This effect is caused by the specific non-uniform parabolic distribution of fat replacement along the proximodistal muscle axis. However, this is not specific for DMD or for fat replacement, as in at least two other muscle diseases non-uniform distributions of muscle fat replacement along the muscle axis [8, 9] have been reported. Muscle tears and injuries are highly location specific and exercise effects are muscle- and location-dependent. Therefore, the impact that accuracy of spatial localization can have on quantification is in fact a very common problem.

However, in the end, it is only relevant to know what the impact of these imperfections in spatial localization will be on a group level basis. For example, in the case of a parabolic distribution, if the slice stack is positioned at the lowest point of the parabola, a shift in any direction will result in an artificial increase of the outcome parameter which cannot be levelled out on a group level. However, slice stacks or volumes are generally located at a specific distance from a bony landmark which does not directly match to the lowest point of the parabola in a specific muscle. As a result, parameter estimates can be under- or overestimated, and this difference could possibly be averaged out on a group level. Ultimately, the effect of these imperfections in spatial localization on quantification will be highly dependent on the shape of the distribution of tissue changes (e.g. linear curve, U-shaped curve, focal lesions, exponential curve) along the length of the muscle. Nevertheless, on a group level basis, it will at least affect the discriminative power of the technique to detect change.

The effect of these imperfections on spatial localization becomes even more complicated in longitudinal study set-ups with pediatric study population and after exercise regimes, as muscles will inevitably change between time-points. This complicates repositioning according to bony landmarks and internal references. In addition, the intrinsic parameters involved in the methodology of most imaging and spectroscopy approaches, e.g. slice gaps, slice thickness, field-of-view and restricted voxel size, could result in limited and location-specific information. Both these

methodological aspects magnify the impact that spatial localization imperfections can have on quantitative outcome measures. Therefore it is recommended to establish a protocol which can take these imperfections into account, for instance by using 3D acquisitions with full limb coverage which allows accurate offline matching of datasets in a standardized way.

7.3 Multi-parametric MRI in DMD: Insight in the pathophysiology and the value of MR outcome measures to monitor tissue changes

Quantitative MRI and MRS are important non-invasive methods to follow disease progression in DMD and are considered as promising surrogate outcome measures for clinical trials. [10] So far the main focus of the field has been on individual quantitative imaging techniques with the ability to reflect variations in the extent of fat replacement, inflammation, and metabolic changes; and to correlate these with disease progression, age and function. In addition, it is known and has been investigated extensively with qMRI, that muscles become affected at different time points and at different rates.[11-14] However, both the origin of this variation in disease progression and the pathogenic mechanism behind this degeneration is not fully clear. [15, 16] To date, only little is known about the relationship between the various pathophysiological processes and if/how those pathophysiological processes vary within individual muscles. Such knowledge could contribute to a better understanding of the underlying pathophysiology and to potential strategies aimed at preserving muscle tissue.

7.3.1 Variations within individual muscles

Chapter three of this thesis focused on variations in muscle degeneration within individual muscles and showed that muscle fat replacement was non-uniformly distributed along the proximodistal muscle axis in DMD, with higher fat fractions in the end-regions compared to the muscle belly. The detection of this specific degeneration pattern, combined with the non-uniform mechanical strain distribution along the proximodistal muscle axis in healthy muscle tissue, higher expression levels of dystrophin in the muscle end-regions and the susceptibility of dystrophin-deficient muscle to stress-induced injury, all point towards mechanical disruption of the sarcolemma as one of the key factors for muscle degeneration in DMD.[17-21] However, the specific role of the mechanical component in the degeneration process needs to be investigated in further detail. This knowledge could for example contribute to explaining the specific pattern of muscle involvement in DMD. Closely-related factors such as fiber-type composition and the amount of eccentric muscle contractions have already been associated with this specific pattern of muscle involvement. [22, 23] Future research could also include evaluation

of the stress and strain distributions within individual dystrophic muscle fibers, as well as evaluation of the change in these distributions when muscle degeneration progresses. Ultimately, it would be relevant to evaluate how this specific knowledge could contribute to potential strategies aimed at preserving muscle tissue and how it relates to functional measures.

The difference in parabolic curvature between low, intermediate and highly affected muscles, with a more prominent curvature in the intermediately affected muscles, suggests that at least at the start and at the end of the fat transformation process, the progression of the parabolic distribution cannot be homogeneous over time. It can be questioned how this progression will evolve in the intermediate stages of muscle deterioration. A recent study in the arm muscles of DMD patients suggested that muscle fat transformation evolved over time with similar rates along the proximodistal muscle axis. [24] All these findings together suggest that the muscle end-regions seem primarily affected but do not necessarily evolve more rapidly over time. However, a more detailed and specific analysis will be needed to further evaluate this degeneration process over time.

Furthermore, it would be highly interesting to evaluate whether the other pathophysiological processes, such as muscle inflammation and metabolic alterations, show the same parabolic distribution along the proximodistal muscle axis. Based on the notion that metabolic alterations and inflammation-like processes occur prior to more structural changes, and considering that muscle tissue is known to be progressively replaced with fat in DMD, it is likely that this specific distribution may only be visible in the early disease phases. As such, it could be that in order to be able to visualize this, DMD patients below the age of five have to be recruited. Acquisition of MR data sets in such a young population might not be practically feasible without sedation. In addition, this is one of the reasons, why scanning of such a young study population is not allowed by most medical ethical committees. Alternatively, it is also likely that none of the other pathophysiological changes shows a similar parabolic distribution, as the specific shape of the distribution largely depends on the progressive nature of muscle fat replacement with its well defined begin and end stage.

7.3.2 The inter relation between these pathophysiological processes.

Muscles of DMD patients are characterized by a wide variety of histological changes such as inflammation, changes in resting energy metabolism and fat infiltration. [25] However, so far, the exact time course and relation between these pathophysiological changes is not fully understood. In **chapter 4** of this thesis we showed that that it

is possible to distinguish between early and late pathophysiological processes in individual muscles. PDE-levels and water T_2 relaxation times were elevated prior to the occurrence of structural changes, and remained elevated in later disease stages. In contrast, the other metabolic indices (Pi/PCr and intracellular tissue pH) showed alterations simultaneously with the replacement of muscle tissue by fat or did not change at all (Pi/ATP and PCr/ATP). These findings are partly in line with previous work which reported elevated water T_2 relaxation times in muscles with low fat levels. [26, 27] Knowledge about this time relation is useful to define a time frame in which the trajectory of individual pathophysiological processes can be assessed in more detail. In addition, our work and that of others also showed that analysis of all these individual pathophysiological processes, reflecting multiple aspects of muscle damage, provides a much more comprehensive view of the disease state of a specific muscle. [28]

The trajectories of these metabolic indices and fat fraction have been investigated in more detail over a two-year time period in **chapter 5**. We found that none of the metabolic indices differed between the consecutive time points (Baseline, 12-months and 24-months) while muscle fat fraction did increase with time. These findings suggest that the metabolic alterations are not directly associated with the severity of muscle damage in DMD. However, the absence of this relationship may be confounded by the fact that there are both early and late metabolic alterations, as discussed before in **chapter 4**. This notion is supported by work in the arm muscles of ambulant and non-ambulant DMD patients, and by most previous cross-sectional work in older DMD boys/men not on steroid treatment. [29-34] These findings suggest that detecting a relation between metabolic alterations and disease progression is highly dependent on the disease stage in relation to the outcome parameter. Thereby it is highly likely that the relation with disease progression varies between disease phases. A longer follow-up in younger and older DMD patients should be performed to investigate the trajectories of these early and late pathophysiological processes in more detail. The wide range of muscle involvement in a specific patient together with the large variation in pathophysiological changes along the course of the disease, stress the importance of muscle specific measurements while conducting such investigations. However, it is important to consider that, while muscle-specific analyses are much more sensitive, these type of measurements are not always feasible in practice, due to hardware accessibility and time constraints. From a clinical point of view, it would be interesting to find out if some of the early pathophysiological changes have the ability to predict the course of some of the later pathophysiological changes, and ideally to relate those changes to loss of functional ability. Past studies have shown that muscle fat fraction of a single muscle or a group

of muscles, detected with DIXON imaging, has the ability to predict loss of functional abilities. [35, 36] Therefore, it could be that a combination of pathophysiological changes, as it creates a more complete view of the clinical state of a patient, in one muscle or a group of muscles, is more sensitive to predict loss of certain functional abilities or specific function milestones. Ultimately, the ability to differentiate between slow- and fast-progressing patients based on a combination of MR measurements in one or multiple muscles, would be valuable for disease-monitoring purposes but also for identifying selection criteria for therapeutic interventions. For such analysis, large patient cohorts that cross broad age ranges are required and need to be followed for a much longer time period.

Despite the fact that all findings in this thesis point towards using multi-parametric MRI to advance the understanding of the pathophysiology, it is also important to note that more detailed analysis of individual techniques/processes are still required. For instance, acquisition of high SNR spatially-resolved ^{31}P MRS data sets allows one to distinguish between glycerol 3-phosphocholine (GPC) and glycerol 3-phosphoethanolamine (GPE) in PDE, and as such allows the assessment of the origin of the elevation in PDE-levels, which contributes to a better understanding of the pathophysiology. Alternatively, other so far not yet implemented MR techniques need to be explored as they could be of value as outcome parameters. Such techniques include for example ^{23}Na MRI to assess inflammation, T1 rho mapping aimed at measuring fibrosis, Arterial Spin Labelling (ASL) to assess tissue perfusion and MR Elastography to detect differences in tissue stiffness. Subsequently, more dynamic measurements such as the recovery of PCr and blood flow after sub-maximal exercise or the change of fiber length and pennation angle due to motion, may provide insight into factors that play a role in daily life activities.

7.3.3 Potential MR outcome parameter

With the expansion of therapeutical developments in DMD [37-40], numerous studies have focused on mapping of the natural disease progression of DMD with qMRI. Until now, muscle fat fraction and water T2 measurements seem to be the most promising MR outcome parameters in DMD.[28, 41] However, since therapeutic developments at the moment aim at preserving or improving muscle tissue, an early marker with a high discriminative ability to detect changes in muscle tissue will be essential. Both water T_2 and %fat do not fulfill these criteria. [36, 42-44]

This thesis shows that PDE-levels detected with ^{31}P MRS could reflect muscle tissue changes with a high discriminative ability (there was a two-fold increase in patients compared to controls) in both the early and more advanced disease stages. Despite

the fact that the exact origin of the elevated PDE-levels in DMD is not fully clear, these changes in muscle tissue could have value as outcome parameter. However, several issues need to be investigated in more detail in order to explore this. To start with, it would be crucial to find out if in DMD patients PDE-levels detected with ^{31}P MRS are able to revert back to normal values upon therapy, as previously shown in Golden Retriever Muscular Dystrophy dogs by using adeno-associated virus (AVV) vector therapy. [45] At the moment, the only therapy available for DMD patients are corticosteroids which slows the pace of the disease progression, probably as a result of reducing the inflammatory component. [46] Although it is unclear what the effect of corticosteroids will be on metabolic pathways, it could be interesting to test the short- and long-term effects of corticosteroids on several MR outcome parameters. Subsequently, the full trajectory of PDE-levels along the course of the disease should be assessed, as it is highly valuable to know the natural progression of change, to relate potential therapeutic effects to. Lastly, it is also of interest to know how accurate and reproducible PDE-levels can be detected between measurements within a single imaging center but also across centers. Previous studies assessed the reproducibility of %fat and water T_2 measurements in both HC subjects and DMD patients within and between centers and found CV values ranging between 0.8-8%.[47] The CV values found for quantifying PDE-levels in this work, for high and lower SNR conditions, are similar to these values, and below the general acceptable level of agreement (<10%). This suggests that even in more highly affected patients (simulated by the lower SNR data-sets) one can accurately quantify PDE-levels within a center. In other words, this means that PDE-levels could be used to monitor muscle tissue changes across different stages of the disease. For future clinical studies, it is recommended to establish a standardized protocol which can be used to determine the reproducibility of quantifying PDE-levels with spatially-resolved measurements across centers.

The two-fold elevation of PDE-levels compared to controls, its detection prior to structural changes, and its high reproducibility confirm the value of PDE-levels as an MR outcome parameter to monitor muscle tissue changes. However, it can be questioned how feasible the use of spatially resolved ^{31}P MRS is to detect PDE-levels in clinical trials. To date, most hospitals have only clinical MR systems and surface coils at their disposal, which do not allow such advanced measurements. In practice, this will most likely result in surface coil localized measurements, which generate a weighted value from multiple muscles at once and might not be sensitive enough to detect subtle changes in individual muscles. With respect to therapy developments in DMD, so far it is uncertain if and to what extent there will be changes in the muscle with appropriate therapy. At the same time it is

unclear where these potential therapeutic effects will be manifested. Due to this lack of knowledge, it is too early to choose one single MR measure as an outcome parameter. Therefore it is highly recommended to use a multi-parametric approach in which the assessment of metabolic alterations, PDE-levels specifically, and a variety of other pathophysiological processes are embedded.

7.4 Future perspectives: Acceleration

This thesis provides evidence, from both a pathophysiological and methodological perspective, that it is important to use multi-parametric MRI in skeletal muscle disease. The feasibility of reaching that goal depends on finding an appropriate balance between scan duration and the necessary quality of the data. Acceleration of scan sequences can provide freedom in either increasing variety or quality**. Chapter 6** of this thesis showed that implementation of a fast B_1^+ shimming technique, as applied to a whole-body fat-water separation approach, improved data quality without loss of essential scan time. These mapping approaches do not have any direct diagnostic value but do directly influence data quality. Over the past decade, other approaches aimed at acceleration of diagnostic scans, such as parallel imaging, compressed sensing, interleaving and integrating of sequences, have emerged. Acceleration factors of 2-5 fold have been achieved with these various methods without loss of data quality in skeletal muscle applications. [48-50] These acceleration factors can be highly beneficial for the implementation of multi-parametric MRI, but also in exercise challenges, in which blood flow and energy metabolism very quickly return to resting state settings, and in whole body applications. Although the foundations for speeding up of acquisitions are available, they will need to be further developed to become clinically applicable.

7.5 Conclusions

This thesis showed the impact of data quality and imperfections in spatial localization on the quantification of MR outcome parameters, but more importantly, emphasized the essence of high quality multi-parametric MRI in order to be able to ascribe tissue changes to either pathology or confounding factors in skeletal muscle applications. More specifically, this thesis showed that sufficient levels of SNR resulted in a robust estimation of MR outcome parameters, and that MR protocols need to be optimized accordingly. Subsequently, confounding factors need to be measured and accounted for, in order to have truly quantitative measures that reflect pathology-related changes. In addition, this thesis showed how different MR measures can be depicted in a complementary way to describe pathophysiological processes during the course of the disease. The use of muscle-specific measurements and multi-parametric MRI both contributed to a better understanding of the disease-related changes in DMD. In the

future, multi-parametric MRI and new technical developments should complement each other in an effort to advance the understanding of the pathophysiology and to determine the value of MR outcome measures to assess muscle tissue changes. At the same time, it is important to link this comprehensive MR muscle profile to muscle function, functional abilities and functional milestones.

7.6 References

1. Froeling M, Nederveen AJ, Nicolay K, Strijkers GJ. DTI of human skeletal muscle: the effects of diffusion encoding parameters, signal-to-noise ratio and T2 on tensor indices and fiber tracts. Nmr Biomed 2013;26:1339-1352.
2. Damon BM. Effects of image noise in muscle diffusion tensor (DT)-MRI assessed using numerical simulations. Magn Reson Med 2008;60:934-944.
3. Baligand C. Stimulated Echo DTI in skeletal muscle of patients with Becker Muscular Dystrophy. 2017.
4. Towse TF, Elder CP, Bush EC, et al. Post-contractile BOLD contrast in skeletal muscle at 7 T reveals inter-individual heterogeneity in the physiological responses to muscle contraction. Nmr Biomed 2016;29:1720-1728.
5. Williams SE, Heemskerk AM, Welch EB, Li K, Damon BM, Park JH. Quantitative effects of inclusion of fat on muscle diffusion tensor MRI measurements. J Magn Reson Imaging 2013;38:1292-1297.
6. Fischmann A, Hafner P, Fasler S, et al. Quantitative MRI can detect subclinical disease progression in muscular dystrophy. J Neurol 2012;259:1648-1654.
7. Sinclair CD, Morrow JM, Miranda MA, et al. Skeletal muscle MRI magnetisation transfer ratio reflects clinical severity in peripheral neuropathies. J Neurol Neurosurg Psychiatry 2012;83:29-32.
8. Janssen BH, Voet NBM, Nabuurs CI, et al. Distinct Disease Phases in Muscles of Facioscapulohumeral Dystrophy Patients Identified by MR Detected Fat Infiltration. Plos One 2014;9.
9. Gaeta M, Mileto A, Mazzeo A, et al. MRI findings, patterns of disease distribution, and muscle fat fraction calculation in five patients with Charcot-Marie-Tooth type 2 F disease. Skeletal Radiol 2012;41:515-524.
10. Straub V, Balabanov P, Bushby K, et al. Stakeholder cooperation to overcome challenges in orphan medicine development: the example of Duchenne muscular dystrophy. Lancet Neurol 2016;15:882-890.
11. Wokke BH, van den Bergen JC, Versluis MJ, et al. Quantitative MRI and strength measurements in the assessment of muscle quality in Duchenne muscular dystrophy. Neuromuscul Disord 2014;24:409-416.
12. Kinali M, Arechavala-Gomeza V, Cirak S, et al. Muscle histology vs MRI in Duchenne muscular dystrophy. Neurology 2011;76:346-353.
13. Torriani M, Townsend E, Thomas BJ, Bredella MA, Ghomi RH, Tseng BS. Lower leg muscle involvement in Duchenne muscular dystrophy: an MR imaging and spectroscopy study. Skeletal Radiol 2012;41:437-445.
14. Schreiber A, Smith WL, Ionasescu V, et al. Magnetic resonance imaging of children with Duchenne muscular dystrophy. Pediatr Radiol 1987;17:495-497.
15. Marden FA, Connolly AM, Siegel MJ, Rubin DA. Compositional analysis of muscle in boys with Duchenne muscular dystrophy using MR imaging. Skeletal Radiol 2005;34:140-148.
16. Arpan I, Forbes SC, Lott DJ, et al. T(2) mapping provides multiple approaches for the characterization of muscle involvement in neuromuscular diseases: a cross-sectional study of lower leg muscles in 5-15-year-old boys with Duchenne muscular dystrophy. Nmr Biomed 2013;26:320-328.
17. Morgan DL, Proske U. Popping sarcomere hypothesis explains stretch-induced muscle damage. Clin Exp Pharmacol P 2004;31:541-545.
18. Shin DD, Hodgson JA, Edgerton VR, Sinha S. In vivo intramuscular fascicle-aponeuroses dynamics of the human medial gastrocnemius during plantarflexion and dorsiflexion of the foot. J Appl Physiol 2009;107:1276-1284.
19. Samitt CE, Bonilla E. Immunocytochemical Study of Dystrophin at the Myotendinous Junction. Muscle Nerve 1990;13:493-500.
20. Atsuta F, Sato K, Maruyama K, Shimada Y. Distribution of Connectin (Titin), Nebulin and Alpha-Actinin at Myotendinous Junctions of Chicken Pectoralis-Muscles - an Immunofluorescence and Immunoelectron Microscopic Study. J Muscle Res Cell M 1993;14:511-517.

21. Moens P, Baatsen PHWW, Marechal G. Increased Susceptibility of Edl Muscles from Mdx Mice to Damage-Induced by Contractions with Stretch. J Muscle Res Cell M 1993;14:446-451.
22. Willmann R, De Luca A, Benatar M, et al. Enhancing translation: guidelines for standard pre-clinical experiments in mdx mice. Neuromuscul Disord 2012;22:43-49.
23. Hu X, Blemker SS. Musculoskeletal simulation can help explain selective muscle degeneration in Duchenne muscular dystrophy. Muscle Nerve 2015;52:174-182.
24. Ricotti V, Evans MR, Sinclair CD, et al. Upper Limb Evaluation in Duchenne Muscular Dystrophy: Fat-Water Quantification by MRI, Muscle Force and Function Define Endpoints for Clinical Trials. Plos One 2016;11:e0162542.
25. Allen DG, Whitehead NP, Froehner SC. Absence of Dystrophin Disrupts Skeletal Muscle Signaling: Roles of Ca2+, Reactive Oxygen Species, and Nitric Oxide in the Development of Muscular Dystrophy. Physiol Rev 2016;96:253-305.
26. Wary C, Azzabou N, Zehrouni K, et al. One year follow-up of Duchenne muscle dystrophy with nuclear magnetic resonance imaging and spectroscopy indices. Neuromuscular Disord 2014;24:853-853.
27. Forbes SC, Willcocks RJ, Triplett WT, Rooney WD, Lott DJ. Magnetic Resonance Imaging and Spectroscopy Assessment of Lower Extremity Skeletal Muscles in Boys with Duchenne Muscular Dystrophy: A Multicenter Cross Sectional Study (vol 9, e106435, 2014). Plos One 2014;9.
28. Hogrel JY, Wary C, Moraux A, et al. Longitudinal functional and NMR assessment of upper limbs in Duchenne muscular dystrophy. Neurology 2016;86:1022-1030.
29. Newman RJ, Bore PJ, Chan L, et al. Nuclear Magnetic-Resonance Studies of Forearm Muscle in Duchenne Dystrophy. Brit Med J 1982;284:1072-1074.
30. Younkin DP, Berman P, Sladky J, Chee C, Bank W, Chance B. 31P NMR studies in Duchenne muscular dystrophy: age-related metabolic changes. Neurology 1987;37:165-169.
31. Kemp GJ, Taylor DJ, Dunn JF, Frostick SP, Radda GK. Cellular energetics of dystrophic muscle. J Neurol Sci 1993;116:201-206.
32. Griffiths RD, Cady EB, Edwards RHT, Wilkie DR. Muscle Energy-Metabolism in Duchenne Dystrophy Studied by P-31-Nmr - Controlled Trials Show No Effect of Allopurinol or Ribose. Muscle Nerve 1985;8:760-767.
33. Wary C, Azzabou N, Giraudeau C, et al. Quantitative NMRI and NMRS identify augmented disease progression after loss of ambulation in forearms of boys with Duchenne muscular dystrophy. Nmr Biomed 2015;28:1150-1162.
34. Banerjee B, Sharma U, Balasubramanian K, Kalaivani M, Kalra V, Jagannathan NR. Effect of creatine monohydrate in improving cellular energetics and muscle strength in ambulatory Duchenne muscular dystrophy patients: a randomized, placebo-controlled P-31 MRS study. Magn Reson Imaging 2010;28:698-707.
35. Gaeta M, Messina S, Mileto A, et al. Muscle fat-fraction and mapping in Duchenne muscular dystrophy: evaluation of disease distribution and correlation with clinical assessments. Preliminary experience. Skeletal Radiol 2012;41:955-961.
36. Fischmann A, Hafner P, Gloor M, et al. Quantitative MRI and loss of free ambulation in Duchenne muscular dystrophy. J Neurol 2013;260:969-974.
37. Niks EH, Aartsma-Rus A. Exon skipping: a first in class strategy for Duchenne muscular dystrophy. Expert Opin Biol Ther 2017;17:225-236.
38. Buyse GM, Goemans N, van den Hauwe M, et al. Idebenone as a novel, therapeutic approach for Duchenne muscular dystrophy: results from a 12 month, double-blind, randomized placebo-controlled trial. Neuromuscul Disord 2011;21:396-405.
39. Mendell JR, Rodino-Klapac L, Sahenk Z, et al. Gene therapy for muscular dystrophy: lessons learned and path forward. Neurosci Lett 2012;527:90-99.
40. Finkel RS, Flanigan KM, Wong B, et al. Phase 2a study of ataluren-mediated dystrophin production in patients with nonsense mutation Duchenne muscular dystrophy. Plos One 2013;8:e81302.

41. Willcocks RJ, Rooney WD, Triplett WT, et al. Multicenter prospective longitudinal study of magnetic resonance biomarkers in a large duchenne muscular dystrophy cohort. Ann Neurol 2016;79:535-547.
42. Arpan I, Willcocks RJ, Forbes SC, et al. Examination of effects of corticosteroids on skeletal muscles of boys with DMD using MRI and MRS. Neurology 2014;83:974-980.
43. Wokke BH, van den Bergen JC, Versluis MJ, et al. Quantitative MRI and strength measurements in the assessment of muscle quality in Duchenne muscular dystrophy. Neuromuscular Disord 2014;24:409-416.
44. Hollingsworth KG, Garrood P, Eagle M, Bushby K, Straub V. Magnetic Resonance Imaging in Duchenne Muscular Dystrophy: Longitudinal Assessment of Natural History over 18 Months. Muscle Nerve 2013;48:586-588.
45. Le Guiner C, Montus M, Servais L, et al. Forelimb Treatment in a Large Cohort of Dystrophic Dogs Supports Delivery of a Recombinant AAV for Exon Skipping in Duchenne Patients. Mol Ther 2014;22:1923-1935.
46. Matthews E, Brassington R, Kuntzer T, Jichi F, Manzur AY. Corticosteroids for the treatment of Duchenne muscular dystrophy. Cochrane Database Syst Rev 2016:CD003725.
47. Forbes SC, Walter GA, Rooney WD, et al. Skeletal muscles of ambulant children with Duchenne muscular dystrophy: validation of multicenter study of evaluation with MR imaging and MR spectroscopy. Radiology 2013;269:198-207.
48. Loughran T, Higgins DM, McCallum M, Coombs A, Straub V, Hollingsworth KG. Improving Highly Accelerated Fat Fraction Measurements for Clinical Trials in Muscular Dystrophy: Origin and Quantitative Effect of R2*Changes. Radiology 2015;275:570-578.
49. Hollingsworth KG. Reducing acquisition time in clinical MRI by data undersampling and compressed sensing reconstruction. Phys Med Biol 2015;60:R297-322.
50. Parasoglou P, Feng L, Xia D, Otazo R, Regatte RR. Rapid 3D-imaging of phosphocreatine recovery kinetics in the human lower leg muscles with compressed sensing. Magn Reson Med 2012;68:1738-1746.

Chapter 8

Nederlandse Samenvatting

8

Nederlandse samenvatting

In dit proefschrift zijn verschillende kwantitatieve MRI technieken gecombineerd en vergeleken tussen patiënten met Duchenne spierdystrofie (DMD) en gezonde controle deelnemers. Dit is zowel op cross-sectionele als longitudinale data gedaan. Het doel hiervan was om de onderliggende pathofysiologie beter te begrijpen. Daarnaast keken we of deze kwantitatieve MRI parameters potentie hebben om veranderingen in spierweefsel te meten in een klinische setting. Tenslotte hebben we gekeken naar het effect van data-kwaliteit, meet nauwkeurigheid in longitudinale metingen en verstorende factoren op kwantificatie van deze MR parameters.

In hoofdstuk 2 hebben we het effect van vetfractie, Signaal-Ruis-Ratio (SNR) en T2 relaxatie tijd op DTI metingen in skeletspieren van patiënten met DMD in kaart gebracht. We hebben laten zien dat voldoende SNR essentieel is om een betrouwbare schatting van de DTI parameters te kunnen doen. Daarnaast hebben we laten zien dat in-vivo metingen van vetfractie en water T_2 nodig zijn om te achterhalen of de verschillen die we zagen in de DTI parameters komen door de pathofysiologie of door andere factoren. Na het corrigeren van de DTI metingen voor SNR, T_2 en de vetfractie vonden we geen verschillen in DTI parameters tussen patiënten met DMD en gezonde controle jongens.

In hoofdstuk 3 hebben we naar de vetverdeling binnen één spier gekeken, in DMD patiënten en gezonde controle deelnemers, met behulp van de Dixon techniek. We hebben laten zien dat vetfracties binnen een spier ongelijkmatig verdeeld waren langs de proximo-distale spieras, met hogere vetfracties aan de uiteindes van de spieren in vergelijking tot de spierbuik. Daarnaast hebben laten zien hoe belangrijk het is om op exact dezelfde locatie te meten binnen één spier. Een kleine verschuiving (15mm) van de meetlocatie langs de proximo-distale as resulteerde in een verschil in vetfractie van 1-2% en kon oplopen tot 12%. Dit kan een enorme invloed hebben op het gebruik van kwantitatieve MRI metingen als potentiele uitkomstmaat in klinische trials en benadrukt het belang van nauwkeurigheid in herpositionering in longitudinale MRI studies. Daarnaast geven deze resultaten aan dat mechanische verstoring van de spiermembraan één van de belangrijkere factoren in de pathofysiologie van DMD zou zijn.

In hoofdstuk 4 hebben we gebruik gemaakt van verschillende kwantitatieve MR technieken om meer inzicht te krijgen in de relatie tussen de verschillende pathofysiologische veranderingen die voorkomen in de spieren van DMD patiënten. Dit hebben we gedaan door naar ontsteking en metabole veranderingen te kijken in

spieren met en zonder vet infiltratie, met zowel imaging als fosfor spectroscopie. We hebben gevonden dat PDE niveaus en water T_2 waardes al verhoogd waren in spieren die nog geen vet infiltratie lieten zien. De ratio van in-organisch fosfaat over ATP en intracellulaire weefsel pH waren alleen veranderd in spieren die al vet infiltratie lieten zien. Dit betekent dat we in staat zijn om een onderscheid te maken tussen vroege en latere pathofysiologische veranderingen in de spieren van DMD patiënten. Daarnaast hebben we ook gevonden dat PDE niveaus en water T_2 waardes verhoogd bleven in spieren die vet-infiltratie lieten zien. Dit impliceert dat PDE niveaus en water T2 waardes niet alleen kunnen functioneren als een vroege maat, maar misschien in meer aangedane spieren. De potentie van deze uitkomstmaten moet verder onderzocht worden aan de hand van longitudinale studies.

In hoofdstuk 5 hebben we aan de hand van longitudinale kwantitatieve MR data van verschillende onderbeenspieren, het tijdsverloop van veranderingen in PDE niveaus en vet infiltratie bekeken. DMD patiënten en gezonde controles werden drie keer gemeten gedurende een periode van 24 maanden met tussenpozen van één jaar. PDE niveaus waren twee keer zo hoog in vergelijking tot gezonde controles, in alle geanalyseerde spieren op alle tijdspunten met uitzondering van de Tibialis Posterior spier tijdens de baseline meting. We vonden geen verschillen in PDE-niveaus tussen de drie tijdspunten. De vetfractie nam significant toe tussen de tijdspunten in de meerderheid van de geanalyseerde spieren van de DMD patiënten. Dit suggereert dat PDE-niveaus een andere verloop over de tijd laat zien dan de vetfractie. Daarnaast hebben we gekeken hoe reproduceerbaar PDE niveaus gemeten kunnen worden en wat het effect van SNR is tijdens het kwantificeren van PDE. We lieten zien dat PDE niveaus accuraat en reproduceerbaar gemeten kunnen worden met fosfor spectroscopie in hoge en lage SNR datasets. Dit betekent dat PDE niveaus in vroege en latere fase van ziekte betrouwbaar gemeten kunnen worden. Al deze bevindingen samen bevestigen de potentie van PDE niveaus als maat om veranderingen in spierweefsel in kaart te brengen in patiënten met DMD.

In hoofdstuk 6 is de implementatie van een snelle DREAM B_1^+ shimming methode geëvalueerd als toepassing voor beeldvorming van het hele lichaam op 3T MRI scanner. Beeldvorming van het hele lichaam is een toepassing die erg gevoelig is voor ongelijkmatigheden in het excitatie (B_1^+) veld. Met behulp van B_1^+ shimming worden deze ongelijkmatigheden zo klein mogelijk gemaakt. Het gebruik van deze nieuwe DREAM B_1^+ shimming techniek zorgde voor een significante toename in data-kwaliteit van de beelden gemaakt in de bovenbenen en het bovenlichaam. Naast deze optische verbeteringen in data-kwaliteit in deze regio's vonden we ook nauwkeurigere excitatie hoek en een homogener B_1^+ veld gemeten in de

bijbehorende B_1^+ mappen. Tenslotte zorgde de nieuwe DREAM methode voor een versnelling van een factor van 10 in vergelijking tot de tot dan toe beschikbare B_1^+ shimming methodes. Dit suggereert dat DREAM B_1^+ shimming een veelbelovende techniek is die niet alleen gebruikt kan worden voor beeldvorming van het hele lichaam maar ook van belang is voor toepassingen in regio's die gevoelig zijn voor artefacten door een inhomogeen excitatie veld.

8

List of Publications

Journal Publications

1) Wokke B.H.***, Hooijmans M.T. *,** Bergen J.C., Webb A.G., Verschuuren J.J.G.M ., Niks E.H., Kan, H.E. Muscle MRS detects elevated PDE/ATP ratios prior to fatty infiltration in Becker Muscular Dystrophy. *NMR in Biomedicine (2013), 27 (11). 1371-1377 (* shared first author)*
2) **Hooijmans M.T.,** Dzyubachyk O., Nehrke K., Koken P., Versluis M.J., Kan H.E., Boernert P. Fast multistation water/fat imaging at 3T using DREAM-based RF shimming. *Journal of Magnetic Resonance Imaging (2014), 42 (1), 217-223*
3) Wokke B.H., van den Bergen J.C., **Hooijmans M.T.,** Webb A.G., Verschuuren J.J.G.M., Niks E.H., Kan H.E. T2 relaxation times are increased in skeletal muscle of DMD but not in DMD patient. *Muscle & Nerve (2013) 53 (1), 38-43*
4) **Hooijmans M.T.**, Damon B.M., Froeling M., Versluis M.J., Burakiewicz J., Verschuuren J.J.G.M., Niks E.H., Webb A.G., Kan H.E. Evaluation of skeletal muscle DTI in patients with Duchenne Muscular Dystrophy. *NMR in Biomedicine (2015), 28 (11), 1589-1597*
5) **Hooijmans M.T.,** Niks E.H., Burakiewicz J., Verschuuren J.J.G.M., Webb A.G., Kan H.E. Elevated Phosphodiesters and T2 levels in the absence of fat infiltration in Duchenne Muscular Dystrophy Patients. *NMR in Biomedicine (2017), 30 (1*), doi: 10.1002/nbm.3667
6) **Hooijmans M.T.,** Niks E.H., Burakiewicz J., Anastasopoulos C., Verschuuren J.J.G.M., Webb A.G., Kan. H.E. Non-uniform muscle fat replacement along the proximal distal muscle axis in Duchenne Muscular dystrophy patients. *Neuromuscular disorders (2017), 27 (5), 458-464.*
7) Burakiewicz J., **Hooijmans M.T.,** Webb A.G., Verschuuren J.J.G.M., Niks E.H., Kan H.E. Improved olefinic fat suppression in skeletal muscle DTI using a magnitude based Dixon method. *Magnetic resonance in Medicine (2017*), *doi:10.1002/mrm.26655*
8) Doorenweerd N., **Hooijmans M.T.,** Schubert S.A., Webb A.G., Straathof C.S.M., van Zwet E.W., van Buchem M.A., Verschuuren J.J.G.M, Hendriksen J.G.M., Niks E.H., Kan H.E. Proton Magnetic Resonance Spectroscopy indicates Preserved cerebral biochemical composition in Duchenne Muscular Dystrophy Patients. *Journal of Neuromuscular Disorders (2017), 4 (1), 53-58.*
9) **Hooijmans M.T.,** Doorenweerd N., Baligand C.J., Verschuuren J.J.G.M., Ronen I., Webb A.G., Niks E.H., Kan H.E. Spatially localized ^{31}P MRS in skeletal muscle: 24-month follow-up study. *Plos one(2017), 12 (8), 1-15.*

Conference Proceedings

1) **Hooijmans M.T.,** Doorenweerd N., Baligand C.J., Verschuuren J.J.G.M., Ronen I., Webb A.G., Niks E.H., Kan H.E. Phosphodiester-levels in muscle assessed using ^{31}P MRS are an early marker for disease activity in DMD
    - ISMRM 2017, Honolulu Hawaii, 22-27 April — *Electronic poster*
    - ISMRM Benelux 2017, Tilburg The Netherlands, 20 January — *Traditional poster*
        - ***Best Poster Presentation Award***

1) **Hooijmans M.T.,** Niks E.H., Burakiewicz J., Anastasopoulos C., Verschuuren J.J.G.M., Webb A.G., Kan. H.E. Fat infiltration is non-uniform along the proximodistal muscle axis in Duchenne Muscular Dystrophy
    - ISMRM 2016, Singapore, 7 -13 May - *Electronic poster*

2) **Hooijmans M.T.,** Niks E.H., Burakiewicz J., Verschuuren J.J.G.M., Webb A.G., Kan H.E. A multimodal MR approach to evaluate complex muscle degeneration processes in Duchenne Muscular Dystrophy
    - ISMRM 2016, Singapore, 7 -13 May -- *Oral presentation*
        - ***Summa Cum Laude Award***
    - ISMRM Benelux 2016, Eindhoven, 22 January – *Traditional poster presentation*

3) **Hooijmans M.T.**, Damon B.M., Froeling M., Versluis M.J., Burakiewicz J., Verschuuren J.J.G.M., Niks E.H., Webb A.G., Kan H.E. Evaluation of skeletal muscle DTI in Duchenne
    - ISMRM 2015, Toronto Canada, 30 May- 5 June -- *Electronic poster*
    - ISMRM Benelux 2015, Ghent Belgium, 16 January – *Oral presentation*

4) **Hooijmans M.T.,** Wokke B.H., Goemans N., Champion G., Verschuuren J.J.G.M ., Niks E.H., Kan, H.E. Longitudinal quantitative muscle MRI in 5 Duchenne boys treated with exon 51 skipping – an off treatment follow-up.
    - WMS 2014, Berlin Germany, October 2014 – *Oral presentation*

5) **Hooijmans M.T.**, Ercan E.A., Webb A.G., Kan H.E., Ronen I. ^{31}P DWS of different muscles in the lower leg
    - ISMRM 2014, Milan Italy, 10-16 May – *Traditional poster*
    - ISMRM Benelux 2014, Maastricht The Netherlands, 20 January – *Traditional poster*

6) **Hooijmans M.T.,** Dzyubachyk O., Nehrke K., Koken P., Versluis M.J., Kan H.E., Boernert P. Improved fast multi-station water-fat imaging at 3T
    - ISMRM 2014 Milan Italy, 10-16 May -- *Power poster Session: ISMRM 2014*
        - ***Magna Cum Laude Award***

7) **Hooijmans M.T.,** Wokke B.H., Bergen J.C., Webb A.G., Verschuuren J.J.G.M ., Niks E.H., Kan, H.E. Elevated muscle metabolites in Becker Muscular Dystrophy detected by MR spectroscopy
    - WMS 2013, Asilomar State Beach USA , October 2013-- *Traditional poster*
    - ISMRM Benelux 2013, Rotterdam The Netherlands, 14 January – *Oral presentation*

Curriculum Vitae

Melissa Tamara Hooijmans was born on July 3rd 1989 in Zoetermeer, The Netherlands. After graduating from the Erasmus College in Zoetermeer in 2007, she continued her studies in Human Movement Sciences at the VU University in Amsterdam. She obtained her Bachelor of Science degree successfully in 2010. During her bachelor Melissa worked as a student assistant at the faculty of Human Movement Sciences at the VU University in the disciplines Human Anatomy of the Muscular System and Neurosciences. After finishing her bachelor, she obtained her Master of Science degree in 2011 with a specialization in Rehabilitation. In 2012, she started as a PhD candidate at Leiden University Medical Center at the C.J. Gorter Center for High Field MRI. Under supervision of Dr. Hermien Kan, Dr. MD. Erik Niks, Prof. MD. Jan Verschuuren and Prof. Andrew Webb she conducted her research project ' Longitudinal quantitative MR in skeletal muscle in DMD and BMD patients' of which the work is culminated in this thesis. She is currently appointed as postdoctoral researcher in the group of Prof. dr. Gustav Strijkers and Prof. Ir. Aart Nederveen at Amsterdam Medical Center. She will pursue to do research with quantitative MR techniques in skeletal muscle.

Dankwoord

Allereerst wil ik in het bijzonder alle deelnemers en hun familie bedanken voor hun inzet. Jullie hebben me aan het huilen gemaakt van het lachen en zo ongelofelijk trots, die momenten zal ik niet vergeten.

Aan al mijn collega's van het C.J Gorter Centrum, wat zijn jullie fantastische, intelligente en enthousiaste mensen. Bedankt dat ik me zo thuis heb gevoeld bij jullie.

A special thanks for my promotor Andrew and copromotors Hermien and Erik. Dear Andrew, I am very grateful that I got the opportunity to work with you. You showed me how important it is to do what you like, thank you for that! Hermien, bedankt voor al het vertrouwen, de begeleiding, de kansen en de vrijheid die je me hebt gegeven om de wetenschap te ontdekken. Erik, dankjewel voor je waardevolle input, kritische kijk op mijn manuscripten, en je ideeën om ook het klinische aspect voldoende te belichten. Jan, wat fijn dat je van het begin af aan betrokken bent geweest bij mijn onderzoek, ik heb je ideeën en suggesties altijd als zeer waardevol beschouwd en je bemoedigende glimlach zal ik niet vergeten. Many thanks to Peter, when we started my first project together, I had no clue about MR. Your enthusiasm, ability to explain, knowledge about MR and endless patience helped me through, thank you.

Lieve Nathalie, dankjewel voor al je steun (en natuurlijke alle leuke dingen) de afgelopen jaren. Vanaf dag 1 stond je klaar om me op te vangen, daardoor heb ik nooit het idee gehad dat ik het alleen moest doen. Ook mijn kamergenootjes uit de bunker (C2-195), onwijs bedankt, ik heb alle jaren met veel plezier bij jullie op de kamer gezeten. Ook wil ik graag alle collega's uit het Duchenne team en mijn scanmaatjes bedanken, ik heb met veel plezier met jullie samengewerkt. Martijn, Jos, Linda en Jules bedankt voor de mooie samenwerkingen en congressen. Ook wil ik graag alle collega's van Zo bedanken voor het warme welkom dat jullie me hebben gegeven in het AMC.

Mijn paranimfen, wat ben ik blij dat jullie er zijn en dankbaar dat jullie vandaag naast me willen staan! Lieve Mathijs, voor andere zijn we waarschijnlijk als water en vuur, maar wat hebben we veel gelachen en gedaan, bedankt dat je voor altijd mijn maatje bent! Lieve Nadina, wat een prachtig mens ben je toch, bedankt voor het perspectief dat je me geeft!

Mijn fantastische spetters, Milou, Janneke, Kim-manou, Maaike, Susan, Claudia, Shanna, Celine, Merel, Anne en Paul, dankjewel voor jullie vriendschap in goede en slechte tijden, ik ben trots op jullie. Lieve Maaike, helemaal aan de andere kant van de wereld zit je nu, wat ben ik trots dat je die keus hebt gemaakt en dankbaar dat je altijd voor me klaar staat. EC-dames, wat is het mooi om te zien hoe we allemaal onze eigen weg zijn gegaan, maar toch nog de tijd vinden om mooie ervaringen en verhalen te delen. Marinka, kleine meisjes worden groot, dankjewel dat je er voor me bent. Aan alle meiden van de Westlandgracht, dankjewel voor mijn fijne thuis, altijd iemand met een luisterend oor en onwijs veel gezelligheid. Loes en Larissa dankjewel voor de ontspanning in en buiten de turnzaal, die hebben me tot veel goede inzichten gebracht.

Tenslotte mijn lieve familie. Mandy, wat een mooi stoer mens ben je toch, dankjewel voor je onvoorwaardelijke vertrouwen in mijn kunnen, je oprechte interesse en steun, zoals je merkt is het gelukt. Mike, dank voor je unieke zelfspot. Je maakt me daarmee altijd aan het lachen, ik ben benieuwd wat er nog meer gaat komen. Lieve paps en mams, dankjewel voor alle kansen die jullie me hebben gegeven en voor jullie betrokkenheid, wijsheden en onvoorwaardelijke vertrouwen en liefde. Jullie hebben altijd voor me klaar gestaan, wat mooi dat ik dit moment nu met jullie kan delen.